Analysis of Intake Charge Temperature and EGR Stratification Effects on HCCI Combustion

by

Angelo P. Chialva

A thesis submitted in partial fulfillment
of the requirements for the degree of

Master of Science
(Mechanical Engineering)

at the

University of Wisconsin – Madison
2006

Approved: _____

David E. Foster

Professor – Mechanical Engineering
University of Wisconsin – Madison

Date: _____

ABSTRACT

HCCI combustion is characterized by a near homogeneous composition and temperature mixture of air, fuel and post-combustion products. HCCI related research work around the world defines different strategies for achieving HCCI combustion based on intake charge characteristics, fuel type, and fuel and residual gas mixing methodologies. Engine specific characteristics that defined our HCCI combustion research can be listed as follows: - Fuel injection was always performed upstream of the intake port to ensure that a fully homogeneous air and fuel mixture charge was delivered into the engine. – Low levels of in-cylinder residual gas were achieved by a late EVC timing and a minimum of NVO for the purposes of mitigating the in-cylinder temperature, air-fuel ratio and diluent stratification effects imposed by the trapped residual gas. – Externally added EGR helped achieve HCCI combustion within the desired limits of combustion variability and ringing index, and also allowed running the engine fully unthrottled. – Cylinder head split port and dual intake surge tanks / dual intake runners made possible it to inject two fully independent charges into the engine. – Fuel type used to run these experiments was isooctane. This fuel was chosen due to its characteristics as a single stage ignition fuel.

A very specific intake port and intake system setup has been designed and installed in a single cylinder engine to analyze and characterize the effects of imposed intake charge temperature and composition stratification on combustion and emission metrics. The characteristics of this particular engine intake port and intake system setup allowed us to establish different sorts of charge stratification, such as thermal and composition stratification.

The main objective of this research work was to conduct HCCI combustion and emission studies through the isolation of combined effects imposed by the stratified charge. Thermal and composition intake charge stratification effects could be imposed by applying separately diluent or charge composition and thermal stratification effects throughout the intake charge. The list of combined effects within the stratified charge was detailed as follows: local air-fuel ratio effects, thermal charge gradient effects caused by differences in charge specific heat ratios, diluent stratification and fuel number density non uniform spatial distributions.

Experimental results have shown that: - Combustion phasing is sensitive to thermal and diluent stratification effects. – The combustion event was a unique function of Combustion Phasing CA50. - With thermal charge stratification, combustion advances at a fixed intake charge temperature. - With diluent stratification, combined effects take place to modify ignition timing. - Stratified charge effects such as A/F, Non-uniform Spatial Distribution of Mixture Gamma, Fuel and Diluent are all interconnected. Combustion phasing is strongly sensitive to each one of these individual effects.

ACKNOWLEDGEMENTS

First of all, I would like to thank my project advirors, Professor Dave E. Foster and Professor Jaal B. Ghandhi for their support, dedication, enthusiasm, and knowledge. I highly appreciate the experience and expertise that both of them bring to many of the research topics that have been relevant for my research work.

I would like to thank also my thesis committee members, Professor Rolf D. Reitz and Professors Timothy A. Shedd for their support, for their inputs regarding my thesis, as well as for sharing their knowledge in the field of internal combustion engines.

General Motors is gratefully acknowledged for making the GM Gasoline HCCI project possible. I would particularly like to express my gratitude to Dave Reuss and Paul Najt from General Motors and to James Eng, former General Motors engine scientist.

My thanks go especially to my GM Gasoline HCCI project partner, Randy Herold a Ph.D. student involved in the HCCI project described in this thesis. It has been a great pleasure to work and share my Engine Research Center (ERC) office with him for over two years. Also, I would like to extend my thanks to Rinaldo Augusta. He provided me with valuable help during the starting stages of my research work. I also would like to mention the valuable support I got from the following people during my engine lab setup and engine maintenance activities: Ralph Braun for his technical advice and assistance in the ERC, Manuel Gonzales and Roger Krieger, and the following ERC hourly students Loney Peet, Aaron Arnold and Andy Baalrud.

I would like to thank very much my parents and my sister in Argentina for their long-distance support and their important advices they have given me.

TABLE OF CONTENTS

LIST OF TABLES

LIST OF FIGURES

GLOSSARY OF NOMENCLATURE

A/F air/fuel ratio
aTDC after top dead center
bTDC before top dead center
CA crank angle
CA 10 10% burn crank angle location
CA 50 50% burn crank angle location
CA 90 90% burn crank angle location
cc cubic centimeter
CH_2O formaldehyde
CI compression ignition (diesel) engines
CO carbon monoxide
CO_2 carbon dioxide
COV coefficient of variation
CR compression ratio
deg degree
EGR exhaust gas recirculation
EI emission index
EI_{CO} emission index of carbon monoxide
EI_{HC} emission index of hydrocarbons
EI_{NO} emission index of nitrogen oxides
EPA environmental protection agency
FWHM full-width half-maximum
HC hydrocarbons
HCCI homogeneous charge compression ignition
IMEP indicated mean effective pressure
N_2 nitrogen
NA naturally aspirated
NO_x nitrogen oxides
NTC negative temperature coefficients
PP peak pressure
PRF primary reference fuel (mixture of isooctane and n-heptane)
PRF 87 primary reference fuel with an octane number of 87
RPM engine revolutions per minute
s seconds
SI spark ignition
TDC top dead center
rc ratio of pressures

Chapter 1 - Introduction

The research work presented in this thesis deals with the analysis of combustion and emission performance data gathered from experiments of an alternative to conventional and well-known concepts of internal combustion engines based on thermodynamic cycles such as; Otto and Diesel cycles. The combustion process in the study is named Homogeneous Charge Compression Ignition (HCCI). Before getting into the details of HCCI combustion and emission characteristics, it is necessary to explain why research into internal combustion (IC) engines has motivated us in the first place.

1.1 Motivation for Internal Combustion Engines Research

Many people's perspectives might associate combustion engines, which are used for purposes such as driving trucks, cars and buses, with large-scale consumption of limited fossil-fuel reserves and the production of exhaust gases that harm both the environment and our health [1, 2]. A second perspective might associate them with the advantages, such as mobility, that are linked to the widespread availability of passenger cars. Regardless of one's perspective, it seems reasonable to expect that the number of vehicles moved by the means of an internal combustion (IC) engine will rise in the future, especially given factors such as the rapid economic development in densely populated areas, such as China and India. Furthermore, trends for passenger cars indicate that vehicle weight and size are likely to increase, together with the power requirements of the growing number of electronic devices on board. All of these factors will keep promoting the increase of fuel consumption, so world-wide fuel consumption and emissions can only realistically be reduced if an alternative for the IC engine is developed with characteristics significantly better in terms of thermal efficiency and pollutant emissions

than those of present engines. Ideally, such an alternative should not be dependent on fossil fuels, emit no harmful products and have a better efficiency.

Concepts such as fuel cells look very promising. Unfortunately, large-scale introduction of this propulsion technology is expected to take another twenty years or more, mainly due to high technology costs, problems with on-board hydrogen storage and the lack of hydrogen infrastructure. Furthermore, the powertrain-to-wheel efficiency of fuel cell powered vehicles with all the necessary auxiliary equipment is estimated to be similar, or even lower, than that of optimized Diesel engines [3, 4]. Production of hydrogen in the vehicle would solve some of the above problems, but as long as fossil fuel reformation is applied, this would not be a sustainable solution. Truly clean fuel cell technology would be based on a renewable source, such as nuclear, wind or solar energy. However, with present technological standards in the renewable energy field, it is far from realistic to believe that a substantial portion of the fossil fuel used for vehicle propulsion could be replaced by sustainable alternatives in the near future.

It is therefore concluded that IC engines are likely to be around for a while and that, as long as no outstanding alternative is available, research focusing on improving the internal combustion engine concept is justified. The issue raised by these considerations is the degree of further improvement that can be expected on IC engines. What characteristics would engines have if unlimited resources were invested in IC research and the results were available today? Similarly, IC engines have been developed for more than a century, how much more can be squeezed out of them? Recent decades have seen impressive evolutionary steps in the development of the IC engine: fuel consumption and emissions have been substantially decreased, while power output has

been raised, mainly due to the application of new technologies, such as the three-way catalyst, enhanced fuel injection systems and improved engine management. Furthermore, other innovative systems and approaches with a wide range of features have recently been introduced or are expected to be applied soon, including: flexible valve operation; cylinder de-activation; cycle-to cycle, model-based engine control systems; and direct-injection of fuel. Bearing these technology advances in mind, together with the strict legislation on vehicle emissions that is to be applied in many countries, it seems reasonable to expect future reciprocating engines to be considerably cleaner and to have better fuel economy than current engines. Without quantifying the possible future improvements, it is concluded that development of IC engines will probably continue during the years to come. One of two possibilities now would be to attempt to improve the conventional Otto and/or Diesel engines. The second would be to focus on alternative combustion modes, such as HCCI combustion. The HCCI concept is promising, as confirmed by the number of research groups and scientific publications dedicated to it [5]. The combustion and emission performance experimental investigation of the HCCI combustion is the topic of this thesis, and the next section, therefore, discusses this IC engine concept more in detail.

1.2 Definition of HCCI Combustion

The characteristics of each of the three combustion concepts, Otto Cycle or Spark Ignited (SI), Diesel Cycle or Compression Ignition (CI) and Homogeneous Charge Compression Ignition (HCCI), used currently in internal combustion engines are very different from each other. Nevertheless, they are all characterized by a common thermodynamic principle that allows the machine to extract energy out of the intake air

and fuel charge. This basic principle is to compress a (more or less) mixture of air and fuel (together with post-combustion products) to high temperatures within the combustion chamber volume. In the case of HCCI combustion, the mixture of air, fuel and post-combustion products tends to be homogeneous. This mixture finally undergoes auto-ignition close to Top Dead Centre (TDC) by the end of the compression stroke. Although this applies for both gasoline and diesel HCCI combustion type engines, the processes involved are often different due to differences in the nature of the fuels; Diesel fuel has a higher vaporization temperature at atmospheric pressure than gasoline and it is less resistant to auto-ignition. For this reason, it is undesirable to inject diesel fuel under relatively cold conditions, i.e., using port-injection or very early direct-injection (e.g., during the intake process). Consequently, it is challenging to obtain a homogeneous mixture of air and diesel fuel at the end of the compression stroke, since too early injection may lead yet to lack of fully vaporized fuel, such as wall wetting, while too late injection can result in insufficient mixing. Furthermore, it may be necessary for HCCI operation to lower the (effective) compression ratio normally used for conventional diesel combustion and to re-circulate cooled combustion products, since diesel fuel auto-ignites relatively easily.

Gasoline fuel, on the other hand, is more resistant to auto-ignition and, in this case, measures are needed to ensure that mixture temperatures near the end of the compression stroke are sufficiently high to facilitate auto-ignition; some of the approaches described in the literature for this involve raising the compression ratio, heating the intake air, variable valve timing, and re-circulating warm combustion products [5].

Since the two fuel-categorized HCCI combustion concepts described above are not universally followed, and various sub-groups can be defined within the two categories, it is necessary to define precisely the concept of HCCI that will be used throughout this research thesis. The definition stated below makes reference to the type of HCCI combustion based on charge characteristics, fuel type, and fuel and residual gases mixing methodologies applied in the single cylinder gasoline GM metal engine.

In this thesis, HCCI is defined as the process in which a near homogeneous mixture of air and fuel (Iso-octane), diluted with excess air, external EGR or external N2 gas, is compressed to such conditions that auto-ignition occurs close to TDC, and a combustion process follows that is usually significantly faster than conventional Diesel and Otto combustion. First of all, heat is added to the intake charge mixture in all cases as required to achieve auto-ignition while using an engine with a compression ratio that stands at the high end of today's gasoline SI engine compression ratios. Second of all, engine exhaust and intake camshaft timings have been selected to give a minimum of negative valve overlap, which results in a minimum amount of in-cylinder trapped residual gas fraction. Therefore, the HCCI combustion heat release rate is modulated with excess of exhaust gas recirculation (EGR), or air or N2 gas; while a late EVC timing configuration is used and IVO at TDC and IVC at BDC are applied to avoid any sort of chamber charge back flow to the intake port. This intake valve timing configuration ensures that gas exchange effects in the intake port can be mitigated in experimental cases which use imposed thermal or composition stratification throughout the intake charge. The fuel is always injected far upstream of the intake port to ensure that fully homogeneous air and fuel charges are provided into the engine. Similarly, homogeneous

intake charge mixtures with excess of EGR or N2 diluent gas are achieved by injecting these excess volumes of intake charge upstream of an intake surge tank, hence providing an adequate time for mixing.

In the definition of HCCI, it is stated that the mixture is near homogeneous. A perfectly homogeneous mixture of air and fuel would release all the heat of combustion simultaneously, since auto-ignition, in this theoretical case, would occur uniformly throughout the combustion chamber [5, 8]. This would require lower intake charge temperatures at a fixed engine compression ratio, but instead providing much narrower HCCI temperature operating windows. Therefore, sources of in-cylinder inhomogeneities like excess of diluent gas externally added is used to stretch out this HCCI operating window in this engine configuration which is characterized by an almost null level of residual trapped gases. Low levels of residual gas trapped in the cylinder mitigate the air-fuel ratio and diluent gas stratification effects on combustion. Nevertheless, it is important to consider that there are some other sources of mixture charge inhomogeneites, still while injecting a fully homogeneous intake charge into the engine. As a result of inhomogeneites, the mixture is not perfectly homogeneous at the moment the auto-ignition event occurs and stratifications in mixture temperature are created [6, 7]. This inhomogeneity may be due to heat losses to the combustion chamber walls and asymmetric heat losses to the end of the intake port and/or intake port septum by the intake charges entering into the combustion chamber through the dual intake valves setup. The degree of stratification is likely to be of major importance for the charge ignition timing. This identifies one of the major focuses of this HCCI combustion and emission research work.

HCCI combustion is also significantly influenced by the overall burn duration, which limits the load range for which stable HCCI operation is possible; too fast heat release gives rise to violent, knocking combustion, whereas a too long burn duration causes incomplete combustion, or even misfiring, due to the falling mixture temperature in the expansion stroke.

Related to the discussion regarding the burn duration is the fact that the mixture is often diluted. If the mixture of fuel and air is diluted using excess air or EGR or N2 gas, the burn duration can be affected due to the following reasons:

1. The dilution acts as a heat sink during combustion, thus lowering the maximum combustion temperature. As a result, NOx emissions from HCCI engines can be considerable lower than those from conventional engines [6, 7].

2. Diluted mixtures burn more slowly, resulting in a less rapid heat release process and reducing the possibility of knock (i.e. too violent heat release) occurring.

As explained before, the HCCI combustion experiments performed throughout this research work neglects the effects of residual gas trapped on ignition timing and burn duration; therefore, minimizing to a large extent the amount of thermal, air-fuel ratio and hot diluent combined effects on HCCI combustion that are mostly imposed by the post-combustion chamber trapped gases.

A second reason for using a fuel with a high resistance to auto-ignition is that gasoline-fuelled engines can be operated in both HCCI and conventional spark-ignited (SI) mode, while using the same engine geometry. The operating range for stable HCCI combustion that can be achieved at present is certainly narrower than the corresponding range for SI operation, which means that it is probably necessary to switch from HCCI

combustion to SI and vice versa during operation in practice. This offers a tremendous potential for a practical goal, which is to adapt an SI engine to enable it to operate in HCCI mode with as few changes as possible.

The injected fuel amount is used to control the load. In this thesis, the fuel amount has been kept constant for each of the experimental cases run. The engine was run constantly unthrottled in HCCI mode. The amount of air was controlled and changed for the different experimental cases as the amount of introduced diluent gas changed, to always maintain a 1bar engine IMAP. A conventional SI engine requires a stoichiometric air-fuel mixture to be burned for the catalyst to work properly. This is due to the fact that unburned hydrocarbons are more likely to react with molecular oxygen than with NOx. Consequently, a catalyst in an SI engine operated with excess air will fail to reduce NOx emissions. In contrast, as HCCI operation results in low emissions of NOx, the engine can be successfully operated on non-stoichiometric mixtures. Nonetheless, it has to be kept in mind that levels of unburned hydrocarbon and carbon monoxide pollutant emissions tend to increase as HCCI combustion concept is established by applying lean air-fuel mixtures which tend to develop in-cylinder combustion temperature approaching the low temperature combustion limits.

Since HCCI engines can be run at wide-open throttle conditions, even for part-load operation, the pumping losses are significantly lower than for SI operation at low and intermediate loads. This contributes to the relatively high efficiency of HCCI combustion at part and light loads operation. Other advantages over SI operation are the faster combustion, which means that the process is more like theoretical constant volume

combustion, and the reductions in heat losses are achieved, due to the lower combustion temperatures characteristic of HCCI operation.

As described earlier, a lean air-fuel mixture is generally reacted in HCCI engines. Furthermore, as much as 50% of the gas in the combustion chamber can consist of internal residuals and/or re-circulated residuals prior to combustion. As a result, the maximum load of (naturally-aspirated) HCCI engines is significantly lower than for SI engines.

1.3 Objective and Approach

Having introduced the HCCI combustion concept, the objective and approach of this HCCI combustion and emissions research presented in this thesis is presented next.

As explained in the previous section, the HCCI combustion experiments performed throughout this research work neglects the effects of residual gas trapped on ignition timing and burn duration; therefore, minimizing to a large extent the amount of thermal, air-fuel ratio and hot diluent effects on HCCI combustion that are mostly imposed by the post-combustion trapped gases. These combustion timing effects turned out to be all combined and interconnected, thus making the understanding of intake charge composition stratification effects on combustion quite complex. The main objective of this research work is to conduct HCCI combustion and emission studies through isolation of the intake charge stratification effects. The two main intake charge stratification effects can be imposed by applying separately diluent or charge composition and thermal charge stratification effects. The purpose of studying the effects of thermal and composition charge stratification separately on combustion initiation, burn duration and emissions is an important key to gain more insight on controlling HCCI

combustion's rapid heat release rates. Besides gaining insight on fuel energy release rates, it is also important to investigate if benefits of charge stratification exist for lowering the required intake charge temperature and expanding the operating HCCI temperature windows for a single engine condition while using lean diluted air and fuel mixtures.

Furthermore, the research work performed has shown that combined-implicit effects are present within the more general composition or diluent gas stratification effect. Therefore, series of experimental cases have been run to distinguish the engine combustion and emission characteristics for each of these combined effects. The list of individual effects were detailed as follows; local air fuel ratio effects, thermal charge gradient effects caused by differences in charge specific heat ratios, diluent stratification and fuel number density. Distinction on the type of air-fuel ratio that is being referred to in the text, will be always made present by stating whether the mixture air-fuel ratio is; the delivered air-fuel ratio which is calculated by the ratio of the delivered air to fuel masses, the in-cylinder trapped air-fuel ratio which is calculated by taking into account the re-introduced oxygen by the EGR mass and the local air-fuel ratio which is calculated at each of the stratified mixture volumes encompassing the engine intake charge.

The approach used in conducting this research was determined first by choosing an engine fueling rate which corresponded to part-load running conditions. Second, homogeneous air, fuel and diluent intake charge mixture combustion experiments were run in the engine to establish HCCI combustion and emission data baselines. Within the first set of baseline data which was run by using external EGR as diluent, a fixed amount of mass of air per engine cycle was inducted into the engine's intake system, hence single

air-fuel ratio conditions were established to run these baselines. Meanwhile, a second set of experimental data baselines were run at different air-fuel ratios while maintaining a constant fueling rate. This was specifically established for cases using different amounts of N2 gas as diluent in the intake. It is important to keep in mind that constant unthrottled or 1bar engine IMAP conditions were always kept as the target when running different diluent amounts as a function of varied air-fuel ratios. More details can be found in Chapter Four which includes the different experimental conditions used to complete this research work.

Intake charge stratification approaches were quite sophisticated in terms of engine and engine intake system hardware setups. The final engine test cell configuration consisted of a set of dual intake surge tanks, dual EGR delivery plenums, dual intake runners and an intake port split port setup. This allowed the handling of the different intake charge strategies with high versatility. The first intake charge stratification strategy was to send equal volumes of a homogeneous air, fuel and dilute mixture through each of the engine valves at different temperatures, hence imposing thermal gradients throughout the intake charge. The second strategy, defined as diluent or composition stratification, was determined by sending two equal volume charge streams into the engine, in which on stream was established as a pure homogeneous mixture of air and fuel, while the second stream had mainly EGR. Similarly, this approach was used to run cases with N2 gas diluent at different air-fuel ratios.

1.4 Scope and limitation

One of the most critical aspects of the experimental data that is acquired throughout the different engine combustion runs is how the data repeats on a daily basis when experimental conditions are unchanged [9]. Significant emphasis was assigned to the repeatability of measuring engine thermodynamic variables such as in-cylinder pressure and intake charge temperature. The GM single cylinder engine used allowed the installation of thermocouples for intake charge temperature control with measurements located by the intake valves inside the cylinder head intake port. Limitations on the degree of intake thermal and composition charge unmixedness were mainly determined by the mixing effects experienced by the intake charge at the time of entering into the cylinder, regardless of the pseudo perfect achievable degree of unmixedness imposed by delivering two fully independent intake charges into the engine. The extent of charge unmixedness inducted into the engine was a no quantifiable magnitude in the metal engine. By in-cylinder flow field analysis performed at the optical engine, it was known that the level of charge unmixedness at early stages of the compression stroke was consistent. However as the piston progresses through the compression stroke and the mixture approaches temperature and pressure conditions that would trigger the start of combustion (SOC), it was seen that a well mixed homogeneous charge pattern was formed throughout the combustion chamber, thus establishing a less stratified or unmixed charge. The heat exchange processes played an important role in studying the effect of thermal stratification, thus slightly changing the temperature of each independently temperature controlled intake charge. Nevertheless, the efforts of installing intake charge thermocouples by in the intake valves made it possible to account for these effects. Intake

charge temperature stratification experiments were also limited by the maximum achievable temperature difference between the two intake charge streams; which was directly affected by the hardware used to condition the charge streams.

Chapter 2 – Literature Review

2.1 Literature Overview

Homogeneous Charge Compression Ignition (HCCI) combustion offers a number of benefits over conventional spark ignited (SI) and compression ignited (CI) combustion methods. These HCCI combustion advantages can be summarized as follows: NOx emissions are much lower due to its relatively low combustion temperature, cycle-to-cycle variation is relatively negligible due to its self-ignition nature, combustion efficiency is higher at part load than its SI counterpart, and soot emissions are low since a homogeneous lean air-fuel mixture is being employed [10]. Unlike conventional SI and CI engines, where combustion is directly controlled by a specifically defined event such as a spark plug actuation or a sudden in-cylinder fuel injection respectively, the combustion in HCCI engines is controlled by chemical kinetics only [8]. It is also known that HCCI combustion presents considerable limitations related to the range of loads that the engine can perform. This is mainly due to the lack of methods to control ignition timing and heat release rate over the entire engine operation range.

The research work presented on this thesis will mainly focus on understanding the effects of intake charge stratification by imposing controlled non-uniform thermal and composition stratified charges in the combustion chamber. The fuel type used was a single ignition stage type fuel [27] isooctane in a single cylinder engine setup with a fixed compression ratio of 10.95:1 and a late EVC timing, hence making very much negligible the amount of negative valve overlap (NVO). Specific control of HCCI combustion initiation was achieved by controlling the engine intake charge temperatures [9]. Furthermore, studies were performed to demonstrate how the set of combined effects

imposed through diluent charge stratification influence the combustion phasing, engine emissions and combustion performance variables. Gaining an understanding of how each of the charge stratification methods affects combustion initiation, emission and combustion performance may help create suitable approaches to control ignition timing and heat release rates of HCCI combustion. Previous research works have observed that the quality of engine charge affects both ignition timing and the heat release rate of HCCI combustion, but a certain charge temperature is essential to start the ignition of HCCI combustion [29].

HCCI combustion is a combustion process which utilizes a homogeneous air and fuel mixture, but combustion is initiated by fuel self-ignition. It therefore combines features of both SI and CI combustion. During the compression process, different parts of the charge mixture have different heat capacities due to local in-homogeneities which results in non-uniform spatial temperature distributions throughout the combustion chamber. When the hotter charge zones are compressed and its temperature is increased enough, ignition of these zones is initiated. The heat energy released from these hotter zones with early ignition warms and compresses the remainder of the charge, increasing the temperature, until full-scale ignition is established after a short time delay [13, 24]. Therefore, HCCI combustion can be defined as a thermal environment related auto-ignition process, but ignition itself is controlled by the chemical kinetics of the mixture with relatively little influence of turbulence and mixing. Nevertheless, it is important to bear in mind that charge stratification effects on HCCI combustion and emission performance are well influenced by the turbulence and mixing process characteristics taking place in the engine cylinder. There is no large-scale flame propagation.

Since the combustion in HCCI engines is controlled by chemical kinetics only direct controlling methods for managing start of ignition are difficult for HCCI engines.

Nevertheless, there are a number of indirect control methods that have the potential of controlling the timing of auto-ignition and the rate of heat release of HCCI combustion. These can be generally divided into two categories: The first category is by modifying the air-fuel mixture properties by increasing intake temperature, adjusting air-fuel ratio, imposing thermal and/or composition charge stratification, using charge diluents, using additives (promoters and inhibitors of ignition), and modifying fuels to establish fuel blends offering different resistance to auto-ignition and different energy release stages as in-cylinder temperature increases. The second category is by modifying engine operation and design parameters, such as the variable compression ratio, variable valve timing, supercharging, and using different concepts of fuel injection.

Research studies on primary reference fuels (PRFs) indicated that the auto-ignition behavior of a fuel depends largely upon its composition, molecular size and structure. For instance, n-heptane is a reactive straight-chain paraffin and has a low octane number and iso-octane is a less reactive branched chain paraffin, and has a higher octane number. Within internal combustion engines, these two fuels behave differently toward auto-ignition. N-heptane is characterised by a clearly distinguished two-stage ignition for most engine operating conditions: the first stage ignition, which is also regarded as “cool flame”, with negative temperature coefficient (NTC) behavior, followed by the main ignition stage. Iso-octane undergoes a single-stage ignition only for most engine operating conditions. The difference between the two ignition mechanisms has important consequences on the control of the HCCI combustion [30]. At low

temperature, the rate of chain branching for a straight-chain paraffin (n-heptane) is much more intense than that of branched-chain paraffin (iso-octane). This is due to the structure of n-heptane radicals which leads to higher rates of RO2 isomerization which causes chain branching from ketohydroperoxide decomposition [37]. Lower reactivity of the branched-chain paraffin (iso-octane) is due not only to the large number of less reactive methyl groups but also to the presence of tertiary and quaternary C atoms in its structure. The homolysis reactions of tertiary and quaternary structures compete with ketohydroperoxide formation, contributing to the lower reactivity of branched-chain paraffins. All of these indicate that a fuel which has a long-chain and many weakly bounded H atoms has high isomerization rates, which leads to rapid ignition. For compact and highly branched fuels with a large fraction of strongly bounded H atoms, ignition is inhibited.

Chain branching processes play a major role in controlling the ignition of hydrocarbons. For hydrocarbons with two stage ignition behavior, the first stage of ignition is the result of “cool flame” combustion and NTC behavior, which is mainly governed by the low temperature (T<1000K) chemical kinetics. At lower temperatures (up to 900K), ignition is controlled by degenerative chain branching processes. These chain branching processes are characterized by producing chain branching precursors, RO2 radicals, which start to decompose above 800K. At an intermediate temperature (900 to 1100K), chain branching is introduced by the following sequences [37]:

RH+HO2 => H2O2+R,

H2O2+M => OH+OH+M,

where M is any non-reactive third-body. This sequence is important since it precedes the second stage of ignition, i.e., the main ignition. During the preceding time with temperatures up to 1000K, H2O2 concentration increases steadily since the decomposition reaction rate is much slower than the production reaction rate. When a temperature of about 1000-1050K is reached, the reaction H2O2+M => OH+OH+M accelerates, which results in producing large amount of OH radicals.

The effect of fuel molecular structure on the first and main stage of ignition is also important [37]. Three isomers of pentane were compared at the same experiment temperature. It was found that n-pentane ignited firstly, followed by neo-pentane and finally iso-pentane. The main ignitions occurred at the same temperature, but the time required to reach such a temperature, which was the ignition delay, was different. N-pentane displayed the highest rate of ignition since its first-stage of ignition provided the highest temperature increase of the three fuels. In other words, the time required for main ignition depends on the heat released from the first stage of ignition, which determines the rate of temperature increase, although the total heat release during the first stage of ignition (low temperature regime) is considerably lower than that in the main ignition stage. Two peaks of heat release rates were observed, where the first peaks indicated the heat released during the first stage of ignition.

A number of worldwide experimental studies using the HCCI combustion concept in 4 stroke engines have been carried out in recent years. The major target among these studies was to achieve a stable HCCI combustion over a wide range of engine operating conditions. In general, two possible directions have been investigated: modifying air-fuel mixture properties, and modifying engine operation and design parameters.

2.2 Air-Fuel Mixture Properties:

The purpose of these air-fuel mixture properties modifications is to alter the reactivity of intake charge by changing its thermo-chemical properties, thus influencing HCCI combustion. 1 - Intake temperature – A higher intake temperature gives a higher heat release rate. It improves the start of first stage ignition (cool flame) and thus reduces main ignition delay. One popular method of generating HCCI combustion and controlling the ignition timing is to adjust the intake air temperature [8, 9, 12]. A higher intake temperature advances HCCI combustion but the controllable range is limited. Outside this range, the engine volumetric and thermal efficiency can be largely reduced, due to the fact that if ignition is advanced into the compression stroke, it will cause significant negative work on the piston. 2 - Air-fuel ratio - The strength of the air-fuel mixture has a direct effect upon ignition timing and its combustion heat release rate [16]. Enriching the mixture decreases the ratio of the specific heats and thus reduces the amount of disposable compression heating in the charge. Consequently, the mixture has to be compressed further to reach ignition temperature. The ignition timing is therefore delayed. 3 - Exhaust Gas Recirculation (EGR) - Two HCCI combustion control strategies with EGR have been identified and one of them will investigated in this research work: trapping hot internal EGR, and adding cool external EGR into the engine fresh charge. Trapping hot residual EGR will increase the engine charge temperature when air-fuel mixture blends with it inside the combustion chamber. By tuning the quantity of residual EGR, ignition delay and heat release rate of HCCI combustion can be adjusted [14, 23, 25]. External EGR has a much lower temperature than internal EGR, and it will reduce the chemical reaction rate, thus delaying the ignition time, reducing the heat release rate,

and lowering peak cylinder pressure [25]. 4 - Externally imposed thermal and compostion charge stratification – Recent research studies have shown that controlled thermal charge differences applied through the intake charge can be used to slow down combustion rates, thus smoothing out the heat release event [12, 13]. Other approaches taken to impose thermal charge stratification effects are: increase of the NVO, hence accentuating the effect of the hotter trapped in-cylinder residual gases [30]. Externally added EGR has also been seen as a potential approach for HCCI combustion rates control; studies demonstrate that effects of in-cylinder heterogeneous EGR zones also presents benefits on slowing down combustion rates while maintaining combustion and emissions metrics within the desired magnitude ranges [14]. 5 - Additives - Some chemical components have the ability to inhibit or promote heat release at the first stage of ignition. If it is mixed with engine charge as an additive, it will affect the heat release of the first stage ignition of HCCI combustion, then further influence the main ignition. Dimethyl-ether (DME) has a low octane number. When it is mixed with conventional fuels, it will promote the rate of heat release at the first stage of ignition, and thus stabilize HCCI combustion. The rate of heat release from the first stage of ignition with methane is very modest. This makes the main ignition of methane very difficult to achieve in an engine cycle compared with other fuels. Experimental results obtained on a Cooperate Fuels Research (CFR) engine [20] showed that improved HCCI combustion could be obtained by adding DME into methane (15% by volume).

6 - Fuel modifications - Fuel reactivity towards self-ignition is influenced by its composition, molecule size and structure. Fuel pre-conditioning or different fuels blending can make some fuels more favorable for HCCI combustion, and make the

combustion controlling process more achievable. The pre-conditioned fuel fraction with lower octane number is more suitable for HCCI combustion due to its superior auto-ignition characteristic. Blending fuels with different auto-ignition abilities can significantly change the HCCI combustion performance. On the other hand, different fuel blending formats can also be used to limit the operational range of the HCCI combustion.

2.3 Engine operation and control parameters

The purpose of modifying the engine operation and control parameters is basically to achieve and to stabilize HCCI combustion by altering the time-temperature history of the engine charge, for various engine operating conditions.

1 - Compression Ratio – A higher compression ratio increases the charge temperature and therefore advances the start of ignition of the HCCI combustion [24]. In addition, higher compression and thus expansion ratios contribute to higher thermal efficiency. However, knock can be a problem when a high compression ratio is used, particularly with lower octane number fuels [35]. 2 - Engine speed - The ignition delay of HCCI combustion depends largely on air-fuel mixture performance and is relatively free from engine speed influences. However, it should be noted that the ignition time of HCCI combustion relative to the engine crank angle should be retarded when the engine speed increases [10]. In the case that ignition occurs before TDC, the temperature rise from compression will compensate the ignition retardation at high engine speed. If ignition appears after TDC, the ignition delay caused by high engine speed will be further retarded by expansion, which slows down the temperature rise. 3 - Variable valve timing (VVT) - Flexible active valve train (AVT) has been used in controlling the HCCI

combustion process [38]. By tuning the engine valve timing, a manageable quantity of internal EGR can be trapped and used to heat fresh charge up to the required ignition temperature [30]. AVT provides promising results in reducing pollutant emissions, fuel consumption as well as in controlling HCCI combustion at lean conditions have been obtained. 4 - Supercharge - Supercharging can be used to increase the engine's IMEP, and extend the operational range of air/fuel ratio of the HCCI combustion. Different fuels have been tested with various compression ratios and boost pressures. Results have shown that supercharging (up to 2bar boost pressure) increases attainable IMEP, and broadens the operational air-fuel ratio range, although the inlet temperature needs additional adjustment [37]. However, supercharging is accompanied by a high cylinder pressure (around 250bar for 2bar boost pressure), this may limit its potential application. 5 - Fuel injection – Direct injection has been under investigation, too. Two direct injection concepts can be used: early fuel injection, and late fuel injection. Using the early in-cylinder fuel direct injection strategy, fuel is injected during the early part of compression stroke. Fuel vaporization draws heat from surrounding gases, and significantly affects the time temperature history of the entire mixture. Experimental results obtained with early injection of diesel fuel show good results regarding emission reduction [22]. The late in-cylinder fuel direct injection strategy is a relatively new approach to obtain "homogenous" diesel HCCI combustion [30]. During low load, fuel was injected around TDC. The ignition timing was managed by EGR, reduction in CR and strong swirl. As a result, combustion appeared well after the end of fuel injection and the combustion jet that is usually associated with conventional CI engines was

eliminated. However, this method suffers from short ignition delay if EGR, reduction in CR and swirl are not employed.

Chapter 3 - Experimental Setup

The HCCI combustion characterization and analysis experiments were conducted in one of the University of Wisconsin, Engine Research Center laboratories and sponsored by General Motors. This engine laboratory, located in room B131 in the basement of the Engineering Research Building, contains a dual engine setup linked to a common dynamometer. A standard engine (metal engine) is at one end of the dynamometer, while the second engine, which is an optically accessible engine (optical engine), sits at the other end. Most of the combustion and emission research studies explained in this thesis were performed in the metal engine. Nevertheless, flow field visualization of the intake charge in the combustion chamber was studied using PLIF techniques at the optical engine. It is important to mention that both engines are nearly identical. This means that both engines intake and exhaust systems, valve train and its configuration, combustion chamber, piston and cylinder head geometry and dimensions are identical copies.

3.1 Engine System

3.1.1 Metal Engine Characteristics

The metal engine is a Ricardo Hydra modular single cylinder four stroke engine. The engine modules provide easy access to the block internal components and easy assembly-disassembly. Starting from the engine block at the bottom of the engine assemby, there is the wet cylinder liner which press fits inside the steel jug which attaches at the top of the cylinder block. There is shim plate in between the engine block and the steel jug. The thickness of this shim plate is a critical dimension since the engine cylinder head clearance volume is a direct function of this shim plate height. Finally, the

aluminum cylinder head with dual over head camshafts attaches to the top of the steel jug. This aluminum cylinder head was built and donated by General Motors Research labs. The main characteristics of this GM cylinder head are its pent roof shape with two intake and two exhaust valves, port fuel injection and spark plug hole features. Engine technical specifications are described below in Table 3-1.

Compression Ratio	10.95:1
Bore	86mm (3.39in)
Stroke	94.6mm (3.72in)
Displacement	550cm^3 (33.58in^3)
Clearance Volume	55.18cm^3 (3.06 in^3)
Connecting Rod Length	152.5mm (6.00in)
Intake Valve Open	360 dATDC
Intake Valve Close	540 dATDC
Intake Valve Lift	5.4 mm
Exhaust Valve Open	131 dATDC
Exhaust Valve Close	375 dATDC
Exhaust Valve Lift	8.6 mm

Table 3-1 Metal Engine Technical Specifications

3.1.2 Coolant System

The engine is water cooled using a closed loop system. The loop consists of a coolant pump, immersion heater, coolant reservoir, cooling tower heat exchanger, and an overflow bottle. The coolant fluid is heated to a set point temperature with an immersion heater before it is circulated into the cylinder head and cylinder liner. From the engine, it flows into the reservoir and heat exchanger before going back to the pump. Figure 3-1 shows a detailed schematic of the engine cooling system.

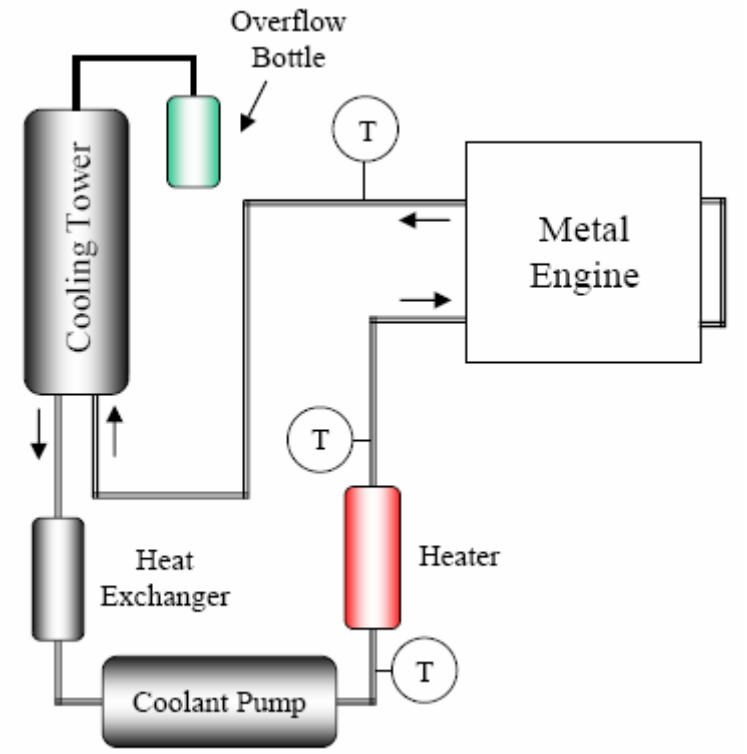

Figure 3-1 Coolant System Schematics

A mixture of 50% distilled water and 50% ethylene glycol is used as the coolant fluid. Prior to running the engine, the coolant fluid is circulated through the engine while being heated to warm up the engine components. This helps the engine achieve steady state conditions faster. During engine operation, the coolant temperature is maintained constant at approximately 95°C by cooling it with city water in a cooling tower heat exchanger. The city water flow is regulated by a solenoid valve which is controlled by an Omega i-series dual output temperature controller. The same controller also regulates the power output of the immersion heater. To monitor the actual coolant temperature at the engine, another thermocouple is installed at the coolant line just after it leaves the engine. During steady state operation, the coolant temperature leaving the engine is always within a range of 93 to 95°C.

The coolant line pressure is regulated using an automotive radiator cap on the reservoir. If the pressure rises above 70 kPa, a relief valve opens to allow coolant flow into the overfill bottle. Once the pressure drops below 70 kPa, the coolant from the overfill bottle is drawn back into the line. All coolant lines are ¾" OD copper tubing except the lines in and out of the engine, which are 5/8" ID silicone hoses.

3.1.3 Lubrication

The closed loop lubrication system consists of a gear pump, oil filter, relief valve, heat exchanger, and an immersion heater. The engine block is equipped with an internal oil gallery that supplies oil to the crankshaft and connecting rod bearings, as well as the camshafts in the cylinder head. The oil supply lines are 3/8" stainless steel tubing and the return lines are ¾" copper tubing. A detailed schematic of the engine lubrication system is shown in Figure 3-2.

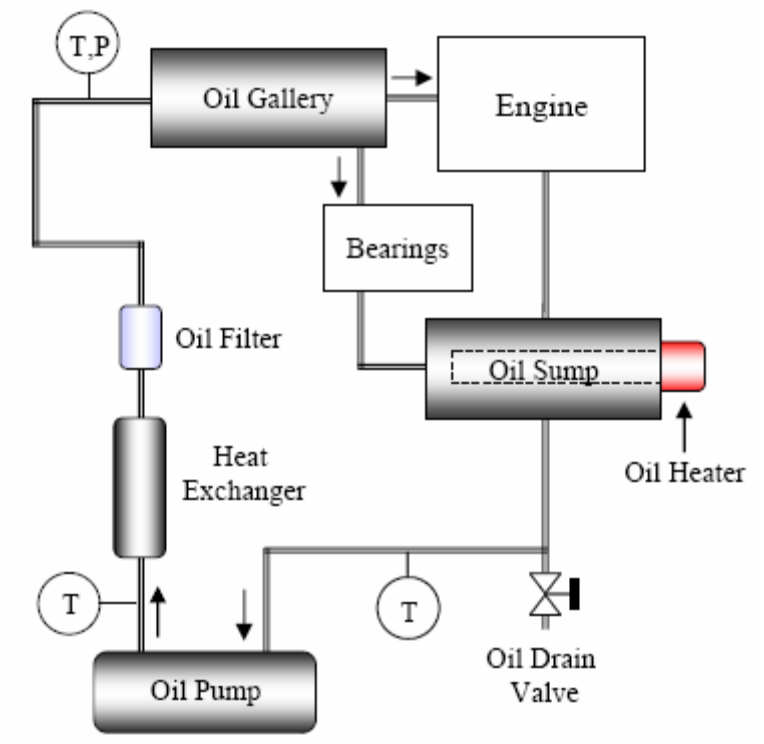

Figure 3-2 Oil System Schematics

To heat the oil to operating temperature, a 1000 W immersion heater is installed in the oil sump. Once the oil reaches the operating temperature of 90°C, the temperature is maintained constant using a heat exchanger in the supply line. Both the water flow to the heat exchanger and immersion heater power are controlled by an Omega i-series dual output temperature controller in the same manner as in the coolant system. The pressure in the oil line is monitored using an Omega PX212 pressure transducer. If the pressure falls below 30 PSIG, the fuel pump and engine ECU power supply will be cut off to prevent engine damage. An adjustable relief valve is installed in the supply line to allow oil flow into the sump when the oil line pressure rises above 40 PSIG.

The oil used in the engine is synthetic 20W-50 engine oil and the oil filter is made by NAPA with part number 21515. The oil level can be checked through a sight glass mounted to the oil sump. To check the oil level, the oil filler cap needs to be removed to release the vacuum in the oil sump. The minimum and maximum oil level is marked in the sight glass. It is important to maintain the oil level within these limits to prevent damage to the immersion heater and the engine.

3.1.4 Dynamometer

The engine is coupled to a General Electric DC double ended dynamometer with a maximum speed rating of 4000 RPM and capable of providing 74.5 kW (100 HP) load to the engine. The dynamometer can spin in either clockwise or counter-clockwise direction. Due to the engine valve train design, the engine can only operate in clockwise direction; therefore only one engine can be coupled to the dynamometer at a time.

The dynamometer is controlled by Dyne Systems Co. DYN-LOC IV digital control system. The torque generated by the engine is measured using an Omega LC101-

2K strain gage load cell which is capable of measuring force up to 8900 N (2000 lbs). Due to the large size of the dynamometer, all brake specific values are close to zero and therefore they will not be considered in this work.

Both the dynamometer shaft and the engine flywheel are equipped with custom metal hubs that allow them to be coupled together using a Falk Wrapflex flexible hard rubber coupling. The hard rubber coupler can be removed easily from the metal hubs to allow switching between standard and optical engine. In addition, the compact design of the coupling minimizes the required distance between the engines and dynamometer, thus allowing both engines to be installed in the available laboratory space.

3.2 Air and Fuel Delivery

The air and fuel delivery systems were designed to accommodate flow to both engines with the capability of shutting off the flow to the non-operating engine. All intake and exhaust system components were designed to handle extremely high temperatures required for HCCI operation. It is also very important to make sure that the air/fuel delivery system is completely sealed from the laboratory environment to prevent any leakage. Air leaks into or out of the system can seriously affect the measurement results and exhaust leaks can be hazardous to the operator. A schematic of air and fuel delivery system can be seen in Figure 3-3.

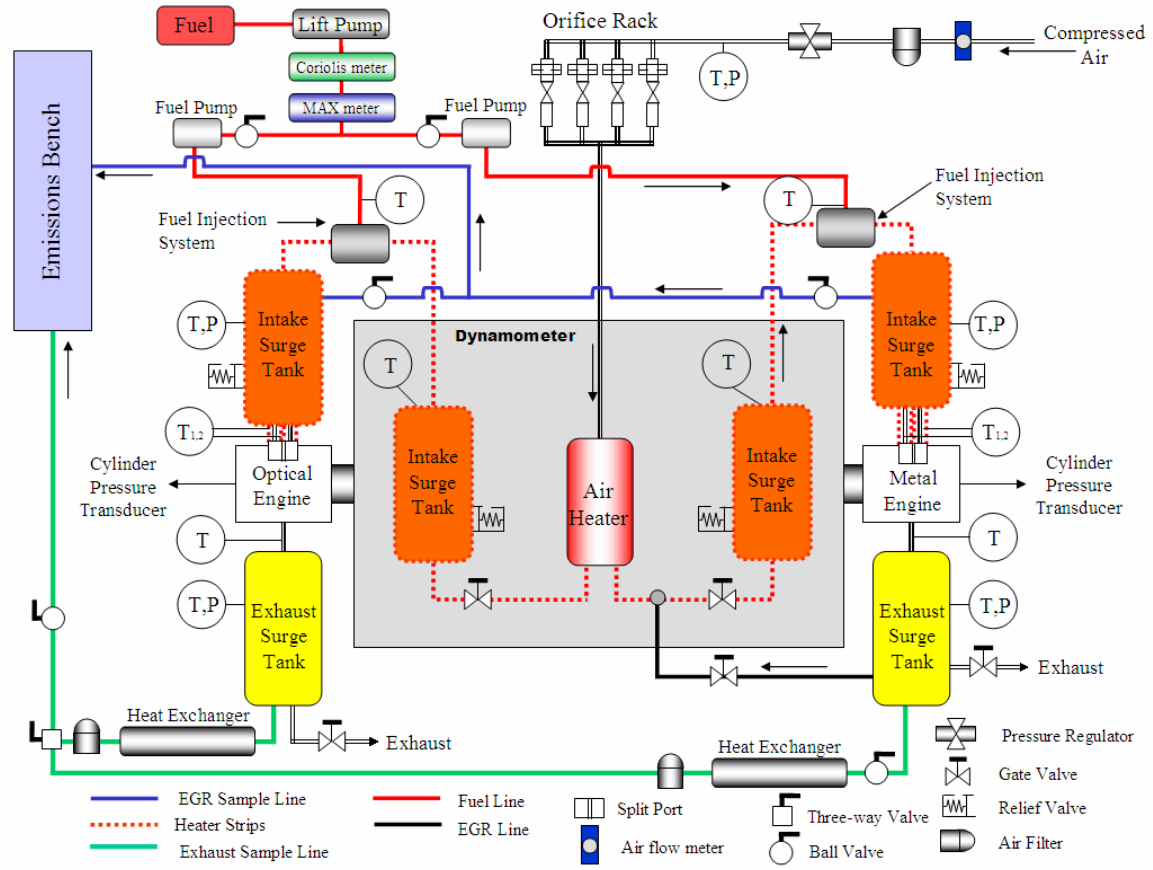

Figure 3-3 Air and Fuel Delivery Schematics – Former Setup

Figure 3-3 shows the former metal engine air, fuel and EGR delivery system setup. The current setup which incorporates a second intake surge tank, dual intake runners, intake port split, and gate valves to handle gas delivery and mixing is shown in Figure 3-4. The current setup shown in Figure 3-4 was also applied for the optical engine in a more simplified manner. Details on critical components of the metal engine schematics shown in Figure 3-4 such as intake runners and intake port split will be explained in subsequent sections. Figure 3-4 can be treated as a zoom-in figure showing details on the air, fuel and EGR delivery system for the metal engine alone.

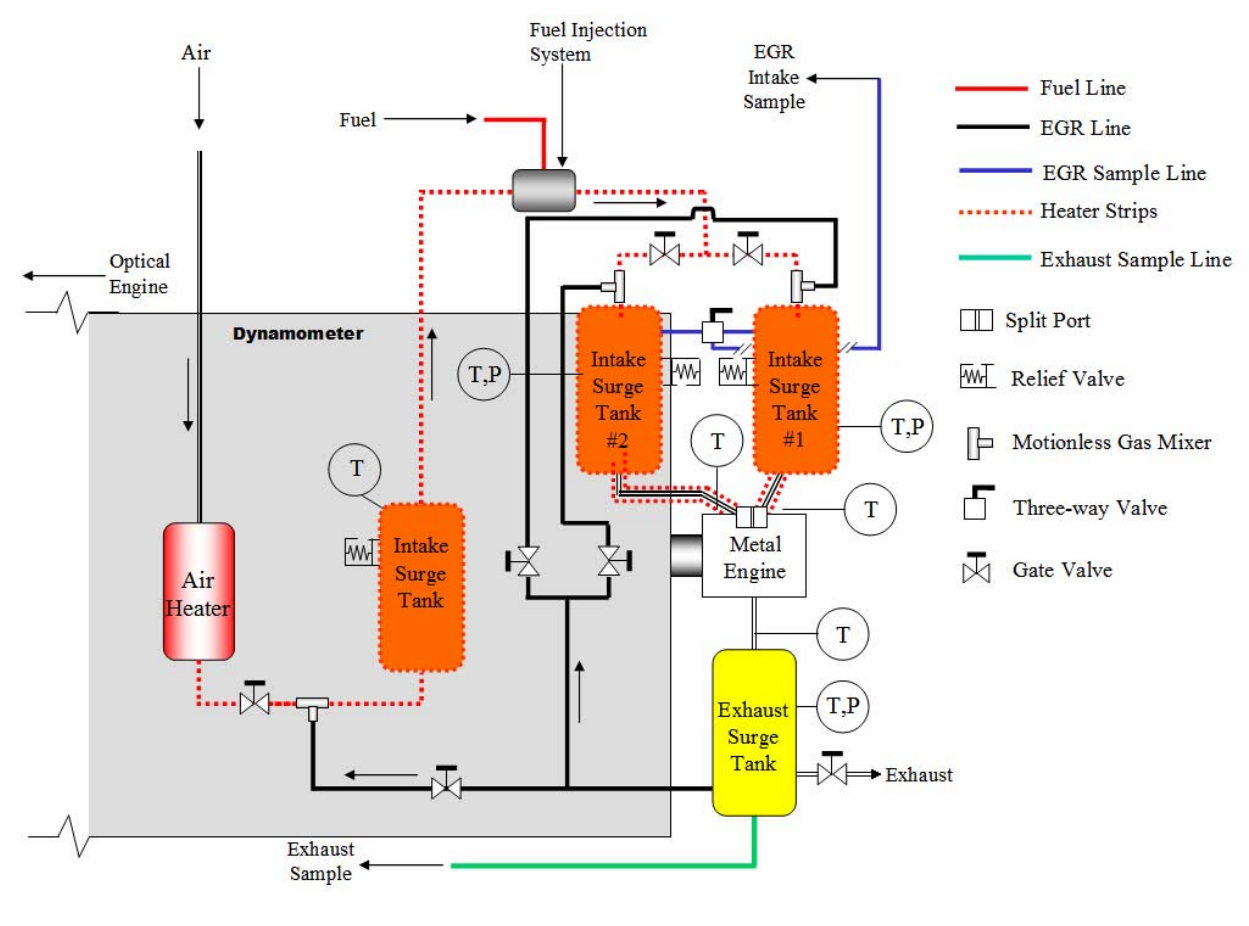

Figure 3-4 Air and Fuel Delivery Schematics – Current Setup

The metal engine schematics shown in Figure 3-3 were used to perform combustion and emissions data analysis for the experimental case of homogeneous air, fuel and EGR intake mixtures. These data established helpful baselines to be compared later against cases run with the current setup shown in Figure 3-4. Since substantial changes were done to the air, fuel and EGR delivery system while upgrading the experimental setup, it was very important to observe the behavior of the engine combustion and emission performance as hardware changes could have modified the fluid mechanics and pressure dynamics aspects of the experiment.

3.2.1 Engine Intake Features

The split port was one of the main and most important engine features that were installed in the cylinder head intake port to allow us to perform thermal and composition charge stratification experiments. These experiments had the particularity of supplying two independent intake charges to the combustion chamber through each of the two intake valves. Therefore, a sort of extended cylinder head septum was fabricated and installed within the cylinder head intake port. This was accomplished by using a $1/16^{th}$ inch aluminum plate which was inserted in the aluminum intake port between the flat bottom of the port and the fuel injector cavity. The top fuel injector cavity added some complexity to the design of this split port. Therefore a cavity plug was built out of aluminum and it was installed to hold the split port plate in place from the top. Figure 3-5 shows detailed schematics of the port split setup installed in the engine intake port.

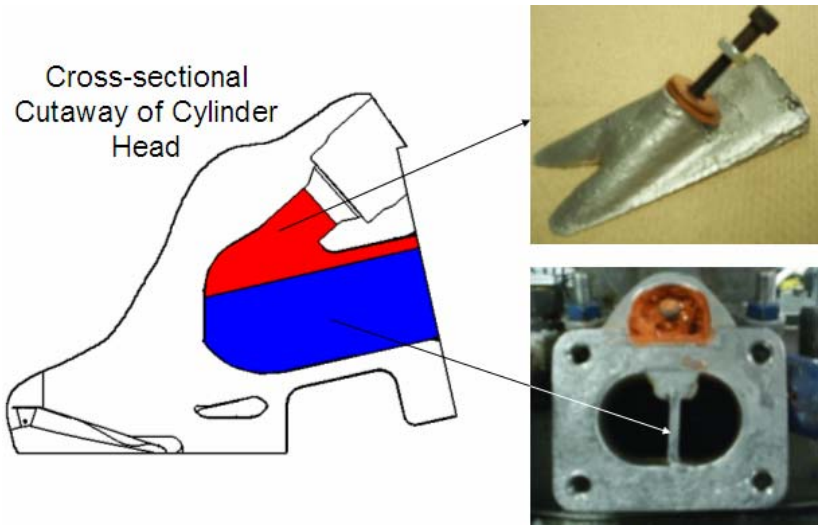

Figure 3-5 Intake Port Split

Two setups of dual intake runners were built out of stainless steel to be used for the purposes of delivering two independent-equal volume charges into the engine. One of the runners consisted of two equal shape and length runners which took equal amounts of air, fuel and EGR charge from a single surge tank to the engine. This setup was used to perform homogeneous charge and thermal stratification experiment baselines. This configuration is shown on the left of Figure 3-6. The second intake dual runner setup had two non symmetric runners. Each of them took approximately equal charge volumes from each of the intake surge tanks into the combustion chamber. This setup was used to perform homogeneous charge, thermal stratification and EGR unmixedness experiment baselines. This configuration is shown on the right of Figure 3-6.

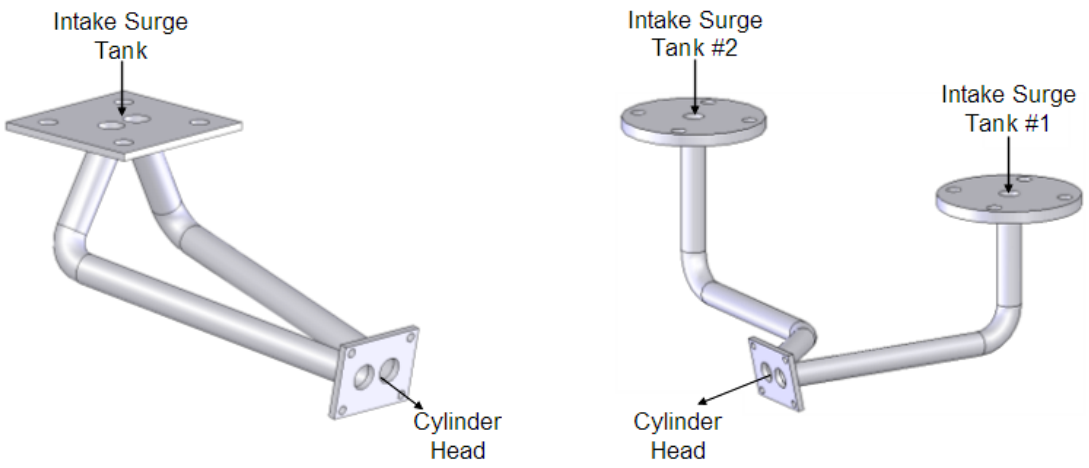

Figure 3-6 Intake Runners Setup

3.2.2 Intake Air

Compressed air at 580 kPa (~85 PSIG) and room temperature 21°C (~70°F) is supplied to the laboratory continuously. The air is filtered prior to entering the intake systems and the flow to the engine is regulated by a pressure regulator and a set of calibrated orifices. There are four orifices installed in the intake system which are selectable depending on the amount of air required. The orifice calibration curves are shown in Figure 3-7.

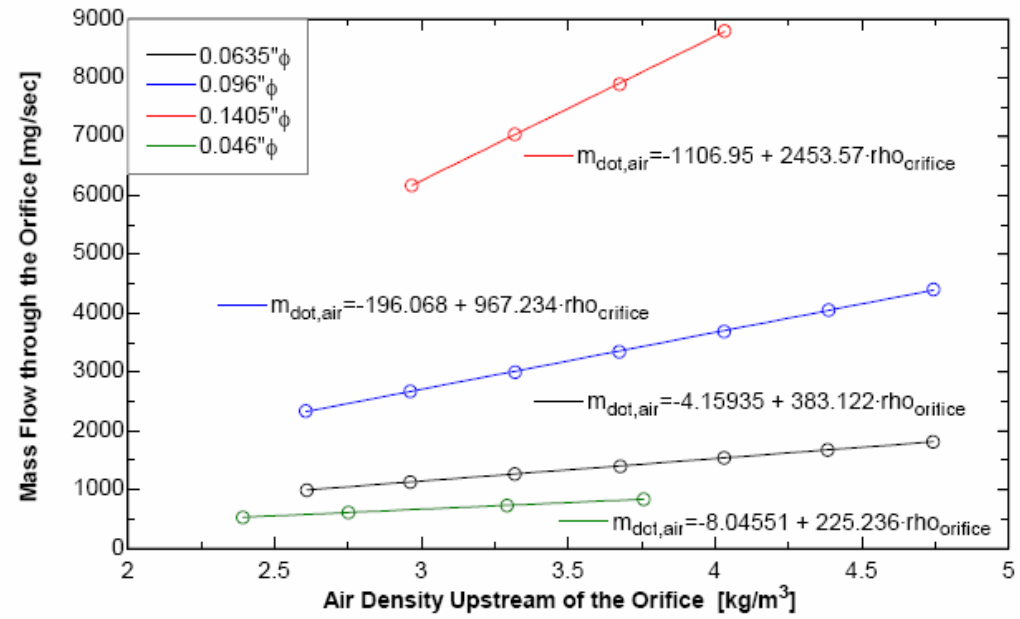

Figure 3-7 Air Orifice Calibration Curves

A Newport Micromega CN77000 controller is used to control the orifice upstream pressure by adjusting the signal to a Parker Pneumatics VIP-F pneumatic control board. This pneumatic control board controls a pneumatic pressure regulator. The Newport controller receives a pressure signal from an Omega PX212 pressure transducer. At steady state conditions, the orifice upstream pressure can be maintained within +/- 1 kPa of the set point.

The pressure and temperature measurement upstream of the orifice are essential for air flow rate calculation. The pressure and temperature were measured using a Dresser DXD combination pressure transducer and thermocouple which has higher accuracy compared to Omega PX212 transducer. Measured temperature values are within +/-0.5°C accuracy, while measured pressure values are within +/-1 kPa accuracy.

From the orifice, fresh air is allowed to flow through an inline heater before entering the first surge tank. When running with premixed fuel injection, fuel is injected into the intake system right after the first surge tank. The air-fuel mixture is allowed to

mix completely in the second surge tank set (dual tanks) prior to entering the engine. The three surge tanks are 37.9 L (10 gal) steel tanks that were installed to damp out the pressure pulses generated during the intake stroke and to facilitate further mixing between fresh air, EGR, and fuel.

For safety reasons, a Kemp FA70-G flame arrestor is installed in the intake system to prevent flame propagation into the first surge tank. A 345 kPa (50 PSI) pop-off valve is installed in each surge tank to release high pressure in the intake system. Another 690 kPa (100 PSI) relief valve is installed in the second surge tank for back-up.

3.2.3 Intake Air Heating

To achieve HCCI combustion with proper phasing, the air-fuel mixture must be preheated to a high temperature prior to entering the cylinder. The fresh air and EGR mixture is initially heated by a Chromolox GCHI 3000 W inline gas heater, which is controlled in an on-off manner with an Omega i-series dual output controller. The main function of this inline heater is to maintain the air in the intake system at a uniform temperature. From the inline gas heater, the mixture flows through heated intake pipes and surge tanks combination. The pipes and tanks were wrapped with heater strips to heat up the mixture to desired temperature. In addition, one heater strip was wrapped around each of the two intake runners to facilitate fine adjustment of the intake charge temperature entering the cylinder. The locations of the heater strips are shown in Figure 3-8.

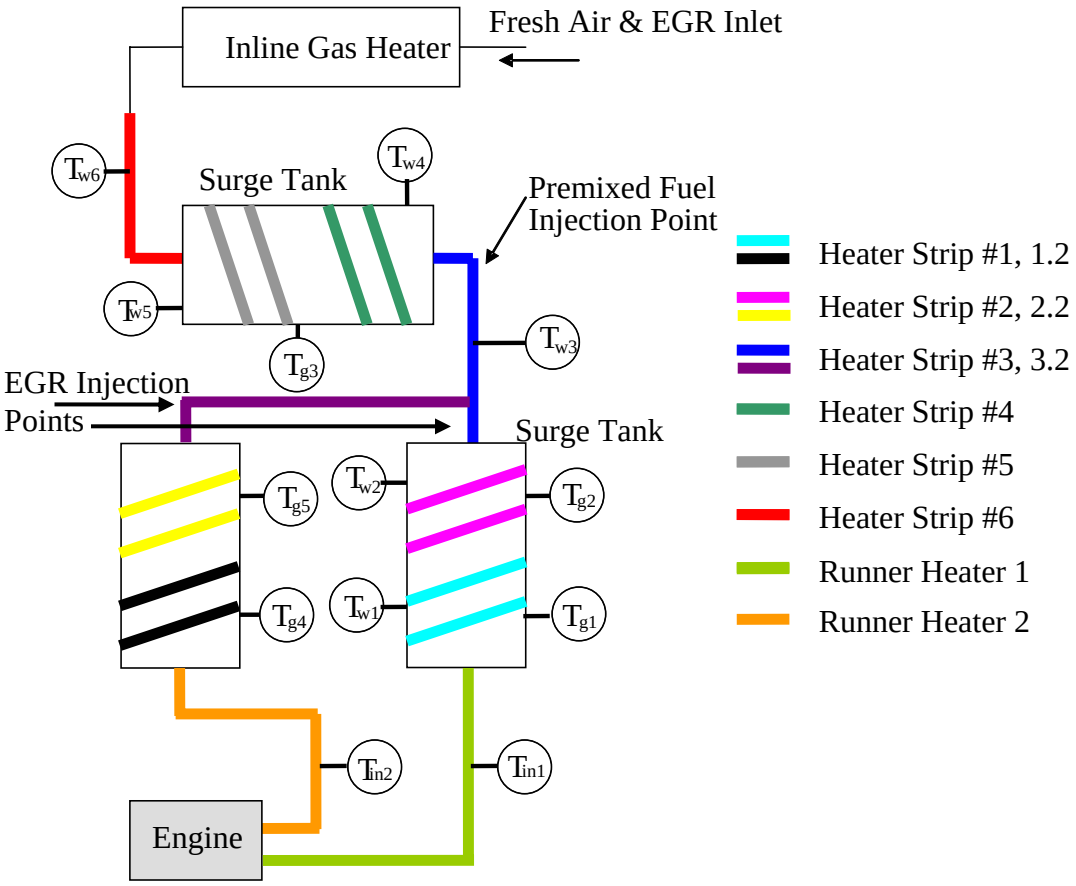

Figure 3-8 Intake Air Heating Diagram

The intake pipes and surge tanks heater strips are controlled by an Omega CN616 controller. The controller adjusts the power to each heater strip independently based on the input signals received from six thermocouples measuring the intake pipes and surge tanks wall temperatures, denoted T_{w1} – T_{w6} in Figure 3-6. The gas temperatures are also measured at three different points along the flow with thermocouples denoted T_{g1} – T_{g6}. The control system is capable of maintaining a close agreement between the actual gas temperature and the average wall temperature.

The intake runner heater strips are controlled by two Omega i-series temperature controllers which receive an input signal from the two thermocouples located in the intake runners approximately 105 mm upstream of the intake valve stems. This methodology of measuring intake charge temperatures in the intake runners was the first approach taken. Nevertheless, an important issue arose when two extra intake charge temperature measurements were taken closer to the intake valves. These extra thermocouples were located 5 mm upstream of the intake valve stems. The temperature readings indicated important differences in temperature between the two intake charges. One intake charge stream underwent more cooling than the other stream while traveling throughout the cylinder head water cooled intake port. The temperature drops experienced in the intake charges, between the original measurement location and the valve stem location were from 60 to 80°C. But more important was the asymmetry found between the intake charge temperatures at the intake valves, which was as large as 15°C. It was noticed that the intake runner with a sharp turn located by the engine cylinder head experienced the largest charge temperature drop. Therefore, the dual intake charges temperature controlling strategy used the temperature readings by the valves as the parameter to control. Figure 3-9 shows schematics of the aluminum engine cylinder head intake port and the four total locations designated for intake charge temperature measurements. Charge intake temperatures measured at the runners was consistent as the measuring charge temperature point across the runner was varied.

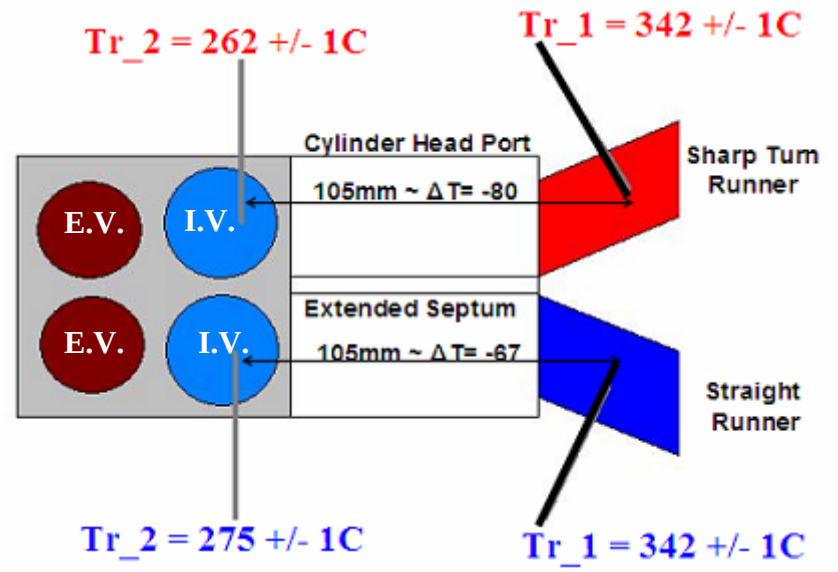

Figure 3-9 Intake Charge Temperature Measurements

By adjusting the power of the intake runner heater strips, the intake charge temperatures leaving the surge tanks can be adjusted 50°C lower or 25°C higher prior to entering the cylinder. The intake heating system control strategy can maintain the two intake charge temperatures within 1.5°C below and 1.5°C above the set point temperature.

3.2.4 Intake Valves Low Profile Cam Lobes

The HCCI combustion heat release rate is modulated with excess of exhaust gas recirculation (EGR), or air or N2 gas. In this particular research engine, a late EVC timing configuration is used to minimze the amount of trapped in-cylinder exhaust gases. Also, an IVO timing at TDC and IVC timing at BDC are applied to avoid any sort of chamber charge back flow to the intake port. These exhaust and intake valves timing configuration ensures that in-cylinder charge composition stratification and premixed charge effects in the intake port are mitigated in experimental cases which use imposed thermal or composition stratification throughout the delivered intake charge. Figure 3-10

shows exhaust and intake valve lift profiles versus engine crank angles. This figure also presents the former intake valve lift profile that was used for previous combustion experiments in this GM engine. It is important to mention that 1-D engine cycle simulation software tools were employed to simulate the changes in intake manifold gauge pressure and pressure wave dynamics that this particular intake valve profile and timing design could have exerted on the engine breathing characteristics. Engine pressure motoring data at constant intake manifold pressure and temperature conditions were compared before and after the engine intake camshaft were swapped. The change in pressure wave dynamics was very small during intake and exhaust strokes, and engine IMAP changes during the intake stroke remained almost unchanged, a drop of 1 - 1.5kPa of IMAP was observed. This was also seen through the engine 1-D cycle simulation results and comparison of cylinder pressure from motoring data.

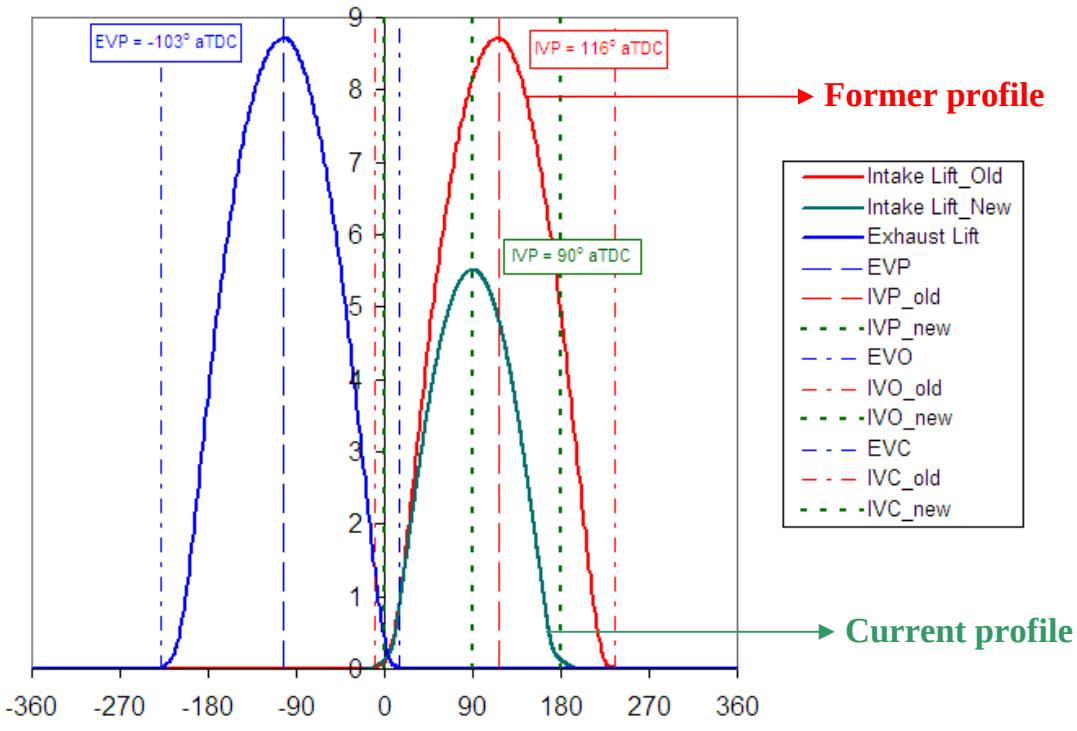

Figure 3-10 Exhaust and Intake Valves Lift Profiles versus Engine Crank Angle

3.2.5 Exhaust Gas

Exhaust gas leaving the engine flows through an exhaust runner to an exhaust diffuser to ensure complete mixing of the exhaust gas components. Part of the exhaust is drawn into the emissions bench, another part flows back into the intake system as EGR, and the rest is drawn by the building exhaust system. A mixing diffuser is installed to ensure that the sample analyzed by the emissions bench is accurate representation of the exhaust gas.

The building exhaust system maintains a constant pressure of 97 kPa absolute (14 PSIA). The pressure can be changed by adjusting the gate valve located in the exhaust line right after the surge tank. For the results presented here, the exhaust pressure was maintained at 97 kPa.

3.2.6 Exhaust Gas Recirculation (EGR)

In HCCI operation, a significant amount of EGR is used to dilute the air-fuel mixture to slow down the combustion reaction rates. Part of the exhaust gas is circulated back into the intake system by means of a positive pressure differential between the engine exhaust and intake surge tank system. The EGR is maintained at temperatures above the water vapor saturation temperature in the exhaust gas stream which is at approximately 1bar of absolute pressure. This ensures that no water condensation would occur inside the steel pipes, otherwise inner pipe surfaces could start oxidizing and delivering ferrous oxide particles into the engine’s chamber. The EGR delivery, as shown in Figure 3-4, is controlled by three gate valves. This setup of valves allows to deliver EGR as a fully intake premixed charge for the homogeneous EGR cases. It also allows

managing the EGR stream in such a way that intake charge composition stratification experiments can be achieved.

The EGR percentage was calculated using equation 3.1. The ambient CO_2 volume fraction is measured in the inlet surge tank prior to running the engine. The volume fraction of CO_2 in the intake and exhaust surge tank is always measured by the Horiba emissions bench CO_2 analyzers.

$$EGR\% = \frac{CO_{2,In} - CO_{2,amb}}{CO_{2,Exh} - CO_{2,amb}} \times 100 \quad (3.1)$$

3.2.7 Premixed Fuel Delivery

The fuel delivery system consists of a low pressure pump, high pressure pump, fuel injector, and air assisted injector. The air assisted injection system, which was designed by Mercury Marine, helps atomizing the fuel as it is injected into the intake system. The atomization process helps the fuel to mix with air more effectively. The low pressure fuel pump sends fuel from the fuel tank to a high pressure pump which supplies the fuel to the injector. Fuel is inducted into a cavity inside the injector before it is injected along with small amount of air into the intake air stream. A schematic of fuel delivery system can be seen in Figure 3-3.

The high pressure fuel pump actually consists of two separate pumps. A medium pressure pump which draws fuel from the float-controlled reservoir and the actual high pressure pump that sends fuel into the injector. The pressurized fuel line pressure is maintained at 90 PSIG (620.5 kPa) with a differential pressure regulator using the injector air pressure as the reference.

The mass flow of air through the air assisted injector was measured using an Omega PMA-A2309 mass flow meter and the value was added to the mass of air flow through the intake system to get the total air flow to the engine.

The low pressure fuel pump is equipped with a return line back to the fuel tank to prevent pressure build up in the fuel line. It is very important to route this return line back into the fuel tank so the fuel is not dumped into the laboratory.

When running the engine with premixed fuel injection, fuel was injected into the intake air stream right after the first surge tank, which is approximately 1.5 meters upstream of the intake valves to ensure formation of homogeneous air-fuel mixture prior to entering the cylinder. The OptiMax air assisted injection system is installed without any modification.

3.2.8 Fuels

The fuel type used in this research work was pure isooctane with an octane number of 100. The properties of the isooctane fuel are listed on Table 3-2.

	Isooctane
Chemical Formula	C_8H_{18}
Chemical Structure	$CH_3C(CH_3)_2CH(CH_3)_2$
Purity	>99%
Molecular Weight	114.23 g/mol
Boiling Point	99.2° C
Lower Heating Value	44.5 MJ/kg
Specific Heat	2.09 kJ/kg-K[a] (1.59 kJ/kg-K)[b]
Auto Ignition Temperature	418° C
Minimum Ignition Energy	27.0 mJ
Octane Number	100

[a] as a liquid at 25° C [b] as a vapor at 25° C

Table 3-2 Fuel properties

3.3 Controls

3.3.1 Engine Operating Controls

The engine operation was controlled by an ECU developed by Mercury Marine for their OptiMax engine. The ECU is suitable for use in the engine because the fuel delivery system also utilizes the OptiMax system. The engine operating parameters such as injection timing and pulse width can be adjusted while the engine is running. All parameters are adjusted from a computer equipped with MotoTune software that interfaces with the ECU. The system is designed to handle eight different injectors and spark signals independently. The knock index analysis software, stratified injection heating chamber, and the CCD camera also receive triggers from the ECU.

3.3.2 Non Engine Controls

Various engine parameters are monitored and controlled continuously to ensure that the operating conditions are repeatable and consistent. Those parameters are displayed at a control panel located in the test cell. The controllers used are Omega I series dual output controllers and Omega CN7700 series controllers. The i-series controllers output are 0-12V proportional DC output and Solid State Relay (SSR) output. The CN7700 controllers have a 4-20 mA proportional output and SSR output. The controllers are wired together in parallel and connected to a computer with RS-485 communication protocol. The data were acquired using LabVIEW data acquisition program. The controlled parameter and its corresponding controller are listed on Table 3-3. In Table 3-3, the parameters recorded by the data acquisition program are marked with an asterisk after the communication ID number.

Parameter	Units	Comm. ID#	Input Type	Output Signal
Oil Pressure	PSI	0040	Pressure Transducer	SSR - Cutout Relay
Stratified Injector Pressure	kPa	0041*	Pressure Transducer	SSR - Injector Power
Orifice Upstream Temperature	C	0042	Thermocouple	NA
Stratified Injector Temp.	C	0001*	Thermocouple	0-12 V DC - Relay
Oil Temperature	C	0002*	Thermocouple	SSR - Heater
				SSR - Solenoid Valve
Coolant Temperature	C	0003*	Thermocouple	SSR - Heater
				SSR - Solenoid Valve
Intake Air Temperature	C	0004*	Thermocouple	SSR - Heater
Exhaust Surge Tank Pressure	kPa	0005	Pressure Transducer	NA
Orifice Upstream Pressure	kPa	0006	Pressure Transducer	4 - 20 mA - Pneumatic Controller
Fuel Temperature	C	0007	Thermocouple	NA
EGR Temperature	C	0008	Thermocouple	SSR - Solenoid Valve
Heated Line #2 Temperature	C	0009	Thermocouple	SSR
Heated Line #1 Temperature	C	0010	Thermocouple	SSR
General Temperature Reading	C	0011	Thermocouple	NA
Engine Coolant Temperature	C	0012*	Thermocouple	NA
Air Assist Injector Flow Rate	SLPM	0013*	Mass Flow Meter	NA
Exhaust Port Temperature	C	0014*	Thermocouple	NA
Intake Surge Tank Pressure	kPa	0015	Pressure Transducer	NA

*Values read and recorded by LabVIEW data acquisition program

Table 3-3 Fixed Experimental Parameters

3.4 Data Acquisition and Analysis

3.4.1 Emissions Analyzer

Exhaust gases from the engine are sampled by a Horiba Instruments emissions analyzer which was donated by General Motors Research.

The emissions analyzer was first calibrated using a Horiba SGR-710C gas divider to ensure accurate exhaust emissions calculation. Considering the age of the instrument, new calibration curves were used instead of the original ones issued by the manufacturer. At the start of each experiment, the analyzers are zeroed and spanned to the calibration value of the reference gas concentration.

This particular emissions bench is a dry type; therefore water must be condensed out of the exhaust gases prior to entering the analyzers. Exhaust gas flows through a heat exchanger immediately after the exhaust surge tank and the water in the exhaust is separated from the flow using a Parker Corp. Balston Division 33G filter. Inside the emissions bench, the exhaust gas also flows through a chiller bath to ensure complete removal of water. It is important to drain the excess water from the emissions bench often to prevent damage to the instrument.

The output from the emission analyzers are sent to a data acquisition computer and displayed real time along with the calculated air/fuel ratio. For data analysis purposes, the emissions values are collected for 1 minute periods and averaged.

3.4.2 Crank Angle Position

The crank angle position is determined by a BEI model H25 optical encoder mounted to the crankshaft. The encoder has a resolution of 720 pulses per revolution, corresponding to one pulse every half degree. The encoder “A” pulse is read by the DSP

system to correlate the pressure signal with the engine volume. In addition, there is a “Z” pulse from the encoder to mark the top dead center location. The encoder top dead center signal is aligned with the crankshaft top dead center position using method described in the paper by Lancaster *et al.* [34].

3.4.3 Cylinder Pressure

The cylinder pressure was measured with a Kistler 6125B quartz pressure transducer. The pressure transducer has a ground insulated design which prevents electrical interference. The measurement range of the transducer is from 0 to 25,000 kPa with an overload pressure of 30,000 kPa. With this particular transducer, thermal shock is not a concern due to the small variation (+/- 2%) in pressure sensitivity over a temperature range of -50 to 350°C. The pressure transducer has a linear response characteristic and the slope of the calibration line is determined with a dead weight pressure tester. In-cylinder pressure measurements were also performed by using a water cooled AVL pressure transducer installed at the cylinder head spark plug hole.

A Kistler 5010B dual mode charge amplifier is used to convert the charge signal from the pressure transducer to a voltage signal which can be read by the data acquisition system. During the experiments, the charge amplifier is operated in “Charge Mode” with a transducer sensitivity of 15.5 pC/MU and a scale of 10 MU/V.

From the charge amplifier, the signal is filtered with an 8 kHz low pass filter. This filtered signal is read by the DSP data acquisition system which consists of a model 4012 TRAQ controller module, an 8 channel 12 bit 100 kHz input module, and an 8 megasamples memory module. The acquired data are analyzed with Redline ACAP v4.0

software which stores engine pressure data as well as calculates other engine parameters such as IMEP, COV of IMEP, and peak pressure.

The pressure signal acquired by the cylinder pressure transducer does not give the actual cylinder pressure values. In order to get the actual cylinder pressure values, the DSP system needs a reference or pegging pressure. The reference pressure is determined by reading the intake surge tank pressure and assigning this value as the actual cylinder pressure when the piston is at BDC of the intake stroke. All other pressure values in the engine cycle can be determined from knowledge of the pegging pressure and calibration line slope.

The number of sequential engine cycles that can be collected is limited by the DSP and computer storage capability. All cylinder pressure data collected in this work were averaged over 500 cycles to minimize cycle-to-cycle variation and obtain good representation of the engine operating conditions.

3.4.4 Lab View Data Acquisition Program

The engine control parameters and exhaust emissions are collected and analyzed by a LabVIEW data acquisition program. The signals were acquired using a National Instruments BNC 2090 16 channel input panel and a National Instruments PCI-6014 data acquisition card. When the program is not recording data, it monitors the engine operating parameters and displays real-time emission values as well as the air-fuel ratio. Every 30 seconds, the program displays averaged values of air flow rate, air-fuel ratio, and fuel flow rate. In addition, every 50 consecutive cycles, the program also displays the averaged ringing index value. In this mode, the program merely displays the values without recording any of them.

In data recording mode, the program reads and averages 30 consecutive readings from the specified Omega controllers as listed in Table 3-4. At the same time, it also averages the exhaust emission data over 1 minute period. After collecting control parameters and emission data, the program collects cylinder pressure data and analyzes the ringing index of 500 consecutive cycles. The average ringing index as well as the standard deviation is recorded and displayed. The procedure for ringing index calculation is detailed in the next section. Finally, the program averages the fuel flow rate data from the Max meter over 5 minutes period. All the values are written into a text file which can be analyzed at a later time. It is important to note that the program does not update any real time displays when it is collecting cylinder pressure and fuel flow data, therefore the operator must pay attention particularly to the engine sounds to ensure that the operating condition does not change significantly during data recording period.

3.4.5 Ringing Index Analysis

Certain operating regimes in HCCI operation are characterized by severe cylinder pressure oscillations, very much like knocking behavior in spark ignition engines. In HCCI, this behavior is called ringing. This behavior generates not only irritating noise; at a certain intensity it can cause mechanical damage to the engine. Due to the possible risk of engine damage, it is very important to monitor the ringing intensity and avoid operating the engine at conditions that produces high intensity of ringing. The ringing intensity is characterized by the ringing index, calculated from the cylinder pressure data.

The ringing index calculation is performed by the LabVIEW data acquisition program. The program collects cylinder pressure data within the interval of 30 deg bTDC to 100 deg aTDC. The voltage signal from the charge amplifier is filtered with a band

pass filter with high and low pass cutoff frequency settings of 6.3 kHz. The signal is multiplied by a factor of 500, and the program looks for a point with largest pressure oscillation. Ringing index is defined as the difference between the highest and lowest voltage values at that point. In data recording mode, the program calculates ringing index from 500 consecutive cycles and displays the average.

In determining the acceptable operating window, the upper limit of ringing index is set at 8 V, which corresponds to a peak-to-peak pressure variation of 16 kPa. If the ringing index rises above 12 V, the data acquisition program displays a warning message to alert the operator of a potential problem.

3.4.6 Fuel Flow Measurement

The fuel flow to the engine can be calculated from the exhaust emission data. However, leakage in the air-fuel delivery system can seriously affect the emission values. To obtain physical measurement of the fuel volumetric flow rate, a Max Machinery Co. model 284 512 flow meter was installed in the fuel line. This flow meter is a positive displacement meter with very small displacement volume to ensure accuracy in small flow rate measurement.

The OptiMax fuel delivery system utilizes a fuel return line and float bowl in the high pressure pump which causes pulsations in the fuel flow. The flow meter always measures positive volume no matter which direction the fuel is flowing, therefore it is necessary to prevent reverse flow through the meter. Check valves were installed in the fuel lines for that purpose. To improve the measurement accuracy, the fuel flow rate data are collected over 5 minutes period and averaged to minimize the effects of pulsating flow. It is also important to make sure that the fuel flow rate calculated from the exhaust

emissions calculation agrees with the flow meter measurement within acceptable error. Significant difference between those two values indicates potential leakage or other problems. The procedure for calculating the air-fuel ratio from the exhaust emissions data is listed in Appendix B.1.

Chapter 4 – Experimental Conditions

4.1 – Experimental Parameters

The HCCI engine experimental parameters can be classified into two groups. The first and second groups define the following parameters respectively: “Fixed or Independent Parameters” and “Variable Parameters”.

4.1.1 – Fixed Parameters

The following experimental parameters were categorized within the “Fixed Parameters” group since they were held constant regardless of the nature of the experiment performed in the engine cell.

Intake Pressure	~97 kPa
Exhaust Pressure	~100 kPa
Coolant Temperature	96°C
Oil Temperature	90°C
Engine Speed	1000 RPM
Engine Fuel	Iso-Octane
Fuel Mass Flow Rate	10mg/cycle
Intake Valves Timing	IVO= 360dATDC, IVC= 540dATDC
Exhaust Valves Timing	EVO= 131dATDC, EVC= 375dATDC

Table 4-1 Fixed Experimental Parameters

Intake and Exhaust Pressure

The values for these two fixed pressure parameters detailed in the table above are approximate. Experiment runs showed that important changes (2-3%) in intake pressures can be perceived within experiments due to the intake charge temperatures and changes in atmospheric air conditions. These changes in intake manifold pressure produced changes in the exhaust manifold pressure, thus resulting in a reasonably constant pressure differential between both manifolds at each experimental condition. This aspect of the

engine is rather important because the positive pressure differential between the exhaust and the intake manifolds is what drives the EGR gases back to the intake system.

Coolant and Oil Temperature

As it has been proved throughout the engine experiment runs, the phasing of HCCI combustion is a strong function of engine intake port and combustion chamber surface temperatures. Therefore, maintaining a constant engine coolant and oil temperature ensured that combustion and emissions performance could be compared between experiments which were able to achieve HCCI combustion at different intake charge temperatures. Nevertheless, heat transfer between the intake charge and intake port surfaces behaved differently due to changes in intake charge temperatures and intake charge compositions. More information regarding the approach that was taken to increase the accuracy of measuring intake charge temperature can be found on Section 3.2.3.

Engine Speed

The engine rotational speed is controlled by a dynamometer. The engine speed is very accurately controlled which makes one aspect of running the engine experiments hassle free. For instance, changes in engine speed would produce oscillation in the intake and exhaust manifold pressures, thus affecting experiments repeatability.

Engine Fuel and Fuel Flow Rate

The fuel chosen for the Gasoline GM HCCI engine experiments was Iso-octane. Characteristics of this specific type of fuel such as a high octane rating (octane number of 100) made it a suitable fuel to be used in our experimental setup. Previous studies have shown that the high intake temperatures used in this research, temperatures above 300°C, can promote partial oxidation of the fuel hydrocarbon molecules with lower octane

ratings, thus affecting the overall combustion and emissions performance [9]. Engine fuel flow rate was held constant at 10 mg/cycle for all the experimental conditions run. Also, a second fueling rate was investigated in the engine to simulate low load conditions such as engine idling conditions. Combustion variability for this lower fueling rate condition (5 mg/cycle) was rather high (from 11 to 4.5 % of COV of IMEP) at the HCCI operating window. This operating window which was identified with high combustion variability would not have provided a reasonable set of data to be able resolve benefits on combustion and emissions performance.

Intake Valves Timing

The intake valve opening and closing timings were held constant through the experiments to ensure that engine breathing characteristics and the pumping work losses associated with it were closely reproduced throughout the span of experiments.

4.1.2 – Variable Parameters

The following table summarizes the parameters which were varied throughout the different engine experiments.

Intake Charge Temperature	240 - 400°C
Air-fuel ratio	20:1 - 38:1
Air Mass Flow Rate	200 - 380 mg/cycle
Diluent Type	EGR and N2
Diluent Percentage	39-42% EGR and 0-45% N2

Table 4-2 Variable Experimental Parameters

The most important parameter varied was the intake charge temperature. This parameter allowed controlling the phasing of HCCI combustion in the engine for each of the experimental conditions within each case of study. The amount of diluent inducted

into the engine underwent changes as the intake charge temperature was varied. Therefore, the amount of diluent was a variable parameter that was measured for each of the experimental cases run. As changes in the intake charge temperature were imposed, changes in the charge density and intake manifold pressure were directly influenced, thus affecting the pressure differential between the exhaust and intake ports. These pressure differential variations between the intake and the exhaust streams determined changes in the delivered diluent amount to the intake system. Therefore, the diluent amount, which was used to maintain a constant intake pressure for each experimental condition, was an intake charge temperature dependent parameter. The diluent amount in percentage by volume of the intake charge was constantly measured for each experimental condition by delivering a sample of intake charge to the Horiba emissions bench and measuring CO2 concentration. Other non-fixed parameters were air-fuel ratio which, was determined by the amount of air delivered to the engine (fuel mass parameter was always maintained constant), and the diluent type. More details on the diluent type and the amount of diluent used will be covered later in this chapter for each of the experimental conditions.

4.1.3 – HCCI Operating Window Definition

The engine operating window can be defined as the range of intake charge temperatures which results in a combustion phasing that spans from a late to an early combustion phasing within an experimental case. Late combustion phasing promoted by locating the intake charge temperature by the low end of the window is characterized by high combustion variability (COV of IMEP) (Reference line #1 in Figure 4-1). However, early combustion phasing (upper operating temperature window limit) is characterized by high engine charge ringing indexes (Reference line #2 in Figure 4-1). The peak of engine

performance output (IMEP) is located at an intake charge temperature window point that tends to approach the high temperature window end (more advance combustion timing) (Reference line #3 in Figure 4-1). Therefore, the lower temperature limit was chosen to the criterion used by General Motors in determining engine drivability. At COV greater than 3%, cycle to cycle combustion and emissions performance variations start experiencing considerable data variability, thus taking the combustion experiments to a zone where judgments on combustion and emissions data is difficult to perform.

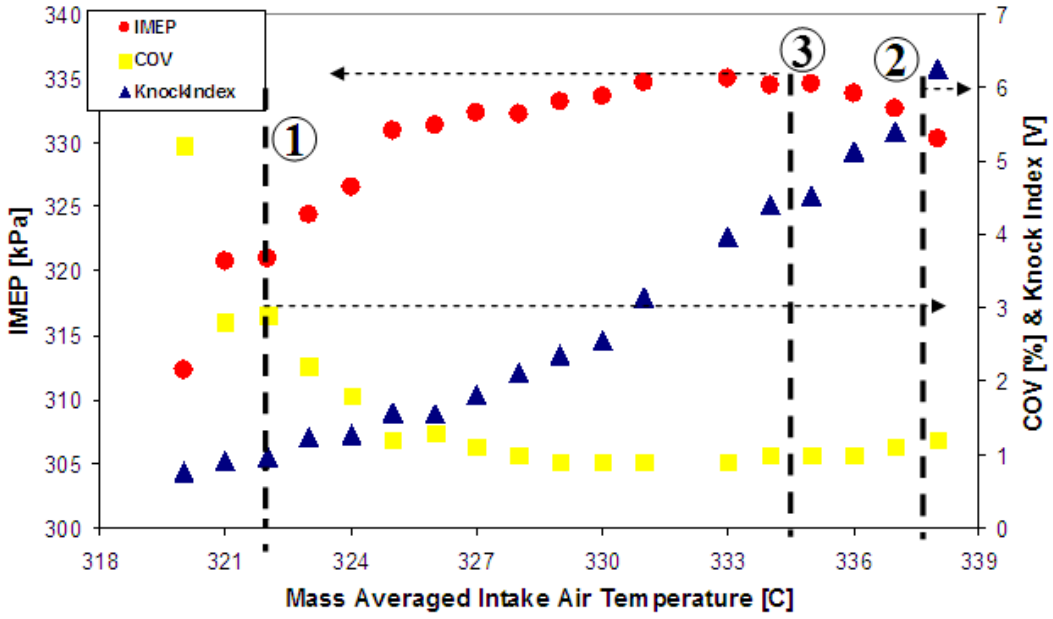

Figure 4-1 HCCI Operating Temperature Window – Homogeneous Intake Charge – A/F=20:1

The upper limit of ringing index was defined from previous experience by running the engine and analyzing the local short-duration and high frequency pressure rises during the combustion heat release event. The cutoff value of 8.0 V was defined as the maximum ringing index at which the engine can be operated safely. Issues associated with engine oil degrading due to high temperatures of the intake charge, made us have the

ringing index cutoff value below 6 - 6.5 V for all of the experiments described in this thesis.

4.2 – Experimental Matrices – EGR Diluent

The first set of experimental matrices was established to observe engine combustion and emissions performance while running the experiments with EGR as diluent. Each of the experimental matrices was run throughout the full span of intake charge temperatures, hence establishing their own operating window and enabling us to analyze combustion and emissions data for each running point as characterized by a specific combustion phasing. Each of these three experimental matrices is identified by its own intake charge handling strategy. The operating conditions for each of these experimental matrices are presented below.

4.2.1 – Matrix #1 – Homogeneous Intake Charge

This experimental matrix data set was obtained while providing to the engine an intake charge composed of fuel, air and EGR diluent uniformly mixed. Fuel injection was performed far upstream of the engine intake port to ensure enough time for mixing of the fuel, air and EGR mixture in the intake surge tank. Also, the diluent was injected into the intake system through a series of motionless mixing tees that were designed to enhance mixing between the air-fuel and the EGR streams. Intake charge composition uniformity was as important as maintaining a temperature uniformity throughout the two intake charges. Combustion and emissions performance were investigated for each of the intake charge temperature points that were run to establish the HCCI operating window.

Window Temperature Range	Variable
Delivered Air-fuel Ratio	20:1
Fuel Mass Flow Rate	10mg/cycle
Air Mass Flow Rate	200mg/cycle
Diluent Type	EGR
Mean Diluent Percentage	40%
Diluent Mixing	Homogeneous
Charge Temperature Difference	0°C

Table 4-3 Homogeneous Intake Charge Experimental Parameters

4.2.2 – Matrix #2 – Temperature Stratification

This experimental matrix data set was obtained while providing to the engine, as well as in Matrix #1, a homogeneous intake charge composed of fuel, air and EGR diluent. This is a homogeneous intake charge which does not present any composition gradients. Nevertheless, thermal gradients were imposed throughout the intake charge by splitting equal volumes of intake charge from a single intake surge tank into two independent intake runners. Each intake runner was wrapped with heating tapes which allowed controlling each runner surface temperature independently, and hence controlling the intake charge temperature very precisely to fractions of degree centigrade. The temperature control for these two intake charges was accomplished by an electronic controller which modulated the electric power delivered to the heating strips until the temperature target for each charge was achieved. Temperature of the intake charges was measured by thermocouples located as closed as possible to the engine combustion chamber. The maximum temperature difference obtained between intake charge streams was of 80°C at the entrance of the aluminum engine cylinder head. Heat losses in the intake port resulted in temperature drops from 60 to 90°C through both intake charges. These were observed while measuring intake charge temperatures before entering the cylinder head port and after the intake port farther inside the head where the intake charge temperature was measured right in front of the intake valve stems. This heat losses

effect brought down the temperature difference to 30°C. Mass average temperatures were calculated by taking into account the temperature of the less hot and hot intake charges. Combustion and emissions performance was investigated for each of the mass average intake charge temperature points that were run to establish the HCCI operating window.

Window Temperature Range	Variable
Delivered Air-fuel Ratio	20:1
Fuel Mass Flow Rate	10mg/cycle
Air Mass Flow Rate	200mg/cycle
Diluent Type	EGR
Mean Diluent Percentage	40%
Diluent Mixing	Homogeneous
Charge Temperature Difference	30°C

Table 4-4 Temperature Stratification Intake Charge Experimental Parameters

4.2.3 – Matrix #3 – Diluent Stratification

This data set was obtained while providing to the engine two sorts of intake charges. One intake charge was composed of a homogeneous mixture of air and fuel at the delivered air-fuel ratio, and a second intake charge composed mainly of EGR. The second intake surge tank, which held mainly EGR (up to 80% of the intake surge tank was occupied by EGR), had also the remainder of the homogeneous mixture of air and fuel at the delivered air-fuel ratio. The average amount of EGR volume throughout one set of experimental conditions was about 40% of the total intake charge volume. This amount of EGR was the required to balance out the intake system pressure to ~1bar at a fixed engine speed of 1000 RPM. Symmetric intake surge tanks and runners system were built to facilitate the stratification of the homogeneous mixture of air and fuel, and the EGR charge. At this time, no thermal gradients were imposed throughout the intake charge. Again, each intake runner was wrapped with heating tapes for controlling each runner surface temperature independently, and hence controlling the intake charge temperature. Combustion and emissions performance was investigated for each of the

mass average intake charge temperature points that were run to establish the HCCI operating window.

Window Temperature Range	Variable
Delivered Air-fuel Ratio	20:1
Fuel Mass Flow Rate	10mg/cycle
Air Mass Flow Rate	200mg/cycle
Diluent Type	EGR
Mean Diluent Percentage	40%
Diluent Mixing	Stratified
Charge Temperature Difference	0°C

Table 4-5 Diluent Stratification Intake Charge Experimental Parameters

4.3 – Experimental Matrices – N2 Diluent

This second set of experimental matrices was established to observe engine combustion and emissions performance while running the experiments with N2 as diluent. Each of the experimental matrices was run throughout the full span of intake charge temperatures, hence establishing their own operating window and enabling us to analyze combustion and emissions data for each running point as characterized by a specific combustion phasing. Each of these three experimental matrices is identified by its own intake charge handling strategy. The operating conditions for each of these experimental matrices are presented below.

4.3.1 – Matrix #1 – Homogeneous Intake Charge

This experimental matrix data set was obtained while providing to the engine an intake charge composed of fuel, air and N2 diluent uniformly mixed. The location of fuel and N2 diluent injections were the same as those for the cases described in the first set of experimental matrices. These set of experiments included two extra variable parameters. These variable parameters were the delivered air-fuel ratio and the amount of N2 diluent which is a function of the amount of air delivered into the engine. The first case was

established by delivering a homogeneous air, fuel and N2 mixture with an air-fuel ratio of 20:1. Further cases provided homogeneous intake charges but with an increase in the amount of delivered air, thus providing leaner air-fuel mixtures until the amount of air delivered was large enough to balance the engine IMAP to ~97kPa, and no N2 diluent was required. Therefore, the first case with an air-fuel ratio of 20:1 resulted with the maximum amount of N2 diluent (45% of the total intake charge volume). The second case, in particular, with an air-fuel ratio of 24:1 would imitate the trapped air-fuel ratio conditions of the homogeneous charge EGR diluted case. Chapter 5 will explain with more detail the experimental approaches used to target certain delivered air-fuel ratios within the N2 gas diluent cases. Combustion and emissions performance were investigated for each of the intake charge temperature points that were run to establish the HCCI operating window.

Window Temperature Range	Variable
Air-fuel ratio	20:1, 24:1, 28:1, 38:1
Fuel Mass Flow Rate	10mg/cycle
Air Mass Flow Rate	200, 240, 280, 380 mg/cycle
Diluent Type	N2
Mean Diluent Percentage	45, 35, 25 and 0%
Diluent Mixing	Homogeneous
Charge Temperature Difference	0°C

Table 4-6 Homogeneous Intake Charge Experimental Parameters

4.3.2 – Matrix #2 – Diluent Stratification

This data set was obtained while providing to the engine two sorts of intake charges. One intake charge was composed of a homogeneous mixture of air and fuel at the delivered air-fuel ratio, and a second intake charge composed mainly of N2. The same approach as that used for the EGR diluent stratification was applied in this case of N2 diluent stratification to control intake charge temperatures and avoid any temperature differences between charges, and meet the IMAP requirement. Combustion and

emissions performance were investigated for each of the mass average intake charge temperature points that were run to establish the HCCI operating window.

Window Temperature Range	Variable
Air-fuel ratio	20:1, 24:1, 28:1, 38:1
Fuel Mass Flow Rate	10mg/cycle
Air Mass Flow Rate	200, 240, 280, 380 mg/cycle
Diluent Type	N2
Mean Diluent Percentage	45, 35, 25 and 0%
Diluent Mixing	Stratified
Charge Temperature Difference	0°C

Table 4-7 Diluent Stratification Intake Charge Experimental Parameters

The remaining volume in the N2 diluted intake surge tank was occupied by a homogeneous mixture of air and fuel at the delivered air-fuel ratio. This remainder of the homogeneous air and fuel mixture was used to balance out the intake system pressure. As the cases progressed, the amount of N2 diluent in the N2 diluted intake surge tank decreased. Thus, the last case which ran with a homogeneous air and fuel mixture had a delivered air-fuel ratio of 38:1, which had zero N2 gas as diluent. This made this last case a homogeneous air and fuel intake charge like experiment at a homogeneous air-fuel ratio of 38:1with equal volumes of air and fuel in each intake surge tank. This case was used to experimentally investigate what would be the required amount of air delivered into the engine to avoid any requirements of N2 diluent in the intake and still run the engine fully unthrottled (~1bar of IMAP).

4.4 – Multiple Intake Charge Effects within Diluent Stratification

The research work performed has shown that combined effects are present within the more general composition or diluent EGR and N2 gas stratification effects. Therefore, a series of experimental cases have been run to aid in distinguishing the engine combustion and emission characteristics for each of these combined effects.

The list of individual effects are detailed as follows; local air fuel ratio effects, thermal charge gradient effects caused by differences in charge specific heat ratios, diluent stratification and fuel number density effects.

Therefore, the following experimental matrices were designed to run series of experiments to aid in the understanding of how each of this intake charge stratification effect individually affect auto-ignition combustion characteristics and combustion emissions.

4.4.1 – Matrix #1 – N2 Diluent Homogeneous Intake Charge – A/F Effect

To isolate the effect of air-fuel ratio on a homogeneous intake charge mixture's combustion characteristics, experiments with varying amounts of total intake air and N2 gas diluent were established to provide air-fuel conditions that spanned from more lean-zero N2 gas diluent at an air-fuel ratio of 38:1 to less lean-45% of N2 gas diluent at an air-fuel ratio which matched the trapped air-fuel ratio conditions establishes for the EGR diluted cases (with a delivered air-fuel of 20:1). The varying amounts of air in the intake, at constant fueling rate conditions imposed changes in the engine IMAP, therefore for each specific air-fuel ratio case only the N2 gas diluent amount that would allow the engine to be unthrottled was used. Differences in the resultant homogeneous charge specific heat ratios were negligible, N2 gas and air specific heat ratios are almost identical.

Window Temperature Range	Variable
Air-fuel ratio	20:1, 24:1, 28:1, 38:1
Fuel Mass Flow Rate	10mg/cycle
Air Mass Flow Rate	200, 240, 280, 380 mg/cycle
Diluent Type	N2
Mean Diluent Percentage	45, 35, 25 and 0%
Diluent Mixing	Homogeneous
Charge Temperature Difference	0°C

Table 4-8 Air-Fuel Ratio Effect on Intake Charge - Experimental Parameters

Air-fuel ratio, air mass flow rate and mean diluent percentage values in Table 4-8 are shown in the order they were applied in the engine experiments.

4.4.2 – Matrix #2 – EGR and N2 Diluents Homogeneous Intake Charge – Gamma Effect

Isolating the effect of homogeneous mixtures specific heat ratios required running a N2 gas diluent case with an air-fuel ratio which would match the EGR diluent trapped air-fuel ratio. The calculation of the trapped air-fuel ratio for the EGR diluent case took into account the intake re-introduced oxygen. This trapped air-fuel ratio for the EGR diluent case was approximately equal to 24:1. Therefore, the chosen air-fuel ratio for the N2 gas diluent case was 24:1, which implied an increase of the amount of air supplied into the engine and a reduction on the required N2 gas diluent. This trapped air-fuel ratio calculations made possbile to compare combustion and emission performance of two homogeneous intake charge cases with equal trapped air-fuel ratios and different specific heat ratio characteristics. Respective performed calculations to estimate trapped and local air-fuel ratio is presented in Appendix B.2.

Window Temperature Range	Variable
Air-fuel ratio "delivered"	20:1 (EGR), 24:1 (N2)
Air-fuel ratio "trapped"	24:1
Fuel Mass Flow Rate	10mg/cycle
Air Mass Flow Rate	200 (EGR), 240 (N2) mg/cycle
Diluent Type	N2 and EGR
Mean Diluent Percentage	40% (EGR), 35% (N2)
Diluent Mixing	Homogeneous
Charge Temperature Difference	0°C

Table 4-9 Gamma Effect on Intake Charge - Experimental Parameters

4.4.3 – Matrix #3 – EGR and N2 Diluents Homogeneous Intake Charge – A/F and Gamma Effects

Matrix #3 shows experimental parameters for two cases, one with EGR gas diluent and the second with N2 gas diluent. This time, the conditions of equal delivered air-fuel ratios was applied, therefore the influences of two combined effects on combustion and emissions were studied.

Window Temperature Range	Variable
Air-fuel ratio "delivered"	20:1
Air-fuel ratio "trapped"	24:1 (EGR), 20:1 (N2)
Fuel Mass Flow Rate	10mg/cycle
Air Mass Flow Rate	200 mg/cycle
Diluent Type	N2 and EGR
Mean Diluent Percentage	40% (EGR), 45% (N2)
Diluent Mixing	Homogeneous
Charge Temperature Difference	0°C

Table 4-10 Air-Fuel Ratio and Gamma Effects on Intake Charge - Experimental Parameters

4.4.4 – Matrix #4 – N2 Diluent Charge Stratification – Multiple Effects

Matrix #4 presents the experimental parameters chosen for three N2 gas diluent cases with increasing air-fuel ratios. The specifics of this N2 gas diluent stratified cases is that as the air-fuel ratio increases, less N2 gas is supplied into the engine, therefore causing mitigation of the effect of diluent charge stratification. This is due to the fact that the volume that used to be occupied by N2 gas diluent, now is taken by a homogeneous mixture of air and fuel at the delivered air-fuel ratio. The decreasing amount of N2 gas in

the diluted surge tank reduced the offset of air-fuel ratio and mixture specific heat ratio between the two intake mixtures coming from separate intake surge tanks. Combined effects imposed by diluent stratification such as local air fuel ratio effects, thermal charge gradient effects caused by differences in charge specific heat ratios, diluent stratification and fuel number density are all interconnected to affect combustion and emission performance. We expected that the effects of diluent stratification would be more noticeable at the less lean air-fuel ratio conditions. This observation takes into account the fact that less lean air-fuel ratio conditions do impose higher fuel number and diluent number density, and larger mixture gamma differences throughout the combustion chamber.

Window Temperature Range	Variable
Air-fuel ratio "delivered"	20:1, 24:1, 28:1
Air-fuel ratio "trapped"	20:1, 24:1, 28:1
Fuel Mass Flow Rate	10mg/cycle
Air Mass Flow Rate	200, 240, 280 mg/cycle
Diluent Type	N2
Mean Diluent Percentage	45, 35, 25 %
Diluent Mixing	Stratified
Charge Temperature Difference	0°C

Table 4-11 N2 Diluent Stratification Effects on Intake Charge - Experimental Parameters

4.4.5 – Matrix #5 – EGR Diluent Charge Stratification – Multiple Effects

Similarly as in Matrix #4, EGR diluent stratification effects are the result of a set of combined effects. These effects are listed as follows: local air fuel ratio effects, thermal charge gradient effects caused by differences in charge specific heat ratios, diluent stratification and fuel number density stratification.

Window Temperature Range	Variable
Air-fuel ratio "delivered"	20:1
Air-fuel ratio "trapped"	24:1
Fuel Mass Flow Rate	10mg/cycle
Air Mass Flow Rate	200mg/cycle
Diluent Type	EGR
Mean Diluent Percentage	40%
Diluent Mixing	Stratified
Charge Temperature Difference	0°C

Table 4-12 EGR Diluent Stratification Effects on Intake Charge - Experimental Parameters

The following thesis chapter, Chapter 5, will present the experimental results and several discussion points for each of the experimental matrices described through out Chapter 4.

Chapter 5 - Experimental Results and Discussion

In this chapter, combustion and emission performance results for the three intake charge handling strategies; homogeneous charge, thermal charge unmixedness and diluent charge unmixedness are presented for the EGR diluted cases. Also, results for the homogeneous and diluent unmixedness intake charge handling strategies are presented as for the N2 diluted cases. Further in the chapter, important discussion points were drawn from comparing cases of the different diluents and different intake charge handling strategies. The purpose of these experimental data comparisons was to try to isolate implicitly imposed effects by EGR and N2 gas diluent stratification throughout the intake charge. These effects have shown considerable influence on the combustion phasing and on the HCCI operating temperature window at different running conditions.

The resulting comparisons between cases are performed by arranging data plots of engine combustion and emissions data outputs mainly as a function of:

- Mass Average Intake Air Temperature

- CA50 Combustion Phasing

Some other data arrangements have been established to compare combustion and emission performance data against CA 90-10 burn duration angle. These cases of data comparison were of particular interest to aid the understanding of the benefits of EGR diluent charge stratification on combustion performance.

The first two sections of this chapter will explain the approach that was taken to define the accuracy and repeatability of the mass average intake charge temperature and CA50 variables throughout the different experimental cases.

Further sections will present the combustion and emissions results for each of the experimental matrices shown in Chapter 4. Furthermore, the final section of this chapter gathers results from cases belonging to different experimental matrices for the purpose of isolating and hence explaining the different effects that were found to be very important on influencing the HCCI combustion phenomenon.

5.1 – Intake Charge Temperature

As it was shown on Section 3.2.3, intake charge temperature has been measured at four different places, two of them within the intake manifold and two within the cylinder head intake port. The intake charge temperature measurements were taken approximately at 11 cm away from the engine intake valve stems, or in other words were measured by the end of the intake runners right before the cylinder head intake port. These are the intake charge temperature data that were used to analyze and report combustion and emission data between the different cases investigated. The other two temperature measurements were performed approximately 5 mm away from the intake valve stems inside the intake port. This location, closer to the combustion chamber, brought the benefit of much more accurate charge temperature control for each of the experiments.

Experimental data showed that the heat losses experienced by the two intake charges traveling through both of the cylinder head half ports resulted in temperature drops of 60-90°C. The largest temperature drop was observed to occur in the intake runner that holds the 70 degrees bend upstream of the intake port. Therefore, for accurate control of the true intake temperature, it was important to monitor and control the temperature at the location closer to the combustion chamber. Thus, more accurate temperature measurements of the delivered charge streams were able to be achieved.

Figure 5-1 shows intake charge temperature readings for the EGR diluted homogeneous and EGR diluted unmixed cases at an air-fuel ratio of 20:1. It is shown in Figure 5-1 that four temperatures could be defined for each running condition within an experimental case. These four measured temperatures, two at the intake port and the others two at intake runners, collapse into one single calculated mass average intake charge temperature (i.e. Homog.EGR20d_R#12_Tavg plot linear fit line). For instance, if the homogeneous charge with EGR diluent case (Homog.EGR20d_R#1 and Homog.EGR20d_R#2 to calculate Homog.EGR20d_R#12_Tavg) is chosen for explanation matters out of Figure 5-1, two temperature measurements determine a single point in the plot. Thus, each plotted point corresponds to a specific intake charge runner temperature and a specific intake charge valve stem temperature (single runner and the respective single intake port half). Therefore, and just as an example, Homog.EGR20d_R#1 reference stands for a point which coordinates are a valve stem temperature as the x-axis coordinate and a runner temperature as the y-axis coordinate. This reference also states that the mixture of air, fuel and EGR diluent is homogeneous and that the delivered air-fuel ratio is 20:1. R#1 means that this set of two temperature readings were taken from one runner and the respective intake port half, while the second set of two charge temperatures were taken from the second runner (R#2), always for a single fixed running condition. Besides these four temperature readings, there was a final temperature value calculated from the charge temperatures measured at the intake runners. This temperature calculation was performed for each experimental point to obtain the mass average intake charge temperature. This mass average temperature was used to compare and record combustion and emission data throughout the series of

experimental cases that were run. Figure 5-1 also shows a trend on the measured charge temperatures as the composition of each charge changes. Composition in the runners changes as the experiments go from homogeneous air, fuel and diluent mixtures conditions to stratified composition charge conditions. For instance, the higher temperature curve fit (blue solid triangle symbols) shows the temperature of the intake charge stream with more EGR diluent (stratified EGR case ~ Unmixed.EGR20d_R#1). This charge runner temperature versus charge valve stem temperature curve holds a 10°C higher runner temperature than for a homogeneous mixture of air, fuel and uniformly distributed EGR (Homog.EGR20d_R#1) and almost 40°C higher runner temperature than its counter stream charge composed of a homogeneous mixture of just air and fuel (Unmixed.EGR20d_R#2). As shown on the Figure 5-1, it can be concluded that intake port heat losses are significant, causing a detrimental effect on the control of intake charge temperatures. Nevertheless, as different intake charge handling strategies are run, EGR diluted homogeneous and unmixed, and different runner and valve stem temperatures are needed for a fixed and equal intake mass average temperature, the calculated intake runners mass average intake charge temperature seems to collapse consistently throughout the different experimental cases (comparing Homog.EGR20d_R#12_Tavg and Unmixed.EGR20d_R#12_Tavg linear curve fits in Figure 5-1).

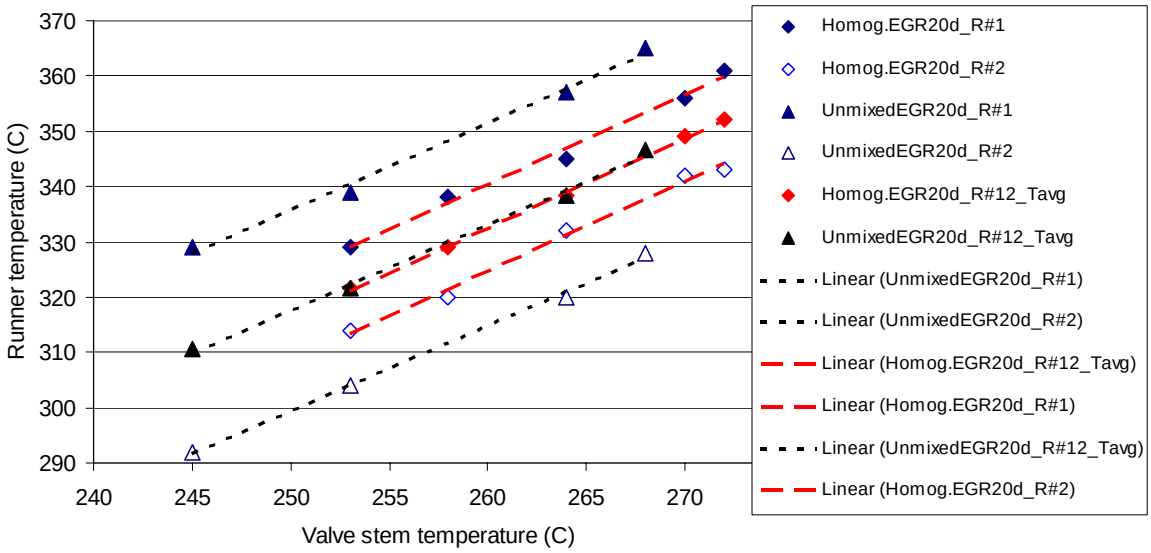

Figure 5-1 Intake Charge Runner versus Intake Charge Valve Stem Temperatures

As a summary, it can be stated that for each experimental condition, there were two temperature measurements for each of the two intake charge streams. In the case of the homogeneous composition and intake temperature, and diluent stratification matrices, the final recorded temperature of the charge was the calculated mass average temperature from the two intake charge temperature readings measured at the intake runners.

Similarly, there were two temperature measurements for each of the two intake charge streams for the temperature stratification cases. The target intake charge temperatures were the ones controlled at the valve stem locations; meanwhile the mass average intake charge temperature was calculated from the two temperature readings at the intake runners. Figure 5-2 shows runner temperature versus valve stem temperature points for a span of mass average intake runner temperatures from 319°C to 340°C (shown by Homog.EGR20d_R#12_Tavg plot points in red). These data conditions correspond to a stratified temperature homogeneous air, fuel and EGR diluent mixture experimental case with a fixed air-fuel ratio of 20:1. Also, Figure 5-2 shows the

maximum achievable intake charge temperature difference between intake charges at the valve stem location throughout the full temperature operating window (319°C to 340°C). This maximum achievable temperature difference was 30°C for a fixed mass average intake charge temperature.

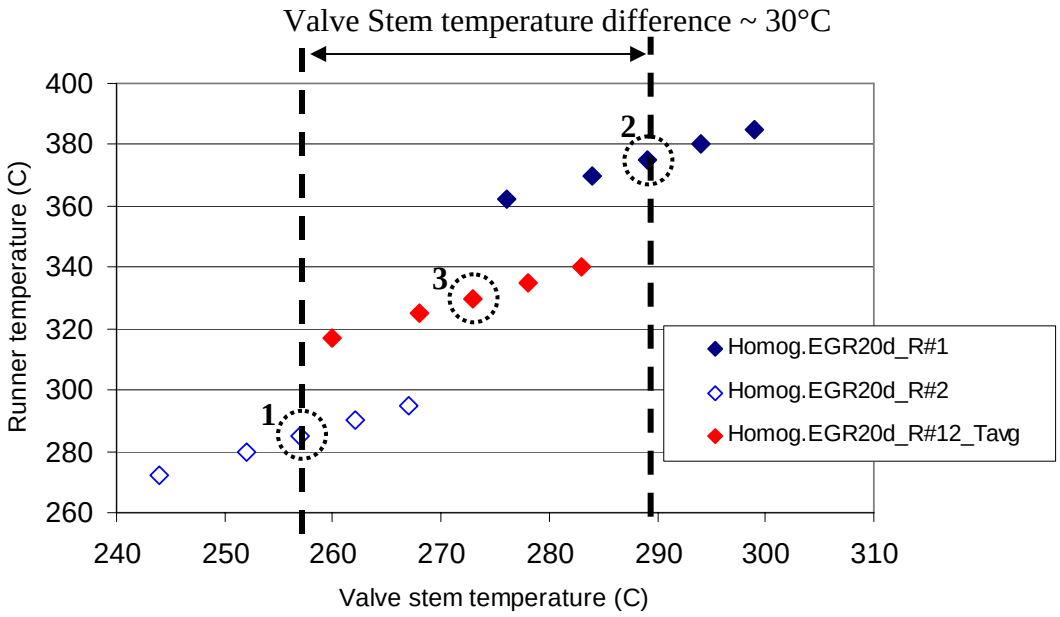

Figure 5-2 Intake Charge Runner versus Intake Charge Valve Stem Temperatures

The two Reference dotted circles # 1 and 2 point out in Figure 5-2 two sets of runner and valve stem temperatures (one set of temperatures for Homog.EGR20d_R#1 and the second set for Homog.EGR20d_R#2), one set for each intake runner and each intake port half. The resultant mass average runner and valve stem temperature is marked by the Reference dotted circle # 3 respectively.

Each run day, tests were performed to observe data repeatability behavior as a function of the mass average intake charge temperature for a specific homogeneous composition and temperature air, fuel and EGR diluent mixture at a fixed air-fuel ratio of 20:1. This condition contained a full sweep of mass average intake charge temperatures,

measured at the runners. These repeatability tests served to define a HCCI operating window as an experimental baseline. Combustion metrics such as IMEP, COV of IMEP, Knock Ringing Index and Combustion Efficiency were found to be sensitive to engine combustion and emission variations induced by changes as small as 1.5-3°C in the intake charge valve temperatures.

The following plots show combustion data from different dates as a function of mass average intake air temperature. Figure 5-3 shows good data repeatability of engine IMEP as a function of the calculated mass average intake charge runner temperatures. The time span for the cases shown on the following four figures corresponds to a total of four months.

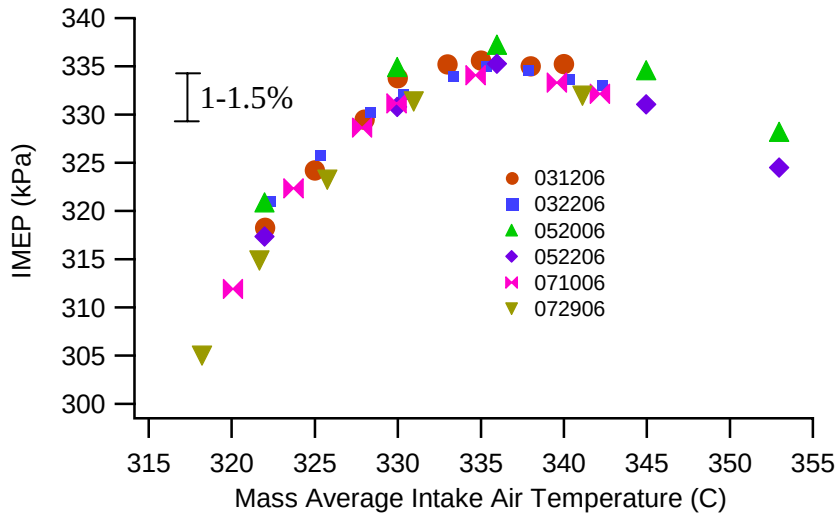

Figure 5-3 IMEP versus Mass Average Intake Temperature

Figure 5-4, 5-5 and 5-6 also show good data repeatability of engine COV of IMEP, Knock Ringing Index and Combustion Efficiency as a function of the calculated mass average intake charge runner temperatures for data sets taken throughout a span of four months.

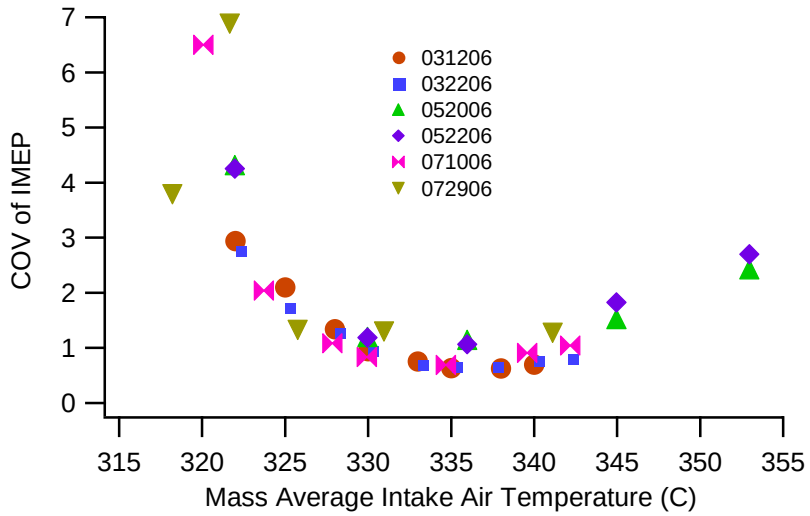

Figure 5-4 COV versus Mass Average Intake Temperature

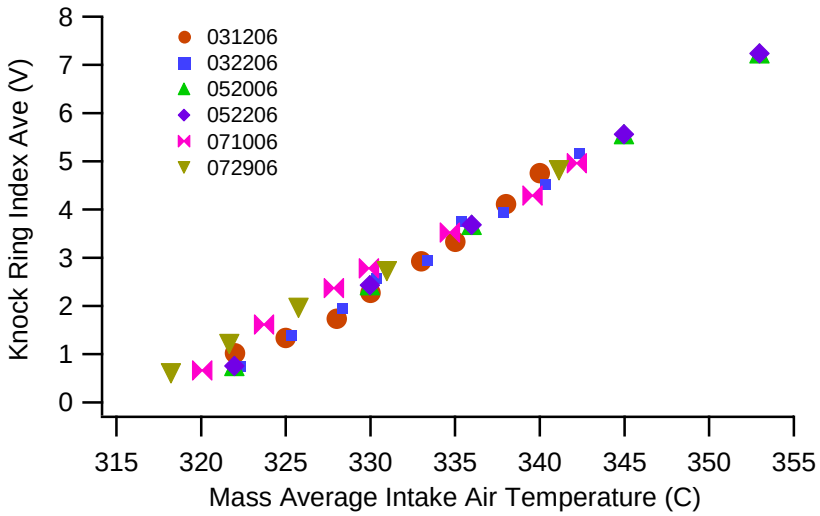

Figure 5-5 Knock Ringing Index versus Mass Average Intake Temperature

The results showed on the previous Figures 5-3,4,5 and on Figure 5-6 showed consistent data repeatability. It is also implicitly shown in the data that not only were the temperature measurements consistent throughout time, but so were emission measurements and cylinder pressure recordings used as a data source for calculations of combustion efficiency, engine IMEP, COV of IMEP and Ringing Index.

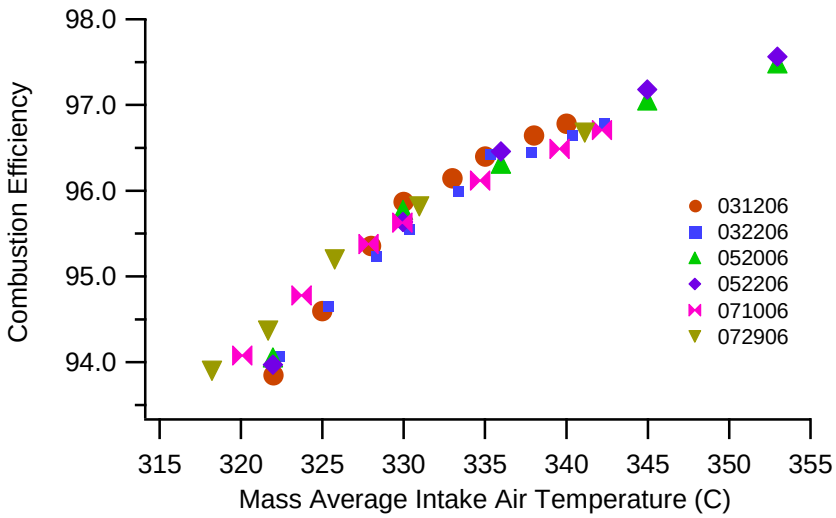

Figure 5-6 Combustion Efficiency versus Mass Average Intake Temperature

5.2 – Combustion Phasing CA50

As was mentioned previously, combustion phasing CA50 will be used as one of the parameters to compare combustion and emission data between different experimental running conditions. The following two figures are presented to show how CA50 correlates with the peak heat release rate locations for different running conditions. Also, results shown on each of the following two figures correspond to two different combustion stability regimes. One combustion regime is characterized as with more advanced CA50 values (3-5 CA degrees aTDC), while the second combustion regime is characterized as with less combustion stability (14.5-17.5 CA degrees aTDC).

Figure 5-7 shows plots of heat release rate versus engine crank angle for homogeneous temperature and composition air, fuel and gas diluent mixtures (The Figure 5-7 legend shows solid lines for heat release rate data from one EGR diluted case, three N2 gas diluted cases and one air diluted case). The vertical dashed lines indicate the specific CA50 for each experimental case shown. For instance, the red continuous

reference line (Homogeneous_EGR_20d) plots heat release rate versus engine crank angle data for an EGR gas diluted homogenous composition and temperature case with an air-fuel ratio of 20:1. Meanwhile, its respective CA50 line (CA50_EGR_20d ~ discontinuous red reference line) indicates the engine crank angle for CA50. Also, the kind of data used to arrange Figure 5-7 can be define as data from more advanced combustion phasing events (3-5 CA degrees aTDC) which provided better COV of IMEP results.

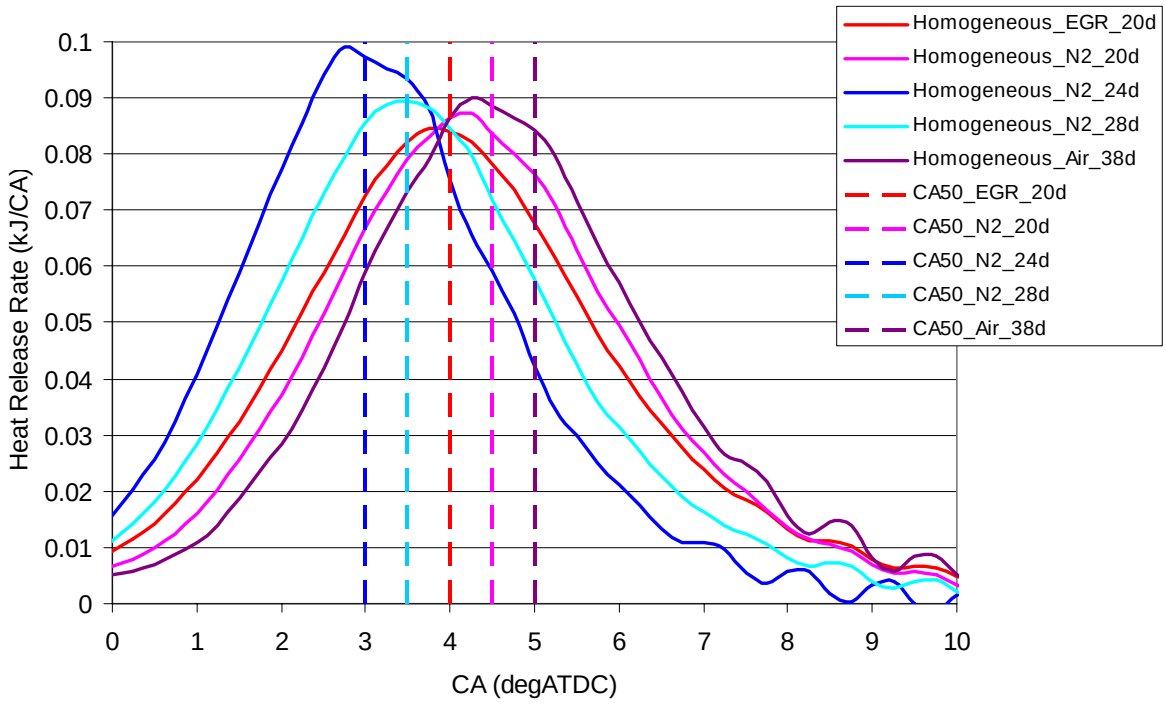

Figure 5-7 Heat Release Rate versus Engine CA and CA50 – COV of IMEP ~1.2%

Figure 5-7 shows that CA50 consistently follows the peak heat release crank angle locations for each of the cases.

Figure 5-8 shows data from cases which were run at the lower operating temperature window limit, hence resulting with much more delayed combustion development and larger COV of IMEP values. Combustion and emissions data obtained

from cases run at larger COV of IMEP regimes did present a broader range of variability of combustion and emission metrics. Nonetheless, CA50 seems to correlate reasonably well while compared to the peak heat release rate location.

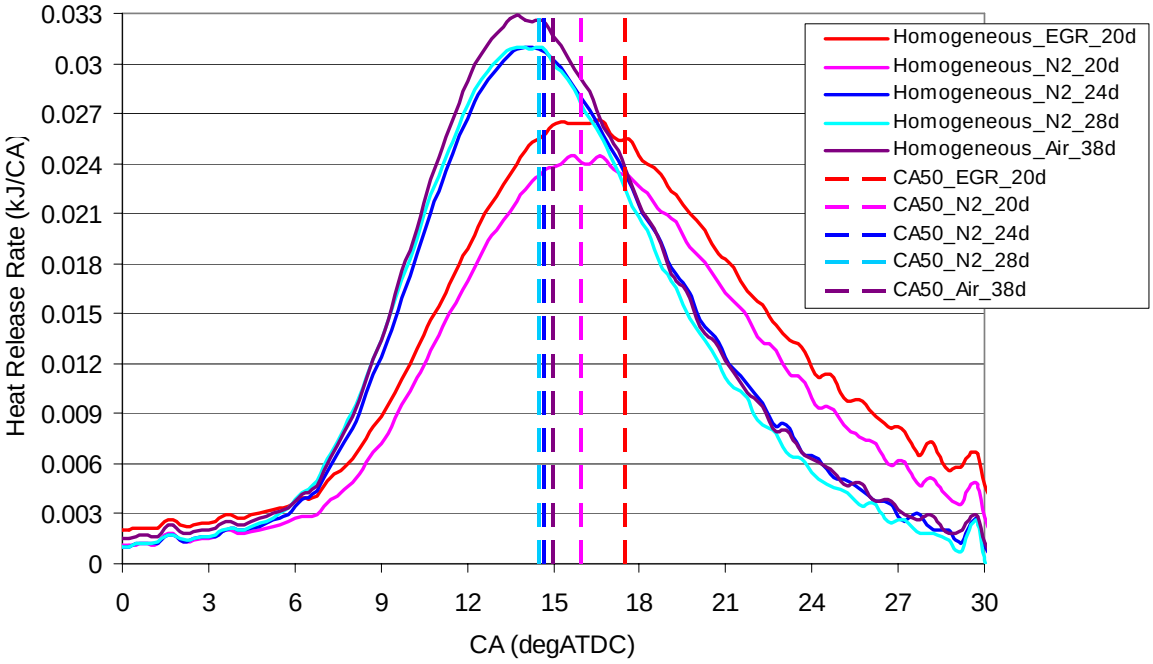

Figure 5-8 Heat Release Rate versus Engine CA and CA50 – COV of IMEP ~6%

Combustion variables such as IMEP, COV of IMEP, Knock Ringing Index and Combustion Efficiency are plotted below as a function of Combustion Phasing, CA50 for one single experimental condition. This single experimental condition was defined as a homogeneous composition and temperature charge using EGR as diluent and with an air-fuel ratio of 20:1. Figure 5-9 through 5-12 shows good data repeatability of engine combustion metric variables as a function of CA50. The time span for the cases shown in the following four figures corresponds to a total of four months.

Details on engine running conditions for the data shown in Figures 5-9 through 5-12 can be found in Table 4-1 and 4-3.

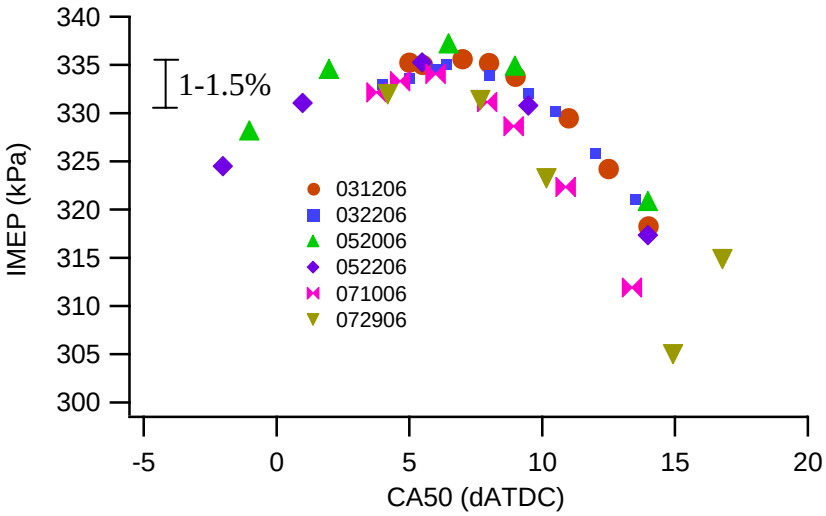

Figure 5-9 IMEP versus Combustion Phasing CA50

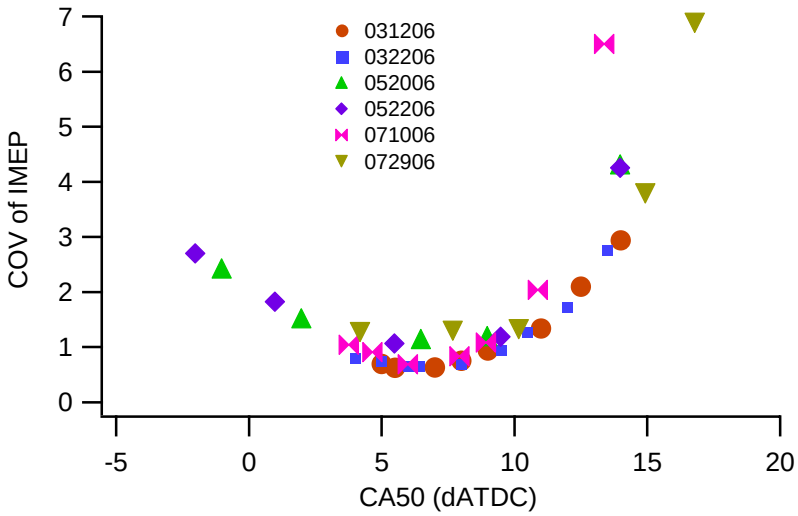

Figure 5-10 COV of IMEP versus Combustion Phasing CA50

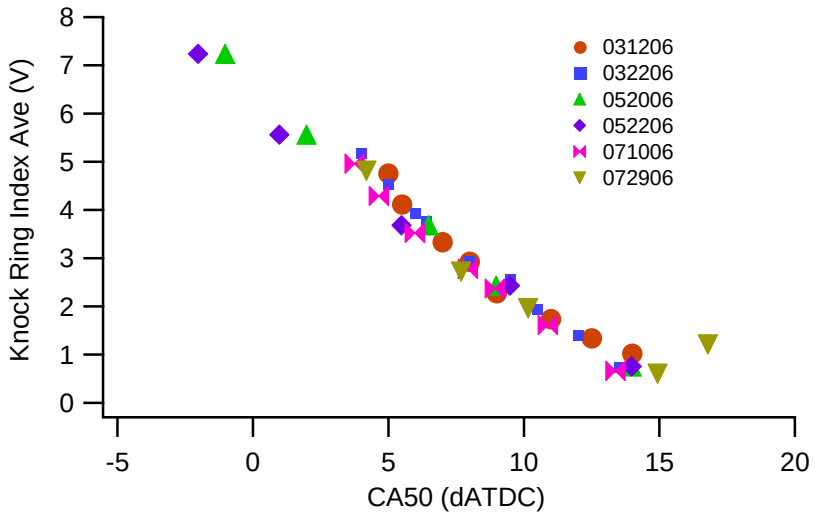

Figure 5-11 Knock Ringing Index versus Combustion Phasing CA50

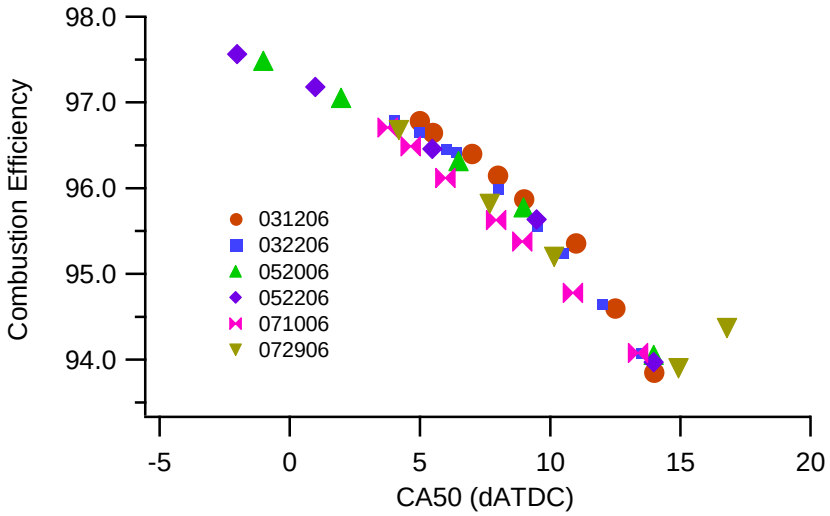

Figure 5-12 Combustion Efficiency versus Combustion Phasing CA50

The combustion results plotted versus CA50 shown in the previous four figures consistently showed a good correlation of the combustion data while plotted as a function of combustion phasing. Therefore, for each CA50 point there was a single output of combustion and emission data, thus the collapsing behavior of the data shown on the previous figures.

5.3 – EGR Diluent Matrices

This section presents combustion and emission performance results for the three experimental matrices using EGR as a diluent. Combustion and emission performance are evaluated relative to the mass average intake charge temperature and CA50 combustion phasing for each EGR diluent case. Experiment running conditions and intake charge strategies used for each experimental matrix are detailed below. Notice in the matrices below, that the HCCI operating temperature window for each of the three EGR diluent matrices has been determined from the data according to the operating window limits explained in Chapter 4 (see Figure 4-1 for reference).

Matrix #1 – Homogeneous Intake Charge

Window Temperature Range	322 - 342°C
Delivered (d) Air-fuel Ratio	20:1
Fuel Mass Flow Rate	10mg/cycle
Air Mass Flow Rate	200mg/cycle
Diluent Type	EGR
Mean Diluent Percentage	40%
Diluent Mixing	Homogeneous
Charge Temperature Difference	0°C

Table 5-1 Homogeneous Intake Charge Experimental Parameters

Matrix #2 – Temperature Stratification

Window Temperature Range	318 - 338°C
Delivered (d) Air-fuel Ratio	20:1
Fuel Mass Flow Rate	10mg/cycle
Air Mass Flow Rate	200mg/cycle
Diluent Type	EGR
Mean Diluent Percentage	40%
Diluent Mixing	Homogeneous
Charge Temperature Difference	30°C

Table 5-2 Temperature Charge Stratification Experimental Parameters

Matrix #3 – Diluent Stratification

Window Temperature Range	288 - 317°C
Delivered (d) Air-fuel Ratio	20:1
Fuel Mass Flow Rate	10mg/cycle
Air Mass Flow Rate	200mg/cycle
Diluent Type	EGR
Mean Diluent Percentage	40%
Diluent Mixing	Stratified
Charge Temperature Difference	0°C

Table 5-3 Diluent Charge Stratification Experimental Parameters

5.3.1 – EGR Diluent and Thermal Stratification Results versus Mass Average Intake Temperature

The following set of results presented on Figures 5-13, 5-14 and 5-15 show plots of combustion performance result such as IMEP, COV of IMEP, Ringing Index, Combustion Efficiency, emissions index variables such as EIHC, EICO and EINO and combustion phasing variables such as CA10, CA50 and CA90.

The data is plotted first as a function of the mass average intake charge temperature. Each set of plotted data is identified on each of the figures' legends. For this specific chapter section (5.3.1), Homogeneous_EGR_20d data set corresponds to the experimental matrix Table 5-1, Tstrat_Homogeneous_EGR_20d data set corresponds to the experimental matrix Table 5-2 and Unmixed_EGR_20d data set corresponds to the experimental matrix Table 5-3. The main distinction between these three sets of data that can be observed from the plots below are the shifts in the operating temperature window for the EGR diluent and thermal stratification cases while compared against the baseline data set (Homogeneous_EGR_20d). A temperature operating window shift of approximately 4-5°C was observed between the homogeneous temperature and

composition data (Homogeneous_EGR_20d) and the temperature stratification data (Tstrat_Homogeneous_EGR_20d). The temperature window shift caused by a split intake charge temperature difference of 30°C was small. The shift in the operating temperature window caused by EGR stratification was large (Unmixed_EGR_20d). The EGR diluent stratification case showed an operating temperature window shift of about 33-34°C. Similarly, an operating temperature window widening was also observed with EGR stratification. This widening was not observed by applying thermal charge stratification. Nevertheless, it is important to keep in mind that the maximum intake charge temperature difference was limited by hardware restrictions and a very high intake charge temperature was required to achieve HCCI combustion. The operating temperature window for the stratified EGR diluent case was almost 10°C wider than the operating temperature window for the homogeneous charge and thermal stratification cases.

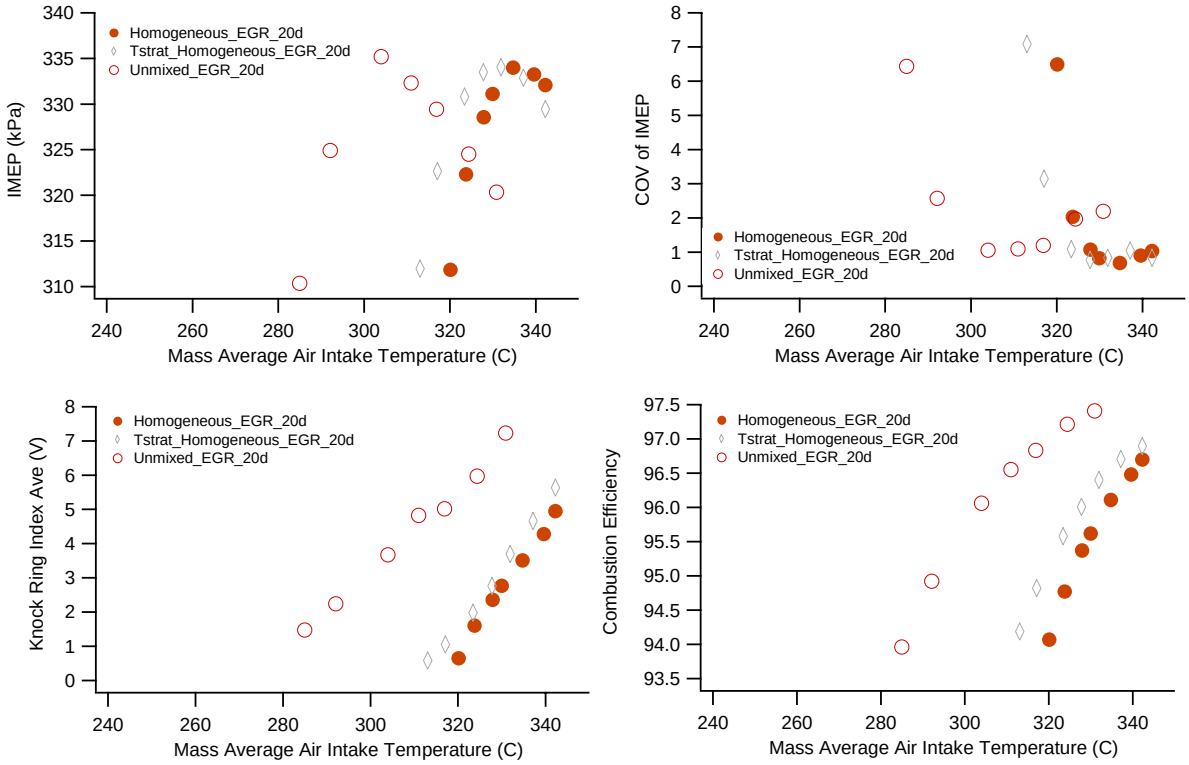

Figure 5-13 Combustion Performance versus Mass Average Intake Temperature

By looking at Figures 5-13 and 5-14 which shows recordings of combustion and emission variables plotted as a function of mass average intake charge temperature, it is observed that there is little difference in the magnitude change of the plotted variables while comparing the two stratified charge cases against the homogeneous composition and temperature EGR diluent baseline. The main effect due to the imposed thermal and composition charge stratification is the lowering of the intake charge temperature. This means that lower intake charge temperatures are required to maintain a constant combustion phasing.

Details on engine running conditions for the data shown in Figures 5-14 through 5-17 can be found in Table 4-1.

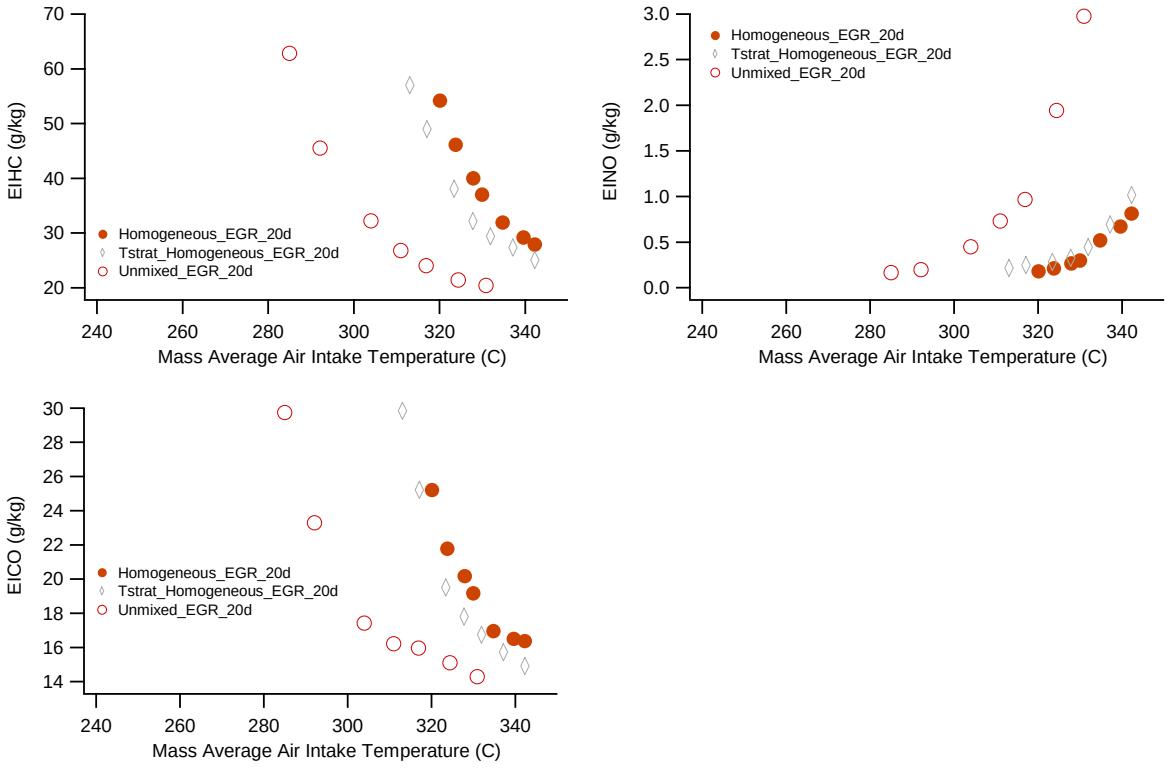

Figure 5-14 Emission Performance versus Mass Average Intake Temperature

In the same manner, it is interesting to observe in Figure 5-15 that the temperature shift between different operating temperature windows remains constant for the different combustion phasing variables plotted such as CA10, CA50 and CA90. There does seem to be a shift toward the lower operating temperature limit (longer combustion phasings) with EGR stratification. while comparing the EGR stratification case against the homogeneous EGR baseline. At this lower operating temperature limit, the combustion regime is characterized by a rise in the COV of IMEP values, which means that start of igniton, intermediate and final combustion stages if combustion (defined by CA10, CA50 and CA90 respectively) show higher combustion variance.

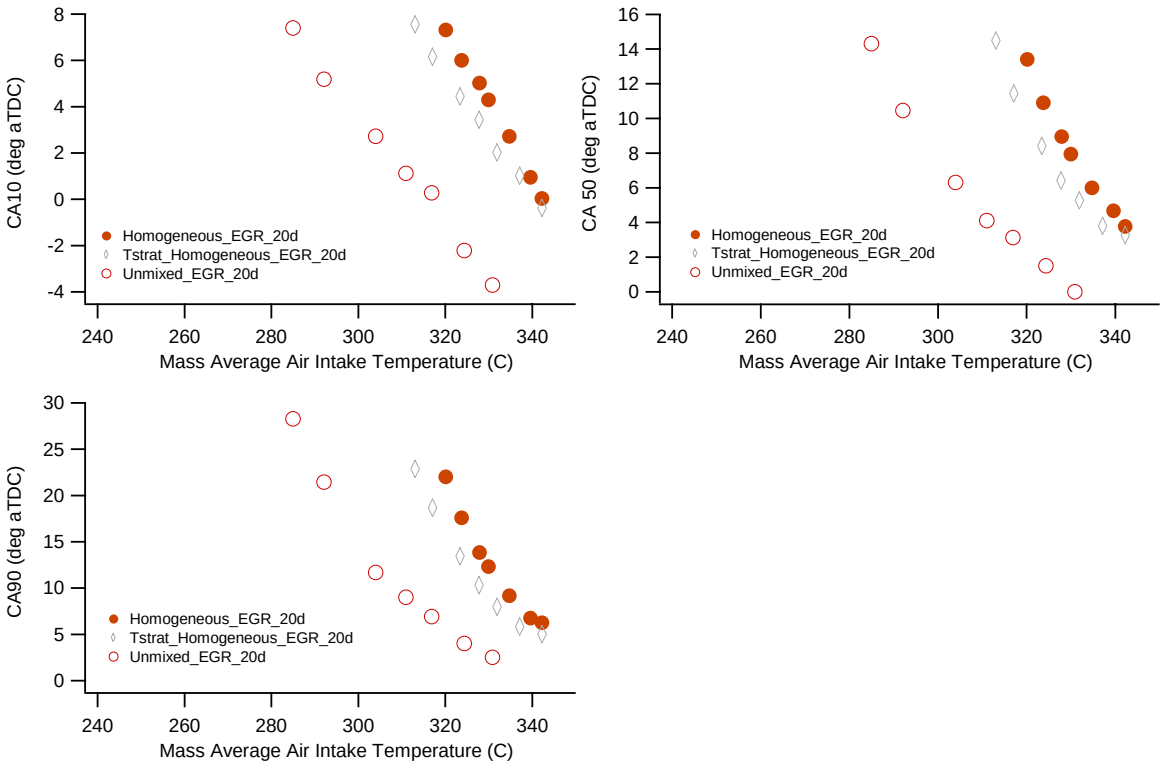

Figure 5-15 Combustion Phasing versus Mass Average Intake Temperature

As stated previously, the operating temperature window for the EGR diluent stratified case resulted to be almost 10°C wider than the temperature operating range for the homogeneous charge and thermal stratification cases. This widening of the operating temperature window may be explained by a slowing of the combustion rates as a result of the imposed EGR diluent stratification. Further explanations will focus on this topic.

5.3.2 – EGR Diluent and Thermal Stratification Results versus CA50 Combustion Phasing

By replotting the data, combustion, emission index and combustion phasing results are displayed versus intermediate combustion stage phasing crank angle (Combustion Phasing CA50). These plots are given in Figures 5-16 and 17.

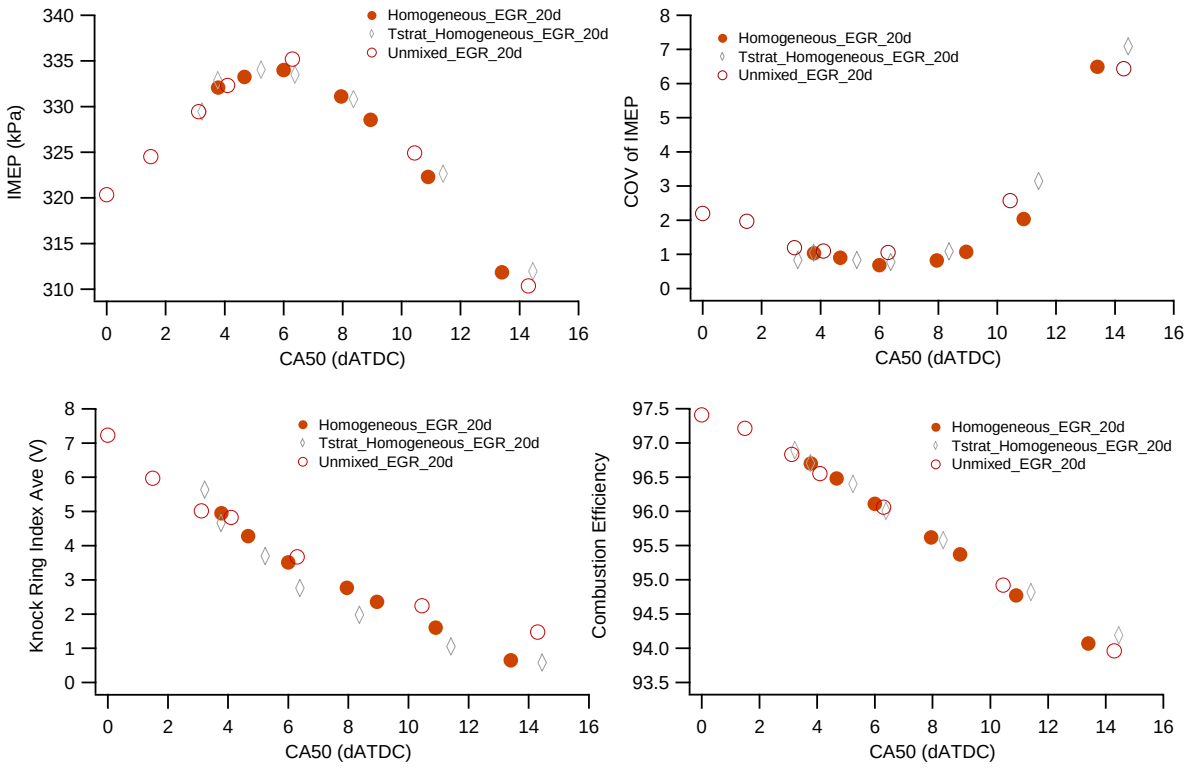

Figure 5-16 Combustion Performance versus CA50

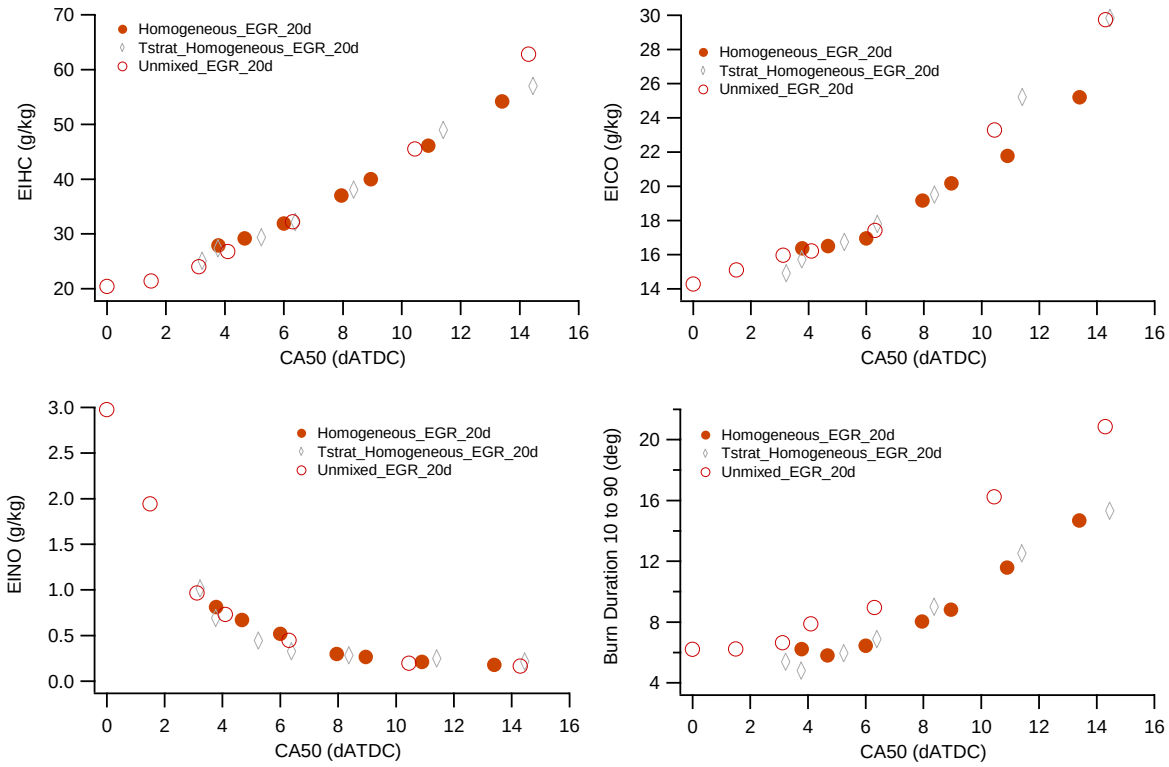

Figure 5-17 Emission Performance versus CA50

The above plots take us back to the earlier statement that the main effect of imposing charge stratification can be described as the lowering of the intake charge temperature required to maintain a constant combustion phasing. Figures 5-16 and 5-17 show that the data collapse reasonably well when plotted versus Combustion Phasing CA50. Nonetheless, it seems that a trend of 2-3 crank angle increase in burn duration is observed for a given CA50 for the case of imposed EGR diluent charge stratification. This effect of slight increase on burn duration is believed to be responsible of the widening of the operating temperature window observed for the EGR diluent stratification case while compared against the homogeneous EGR diluent baseline.

Therefore, the effect of imposing EGR diluent stratification throughout the intake charge seems to result in homogeneous charge like combustion phasing with lower intake charge temperatures. Further explanations will be presented in Section 5.5 including details on the effects that can be attributed to causing shifts in the operating temperature windows.

5.4 – N2 Diluent Matrices

This section will present combustion and emission performance data results for two experimental matrices using N2 gas as diluent. Combustion and emission performance results will be presented in terms of their mass average intake charge temperature and CA50 combustion phasing. Experiment conditions and intake charge strategies used for each experimental matrix are detailed below:

Matrix #1 – Homogeneous Intake Charge

Window Temperature Range	257 - 326°C
Delivered (d) Air-fuel Ratio	20:1, 24:1, 28:1, 38:1
Fuel Mass Flow Rate	10mg/cycle
Air Mass Flow Rate	200, 240, 280, 380 mg/cycle
Diluent Type	N2
Mean Diluent Percentage	45, 35, 25 and 0%
Diluent Mixing	Homogeneous
Charge Temperature Difference	0°C

Table 5-4 Homogeneous Charge Experimental Parameters

Matrix #2 – Diluent Stratification

Window Temperature Range	281 - 311°C
Delivered (d) Air-fuel Ratio	20:1, 24:1, 28:1, 38:1
Fuel Mass Flow Rate	10mg/cycle
Air Mass Flow Rate	200, 240, 280, 380 mg/cycle
Diluent Type	N2
Mean Diluent Percentage	45, 35, 25 and 0%
Diluent Mixing	Stratified
Charge Temperature Difference	0°C

Table 5-5 Diluent Charge Stratification Experimental Parameters

It is important to mention as a sort of a reminder that as the delivered air-fuel ratio increases for each of these N2 diluent cases, the required amount of N2 diluent gas to be supplied into the engine to balance out the engine IMAP decrease.

Details on engine running conditions for the data shown in Figures 5-18 through 5-22 can be found in Table 4-1.

5.4.1 – N2 Diluent Results versus Mass Average Intake Temperature

Similarly as was stated for the EGR diluent cases, the main distinction that can be made between the N2 diluent data sets shown in Figures 5-18, 19 and 20 are the shifts experienced on the N2 gas diluent stratified charge operating temperature window compared against the homogeneous N2 gas diluent baselines. However, as N2 diluent includes cases run at leaner air-fuel ratios, a second effects needs to be recognized, namely that the leaner air-fuel ratios also shift the operating temperature window downward compared to the N2 gas diluent homogeneous charge baseline with a fixed air-fuel ratio of 20:1. The temperature shift caused by the leaner intake charges is, especially when comparing the case with an air-fuel ratio of 20:1 against the case with an air-fuel ratio of 38:1 (leanest air diluted case). This comparison results in a temperature shift of about 46-48°C. Further discussions of the phenomena is provided in Section 5.5.

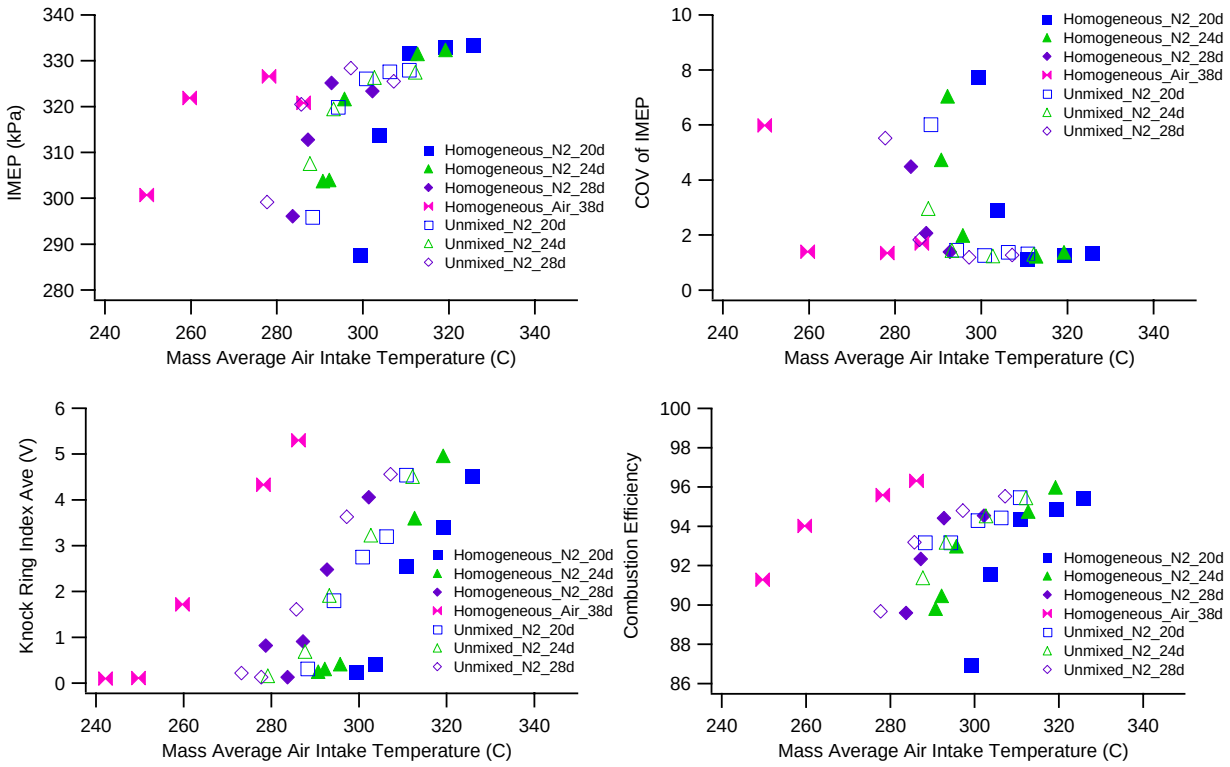

Figure 5-18 Combustion Performance versus Mass Average Intake Temperature

It is also noticed that the maximum temperature shift between the stratified and the homogeneous case operating windows is observed for the N2 diluent case which holds an air-fuel ratio of 20:1. The air-fuel ratio of 20:1 presents the strongest effect seen for composition charge stratification. This case contains the maximum amount of N2 diluent (45% of the total inducted intake charge volume). The impact of charge stratification on the operating temperature window tends to disappear as the mixture air-fuel ratio gets leaner; that is as the amount of N2 gas present in the intake diluted charge decreases. None of the N2 diluent cases resulting in such a pronounced operating temperature window shift as was observed for the EGR diluent stratification case; nor was an operating temperature window widening observed for the N2 diluent as it was for EGR diluent.

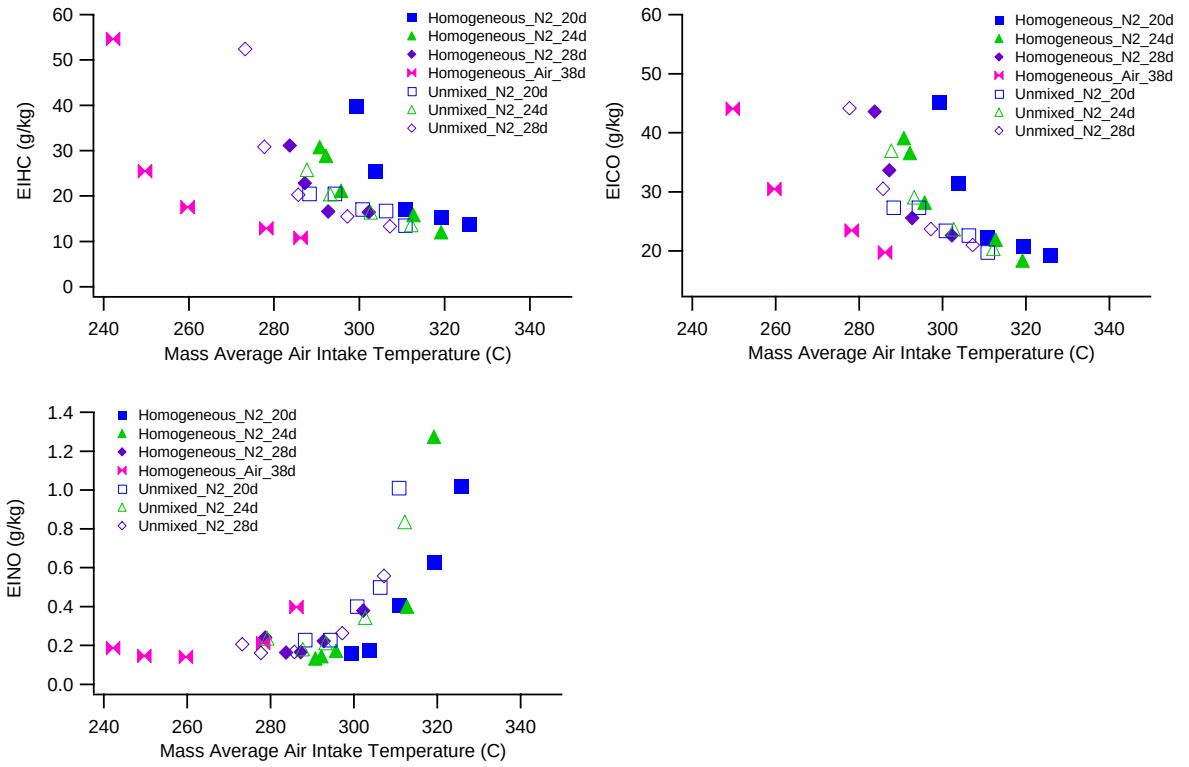

Figure 5-19 Emission Performance versus Mass Average Intake Temperature

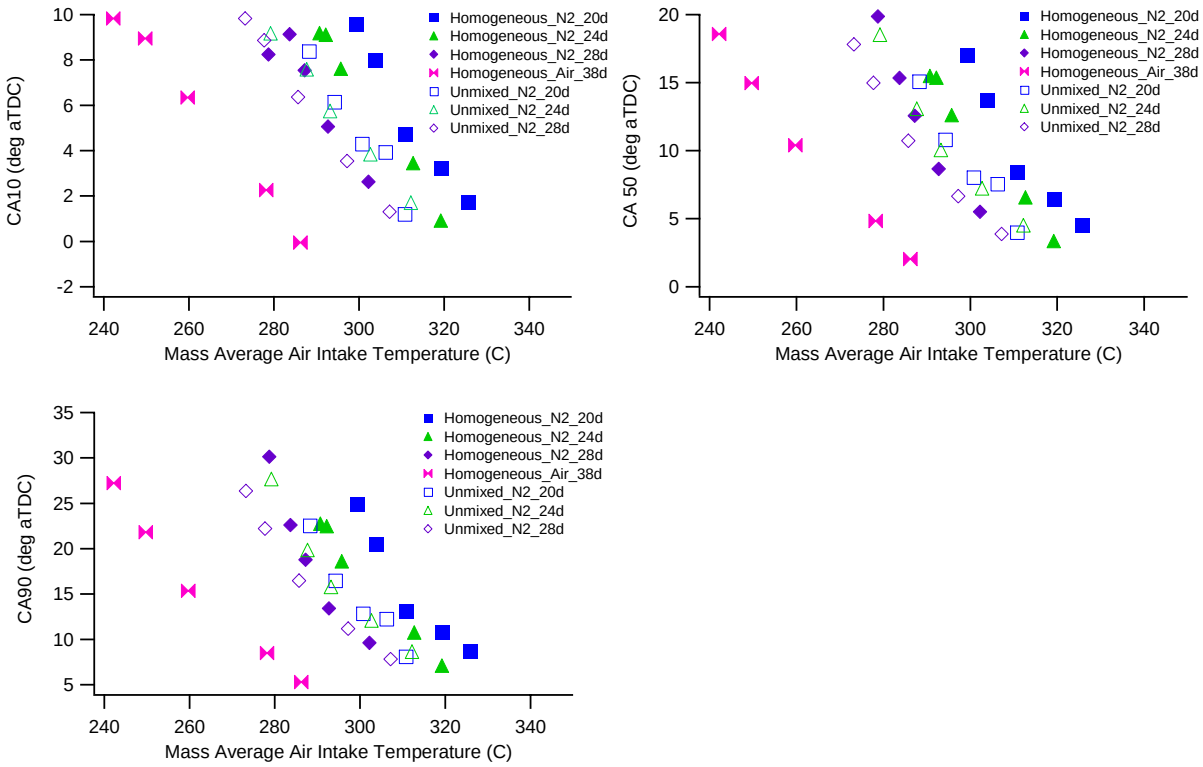

Figure 5-20 Combustion Phasing versus Mass Average Intake Temperature

5.4.2 – N2 Diluent Results versus CA50 Combustion Phasing

The effect of imposing N2 gas diluent stratification throughout the intake charge resulted in reaching homogeneous temperature and composition charge like combustion phasing values at lower intake charge temperatures. Here, once again, the combustion and emission data are analyzed versus combustion phasing CA50; thus bringing a set of results that consistent collapsing trends throughout the different combustion phasings.

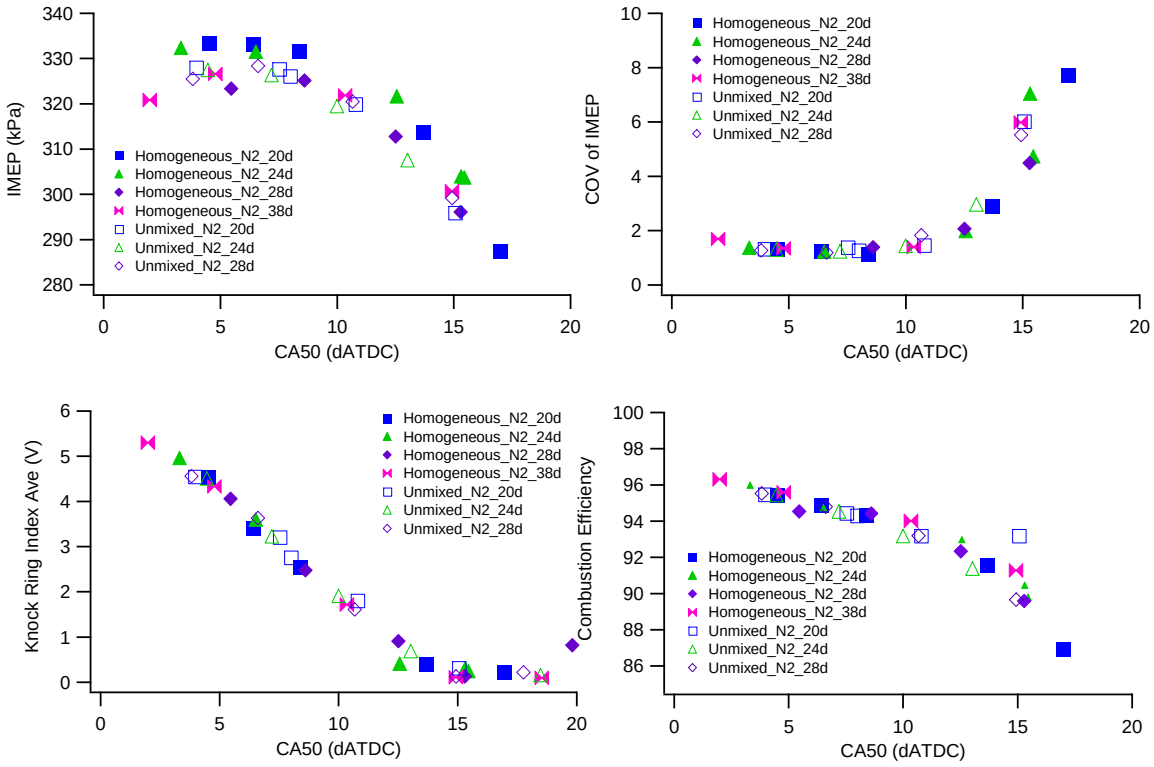

Figure 5-21 Combustion Performance versus CA50

On the basics, changes in air-fuel ratio conditions had no impact on the combustion and emission data results. As with the EGR data, the impact of unmixedness is seen as affecting a change in the charge temperature to maintain combustion phasing throughout the operating temperature window.

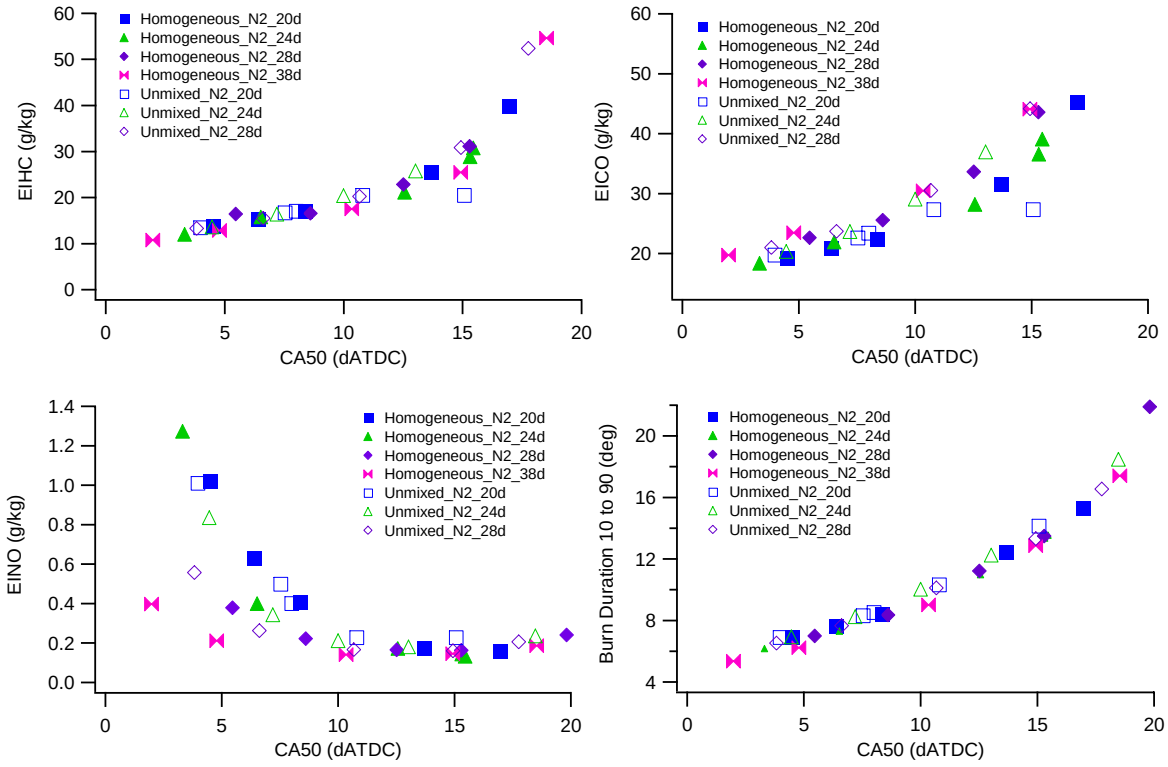

Figure 5-22 Emission Performance versus CA50

Section 5.5.describes calculations explaining the differences in the EINO trends that were observed in the N2 gas diluent cases as the delivered air-fuel ratio increased from 20:1 to 38:1. These EINO differences can be observed by looking at Figure 5-22 at combustion phasing stages which required higher intake charge temperatures to maintain advanced values of Combustion Phasing CA50. This CA50 values fall within the range of crank angles that goes from 10 deg aTDC to a more advanced crank angle of 2-3 deg aTDC.

5.5 – Multiple Intake Charge Effects within Diluent Stratification

The purpose of this section is to show combustion and emission data results in which individual thermodynamic and fluid mechanic effects are isolated. These single intake charge effects have been identified to be relevant in influencing combustion phasing and shifting the operating intake temperature windows. Once the combustion and emission data have been analyzed to characterize each of the cases with single charge effects, explanations will proceed to try to asses situations when multiple effects are present by EGR and N2 gas diluent intake charge stratification. These combined effects imposed by composition charge stratification can be claimed to effectively influence combustion phasing and HCCI operating temperature window for each of the running conditions.

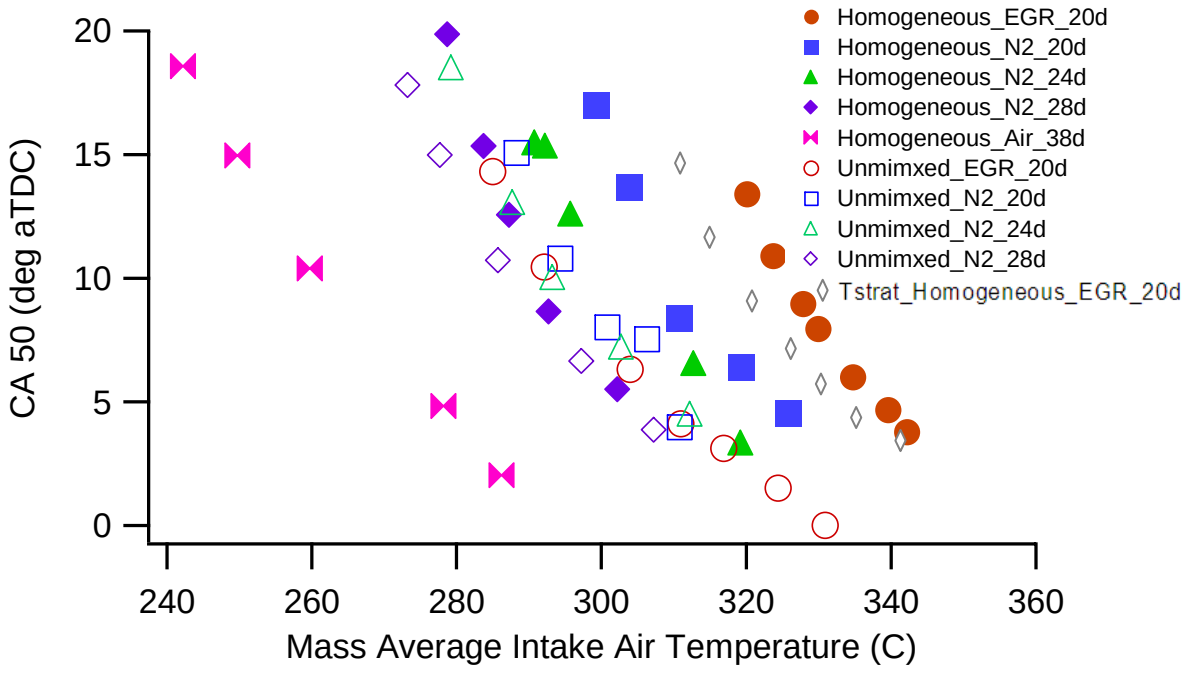

Figure 5-23 CA50 versus Mass Average Intake Charge Temperature

Figure 5-23 above shows the span of Combustion Phasing CA50 for each of the experimental cases run as a function of mass average intake charge temperature. Solid symbols represent homogeneous composition and thermal intake charge cases, while open symbols represent data for the stratified charge cases. Symbol shapes are conserved between equal running conditions such as air-fuel ratio and diluent type to facilitate the task of comparing the operating temperature window shifts between homogeneous and stratified charge cases. The following sections will summarize the results for each of the intake charge treatments, as Combustion Phasing CA50 data is analyzed against mass average intake charge temperatures.

Details on engine running conditions for the data shown in Figures 5-24 through 5-36 can be found in Table 4-1.

5.5.1 – N2 Diluent Homogeneous Intake Charge – A/F Effect

The following experimental matrix presents running conditions for cases run with N2 gas diluent at different air-fuel ratios, i.e. with different amounts of N2 gas in the intake charge. The approach of utilizing N2 gas as diluent instead of EGR was motivated by the fact that EGR reintroduces oxygen into the intake, thus establishing an in-cylinder trapped air-fuel ratio which is leaner than the delivered air-fuel ratio. Also, these experimental runs with N2 gas diulent were intended to eliminate the effects on combustion due to the differences in specific heat ratio (γ) between homogeneous mixtures of air, fuel and EGR at different air-fuel ratios.

Window Temperature Range	267-322°C
Air-fuel ratio	20:1, 24:1, 28:1, 38:1
Fuel Mass Flow Rate	10mg/cycle
Air Mass Flow Rate	200, 240, 280, 380 mg/cycle
Diluent Type	N2
Mean Diluent Percentage	45, 35, 25 and 0%
Diluent Mixing	Homogeneous
Charge Temperature Difference	0°C

Table 5-6 A/F Effect Experimental Parameters

As seen in the experimental matrix above, all the tests were run with homogeneous mixtures of air, fuel and N2 gas diluent, except for the case with the leaner air-fuel ratio (38:1) which was an air diluted (non N2 gas) homogeneous charge mixture. The slight difference in the specific heat ratio between air and N2 gas was neglected.

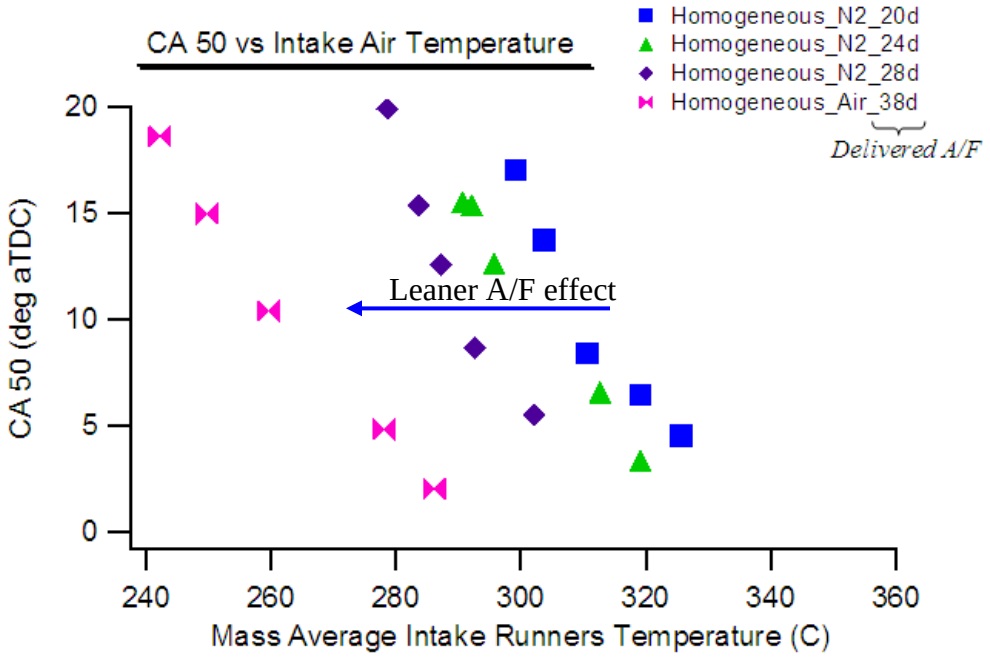

Figure 5-24 CA50 versus Mass Average Intake Charge Temperature

It can be observed in Figure 5-24 that the air-fuel ratio played a very important role in shifting the operating temperature window downward for cases with leaner air-fuel ratios. As the air-fuel ratio increase, combustion phasing was achieved at lower intake temperatures. In other words, leaner air-fuel ratios required a lower intake

temperature for a fixed combustion phasing, thus concluding that intake charge temperature seemed to be strongly sensitive to the air-fuel ratios.

Table 5-7 is a useful arrangement of calculated data showing the resultant specific heat ratio (γ) for each set of mixtures. In this case, we have analyzed homogeneous air, fuel and N2 gas diluent mixtures with different air-fuel ratios, which indicated the non differences between gammas. Also, information is provided to show differences between delivered and trapped air-fuel ratios. The last table column shows the effect of the mixture γ by showing the calculated isentropic compression temperature as the charge undergoes an isentropic compression for a compression ratio of 7:1. The approach used to convert the γ differences into in-cylinder gas temperatures was determined by using a constant IVC temperature of about 500K for all cases.

A/F Effects

Homogeneous N2 Diluent Case	Specific Heat Ratio				Trapped AF				Isentropic Temp. (rc = 7)			
Delivered AF	20:1	24:1	28:1	38:1	20:1	24:1	28:1	38:1	20:1	24:1	28:1	38:1
AIR+FUEL (homog. mixture)				1.332				38				1094
AIR+FUEL+N2 (homog. mixture)	1.333	1.333	1.333		20	24	28		1096	1096	1095	

Table 5-7 Mixture Gamma, Trapped A/F and T_isentropic (C) Calculations

Based on this analysis, the shifts in the operating temperature window can be entirely attributed to the changes in the charge delivered air-fuel ratios.

Experimental Case	CA50 (degATDC)	T_int_avg (C)	T_bulk (CA50) (C)	T_exh (C)	y_res_int %	T_IVC (C)
Homogeneous_N2_A/F_d=20:1	4.5	325	1303	350	7.29	225.2
Homogeneous_N2_A/F_d=24:1	3.5	319	1306	346	7.33	224.1
Homogeneous_N2_A/F_d=28:1	5.2	302	1233	342	7.34	219.2
Homogeneous_Air_A/F_d=38:1	4.5	276	1172	333	7.32	217.5

Table 5-8 N2 Gas Diluent Cases In-cylinder Bulk Temperature (C) Comparisons

Table 5-8 shows data for the mass average intake charge temperature, the calculated bulk gas temperature at CA50, the gas temperature at IVC and the measured exhaust gas temperature for homogeneous mixtures of air, fuel and N2 gas diluent with

increasing air-fuel ratios. The cases shown in this table go from a less lean air-fuel ratio of 20:1 to the leanest case of 38:1. The calculations were performed for experimental cases with similar Combustion Phasing CA50 values; i.e. these Combustion Phasing CA50 values corresponded to combustion regimes of low COV of IMEP, close to maximum engine IMEP. Also, the residual gas trapped mass fraction percentage is shown for each case. The results of this table show that the hotter intake charges burn at higher temperatures, which explains their higher NOx emissions. The trends of increasing EINO emissions for cases that achieved combustion at higher IVC temperatures can be observed in Figure 5-25. The effect of the trapped residual gas temperature as the mixture's air-fuel ratio increases may be because of the small fraction of residual gas trapped (~0.07) in the cylinder relative to the engine's inducted charge.

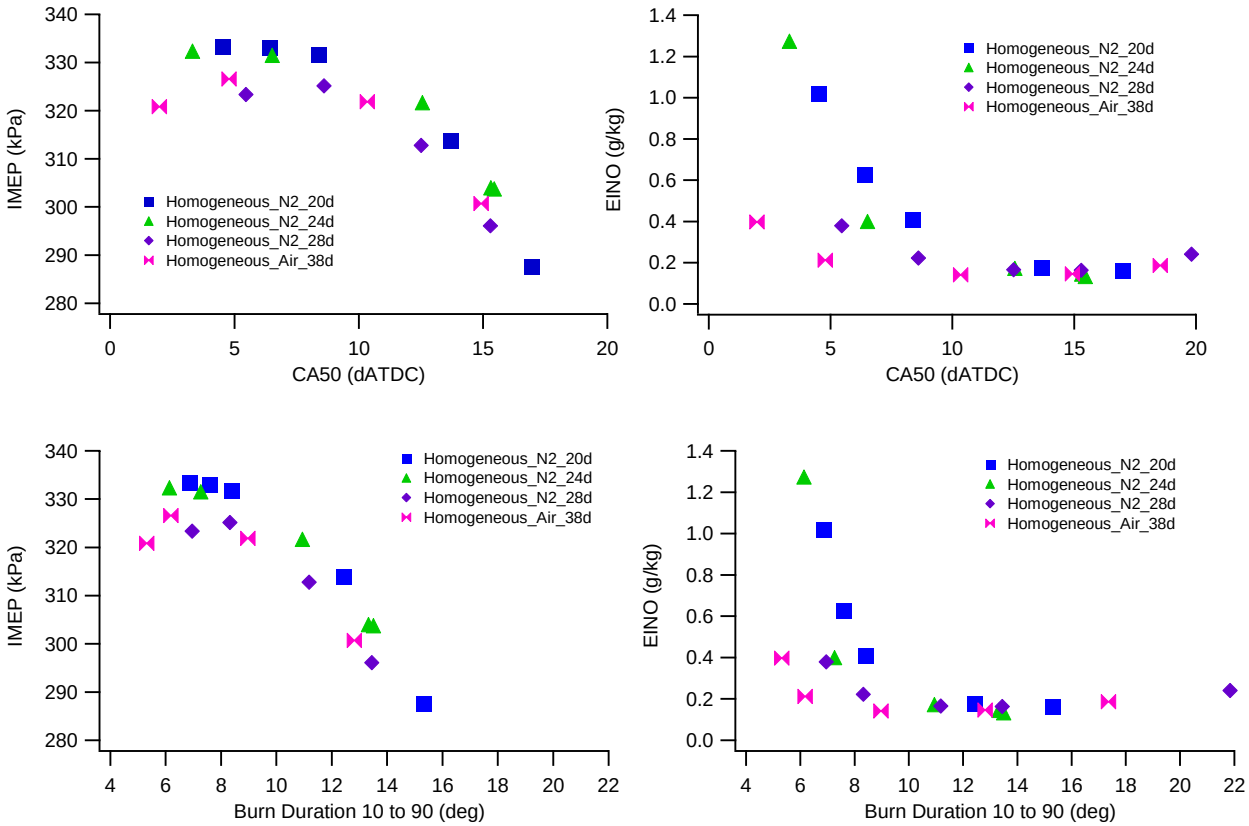

Figure 5-25 IMEP and EINO versus CA50 and CA90-10 angle

It can be also observed stated that there is a noticeable drop of engine IMEP for cases that had lower temperatures for their HCCI operating window. IMEP drops between 4-5% can be seen when comparing the N2 gas diuent cases at their different air-fuel ratio conditions (see Figure 5-25 for reference).

5.5.2 – EGR and N2 Diluents Homogeneous Intake Charge – Gamma and A/F Effects

The following two experimental matrices shown running conditions for cases ran with N2 gas diluent and EGR diluent. The EGR diluent case was run at a constant delivered air-fuel ratio of 20:1, meanwhile the N2 gas diluent case was run at two different air-fuel ratios, 20:1 and 24:1.

The first data analysis was performed by comparing CA50 versus mass average intake temperature between the N2 diluted case with a delivered air-fuel ratio of 24:1 and the EGR diluted case with a delivered air-fuel ratio of 20:1. The purpose of this first analysis intended to isolate the effect of charge specific heat ratio on combustion phasing for each case. EGR recirculates O2 into the engine intake, hence chaning the intake mixture air-fuel ratio to leaner magnitudes.

-Equal Trapped A/F Ratios – Gamma Effect

Window Temperature Range	315-342 °C
Air-fuel ratio "delivered"	20:1 (EGR), 24:1 (N2)
Air-fuel ratio "trapped"	24:1
Fuel Mass Flow Rate	10mg/cycle
Air Mass Flow Rate	200 (EGR), 240 (N2) mg/cycle
Diluent Type	N2 and EGR
Mean Diluent Percentage	40% (EGR), 35% (N2)
Diluent Mixing	Homogeneous
Charge Temperature Difference	0°C

Table 5-9 Gamma Effect Experimental Parameters

-Equal Delivered A/F Ratios – Gamma and A/F Effects

Window Temperature Range	321-342 °C
Air-fuel ratio "delivered"	20:1
Air-fuel ratio "trapped"	24:1 (EGR), 20:1 (N2)
Fuel Mass Flow Rate	10mg/cycle
Air Mass Flow Rate	200 mg/cycle
Diluent Type	N2 and EGR
Mean Diluent Percentage	40% (EGR), 45% (N2)
Diluent Mixing	Homogeneous
Charge Temperature Difference	0°C

Table 5-10 A/F and Gamma Effects Experimental Parameters

We have seen so far that the air-fuel ratio effect strongly shifts the operating temperature window at a fixed combustion phasing.

For the purpose of these analyses, calculations were performed to determine the value of trapped air-fuel ratio for the air, fuel and EGR mixture. EGR gases reintroduce oxygen into the intake. At a 20:1 air fuel ratio condition (200 mg of air and 10 mg of fuel per cycle), it has been measured by the emissions bench that there is 6.2% of oxygen in

the exhaust (EGR), which results in a trapped air-fuel ratio of 23.8:1 (this value has been rounded off through out experimental matrices and plot legends to be 24:1).

Therefore, as it was mentioned earlier, the first data comparison was made between the N2 gas diluent case with an air-fuel ratio of 24:1 and the EGR diluent case with a trapped air-fuel ratio of 24:1. This equal air-fuel ratio mixtures experiment was intended to isolate the effect of gamma in the combustion phasing.

Meanwhile, the second data comparison was performed (experimental details are given in Table 5-10) at equal delivered air-fuel ratios of 20:1 for experimental cases, N2 gas diluent and EGR diluent. For these data, there will be both gamma and air-fuel ratio effects.

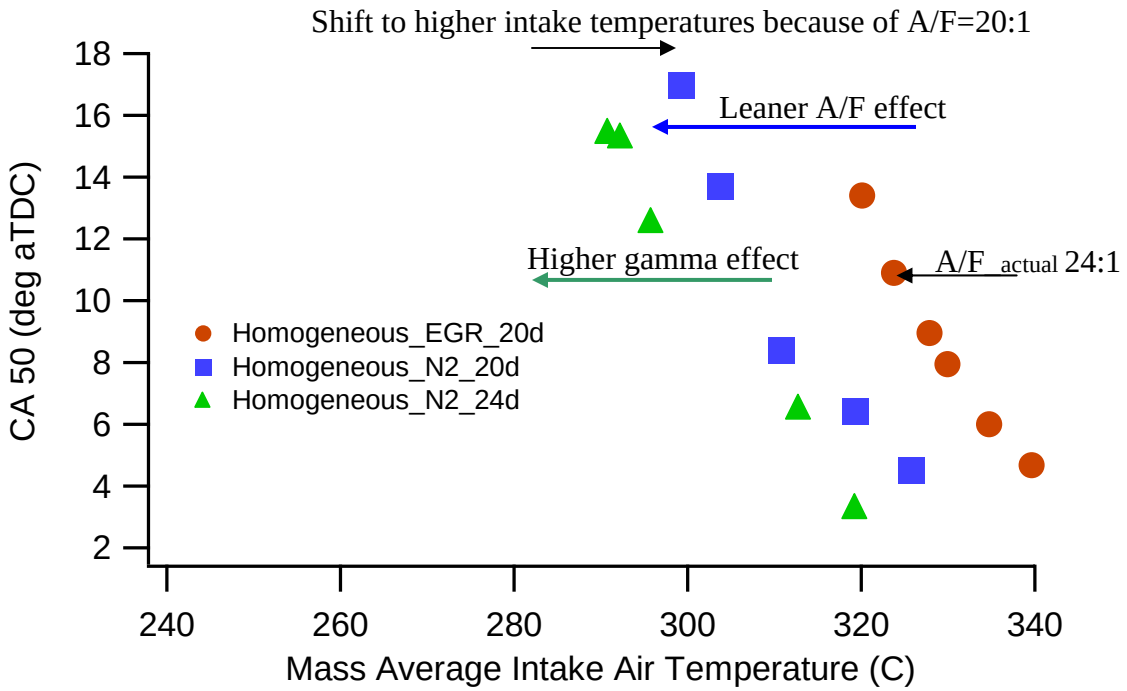

Figure 5-26 CA50 versus Mass Average Intake Charge Temperature

In looking at Figure 5-26, it is clear that a larger operating window temperature shift occurs for the cases in which single charge stratification effect, gamma effect is imposed (Homogeneous_EGR_20d and Homogeneous_N2_24d). This single effect was

imposed by differences on the mixtures specific heat ratio. The second comparison, which considered a N2 gas diluent case with an air-fuel ratio of 20:1 experienced an upward shift in the operating temperature window. Therefore, it can be stated that the effect of higher γ in the charge mixture required (Homogeneous_N2_24d experiment) lower intake charge temperatures for a fixed combustion phasing.

Gamma Effects

Homogeneous - EGR vs N2	Specific Heat Ratio				Trapped AF				Isentropic Temp. (rc = 7)			
Delivered AF	20:1	24:1	28:1	38:1	20:1	24:1	28:1	38:1	20:1	24:1	28:1	38:1
AIR+FUEL+EGR (homog. mixture)	1.316				24				1059			
AIR+FUEL+N2 (homog. mixture)		1.333				24				1096		

Table 5-11 Mixture Gamma, Trapped A/F and T_isentropic (C) Calculations

A/F and Gamma Effects

Homogeneous - EGR vs N2	Specific Heat Ratio				Trapped AF				Isentropic Temp. (rc = 7)			
Delivered AF	20:1	24:1	28:1	38:1	20:1	24:1	28:1	38:1	20:1	24:1	28:1	38:1
AIR+FUEL+EGR (homog. mixture)	1.316				24				1059			
AIR+FUEL+N2 (homog. mixture)	1.333				20				1096			

Table 5-12 Mixture Gamma, Trapped A/F and T_isentropic (C) Calculations

Tables 5-11 and 5-12 show that for a 1% γ difference between equivalent trapped air-fuel ratio mixtures, results in isentropic compression temperature difference of almost 40°C, thus resulting in a (-) 24-25°C operating temperature window shift. This indicates a high sensitivity of ignition timing to changes in mixture γ. The temperature window shift was narrower ((-) 19-20°C) when the mixtures delivered air-fuel ratios were matched at 20:1. This narrower temperature shift indicates that there are interactions that counteract the effects of the air-fuel ratio and γ on combustion phasing. Intake charge temperature requirement decrease as EGR leans out the air-fuel ratio mixture, however the intake charge temperature requirement increases as γ is reduced by the effect of the lower exhaust gas γ.

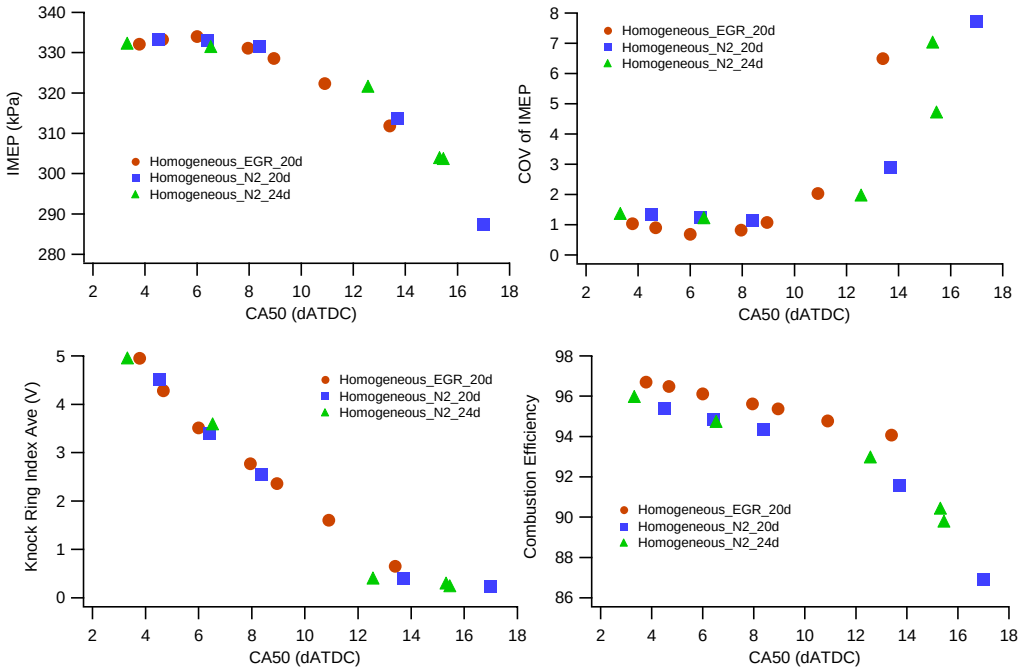

Figure 5-27 Combustion Performance versus CA50

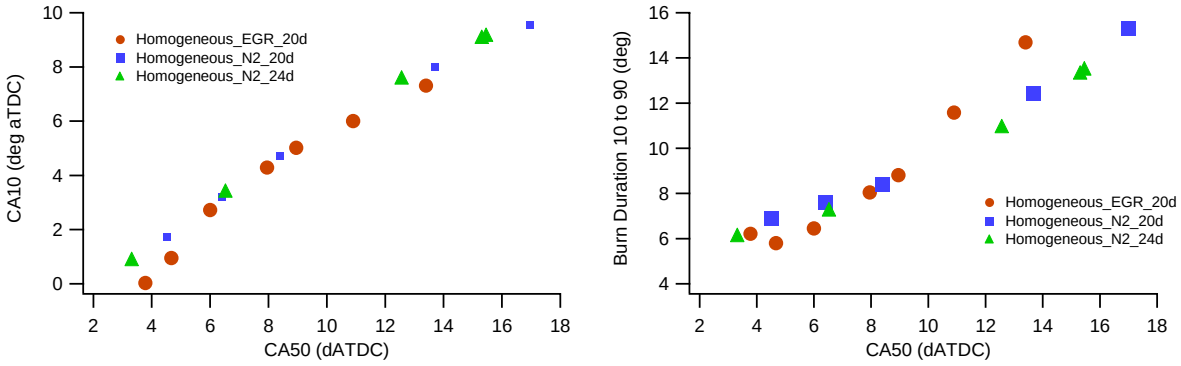

Figure 5-28 CA10 and CA90-10 versus CA50

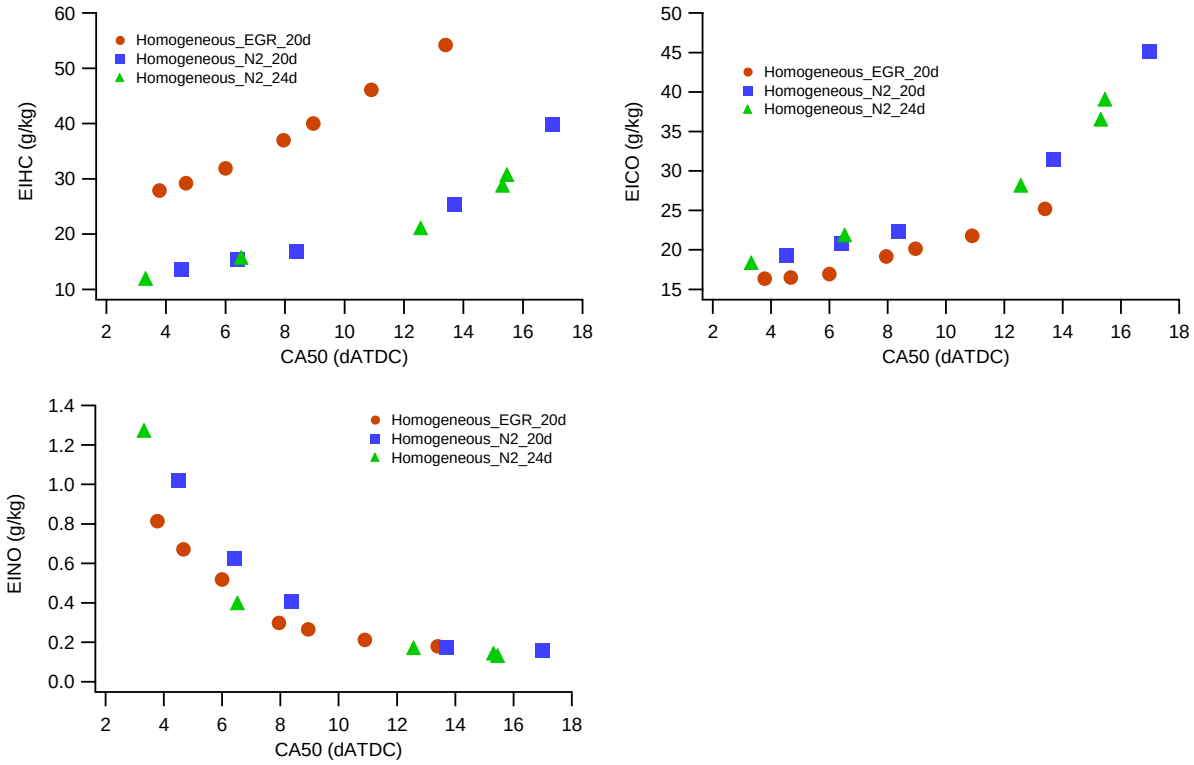

Figure 5-29 Emission Performance versus CA50

Differences in the combustion efficiency and emission indexes seen in Figures 5-27 through 5-29 can be attributed to the fact that experimental cases with operating windows located at higher intake charge temperature ranges achieve combustion at higher in-cylinder temperatures.

5.5.3– EGR Diluent Charge Stratification – Multiple Effects

EGR diluent experiments were performed at a single delivered charge air-fuel ratio of 20:1 with an average amount of EGR diluent of 40% of the total intake charge volume. This experimental EGR diluted case includes one fully homogeneous air, fuel and EGR diluent experimental case and a stratified diluent experimental. The experiment running conditions are presented below in Table 5-13.

Window Temperature Range	318-342°C
Air-fuel ratio "delivered"	20:1
Air-fuel ratio "trapped"	24:1
Fuel Mass Flow Rate	10mg/cycle
Air Mass Flow Rate	200mg/cycle
Diluent Type	EGR
Mean Diluent Percentage	40%
Diluent Mixing	Stratified
Charge Temperature Difference	0°C

Table 5-13 EGR Diluent Multiple Effects Experimental Parameters

As it can be observed in Figure 5-30 an operating temperature window shift of 33-34°C is established by the imposed stratified EGR charge effects.

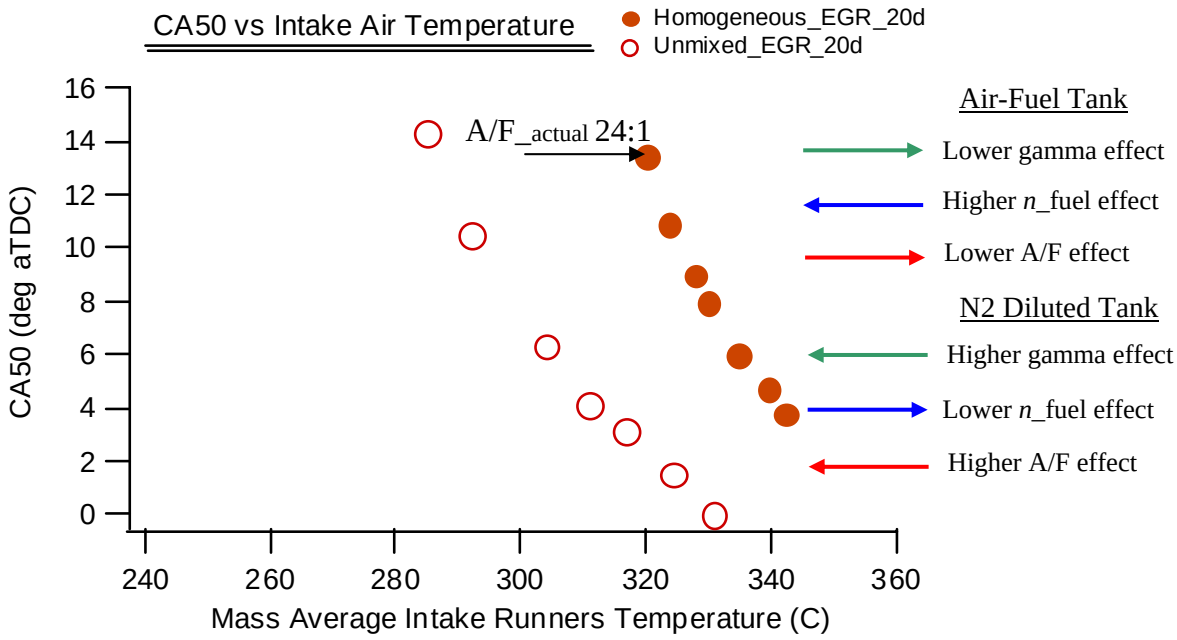

Figure 5-30 CA50 versus Mass Average Intake Charge Temperature

The analysis of this EGR stratification experimental case establishes that the non diluted homogeneous air and fuel mixture tank with an air-fuel ratio of 20:1 has a lower γ compared to the EGR diluted intake surge tank. This is a small difference in γ, which results in slight differences in the isentropic compression temperature, approximately 9°C. The main charge difference between the diluted and the non diluted tanks is their mixture air-fuel ratios and their fuel number densities. The non diluted, air, fuel and tank

introduces into the engine chamber a mixture with a higher fuel number density and a lower air-fuel ratio. Instead, the EGR diluted tank introduces into the engine a much leaner air-fuel ratio and a lower fuel number density. Details of local air-fuel ratios and isentropic compression temperature differences can be found in Table 5-14 below.

EGR Diluent Stratification Effects

Unmixed EGR diluent Case	**Specific Heat Ratio**				**Local AF** (24:1 trapped)				**Isentropic Temp. (rc = 7)**			
Delivered AF	**20:1**	**24:1**	**28:1**	**38:1**	**20:1**	**24:1**	**28:1**	**38:1**	**20:1**	**24:1**	**28:1**	**38:1**
AIR+FUEL (homog. mixture)	1.314				20				1055			
AIR+FUEL+EGR (diluted tank)	1.318				71				1064			

Table 5-14 Mixture Gamma, Trapped A/F and T_isentropic (C) Calculations

The effects imposed by differences in the spatial distribution of fuel, leaner air-fuel ratio zones and different γ zones help to distinguish the interactions that can advance the combustion phasing. For instance, combustion phasing can be advanced due to large energy release events (i.e. higher fuel number density zones). Same manner, the combustion phasing can be delayed due to a lower γ effect or leaner air-fuel ratio effect.

For this EGR diluent stratified case, the effect of air-fuel ratio is dominant. It is important to realize that both stratified charge regions do present competing effects on the combustion phasing. For instance, regions with large amounts of EGR have leaner air-fuel ratios and less fuel spatially distributed within the oxygen molecules, and vice versa for the non EGR diluted air and fuel mixture.

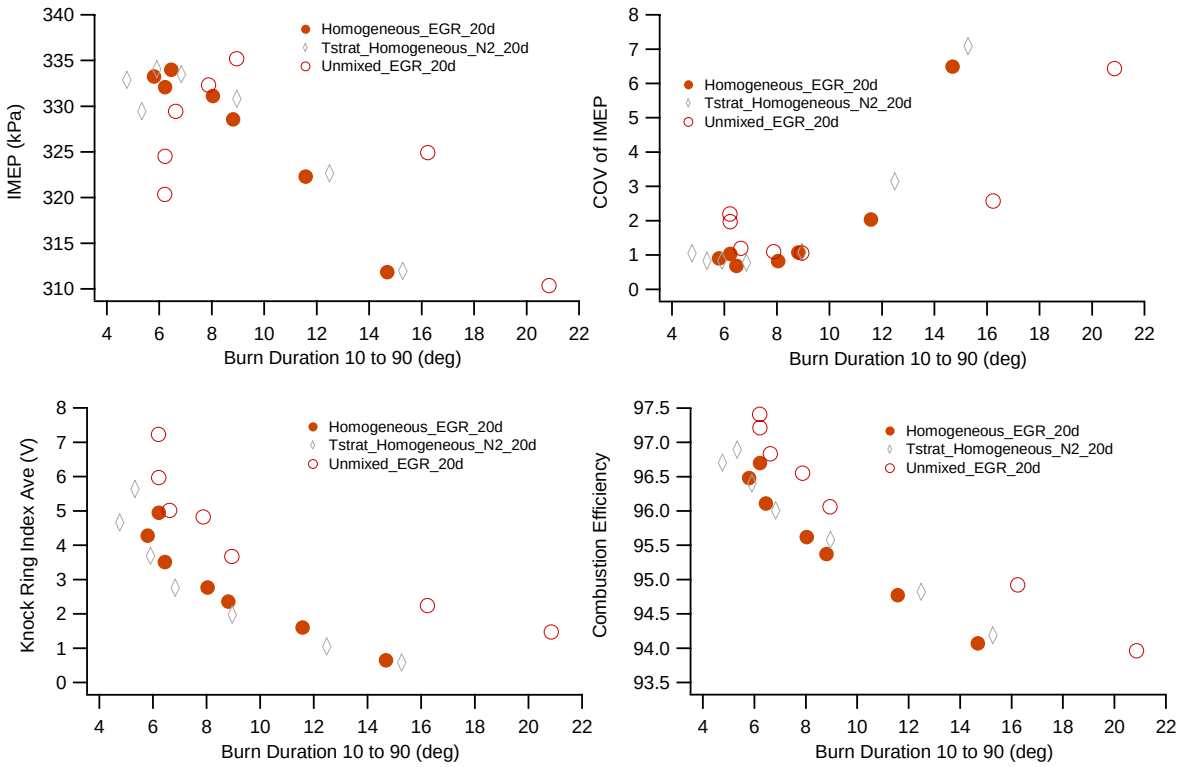

Figure 5-31 Combustion Performance versus CA90-10 angle

Figures 5-31, 5-32 and 5-33 show combustion, emission and phasing variables plotted against CA90-10 burn duration angle. It seems that regardless of which of the basics on which one compares engine performance, i.e. constant combustion efficiency or knock index, the CA90-10 burn duration angles tend to be 1-2 crank angle degrees longer for the EGR diluent stratified cases while compared against the EGR homogeneous baseline. This may explain the widening of the operating temperature window seen for the EGR diluent stratified case.

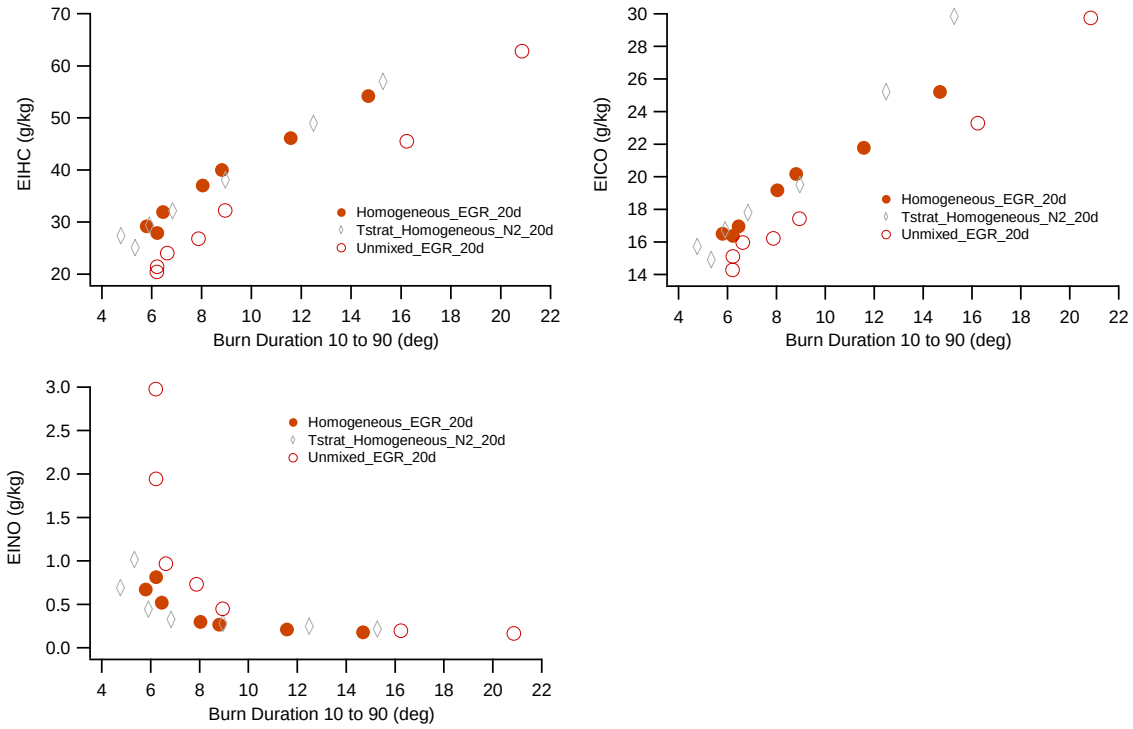

Figure 5-32 Emission Performance versus CA90-10 angle

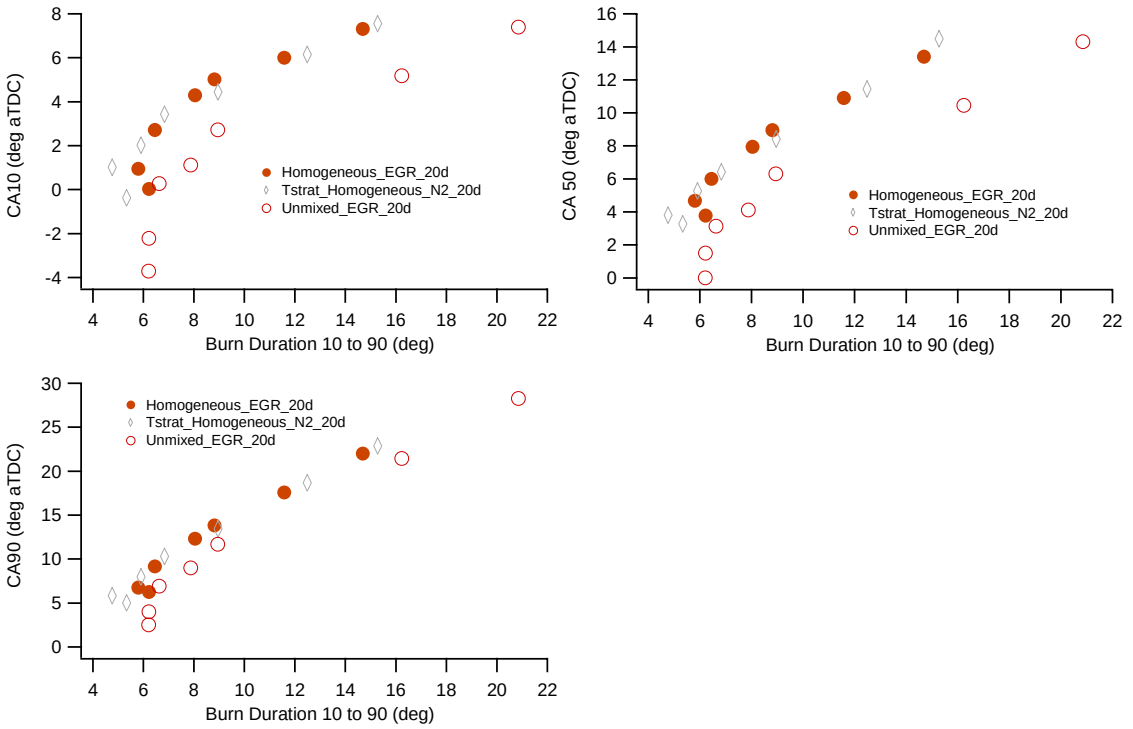

Figure 5-33 Combustion Phasing versus CA90-10 angle

5.5.4 – N2 Diluent Charge Stratification – Multiple Effects

The N2 gas diluent experiments were performed at charge air-fuel rations of 20:1, 24:1 and 28:1, which corresponded to N2 gas dilution of 45%, 35% and 25% of the total inducted charge volume respectively. All the cases maintained a fixed IMAP of ~1bar. Each case includes one fully homogeneous air, fuel and diluent case and its respective stratified diluent case at the same air-fuel ratio. For instance, the case with a mixture of air, fuel and N2 gas diluent at an air-fuel ratio of 20:1 imposes the largest stratified diluent effect on combustion timing due to the larger non-uniform N2 gas diluent spatial distribution (most of the intake second surge tank volume contains N2 gas diluent plus the small reminder of a air and fuel at an air-fuel ratio of 20:1). Table 5-15 describe details on the N2 gas diluent experimental cases run.

Window Temperature Range	302-327°C
Air-fuel ratio "delivered"	20:1, 24:1, 28:1
Air-fuel ratio "trapped"	20:1, 24:1, 28:1
Fuel Mass Flow Rate	10mg/cycle
Air Mass Flow Rate	200, 240, 280 mg/cycle
Diluent Type	N2
Mean Diluent Percentage	45, 35, 25 %
Diluent Mixing	Stratified
Charge Temperature Difference	0°C

Table 5-15 N2 Diluent Multiple Effects Experimental Parameters

Figures 5-34 through 5-36 present CA50 versus mass average intake temperature data comparison for N2 gas diluent homogeneous and stratified cases at air-fuel ratios of 20:1, 24:1 and 28:1.

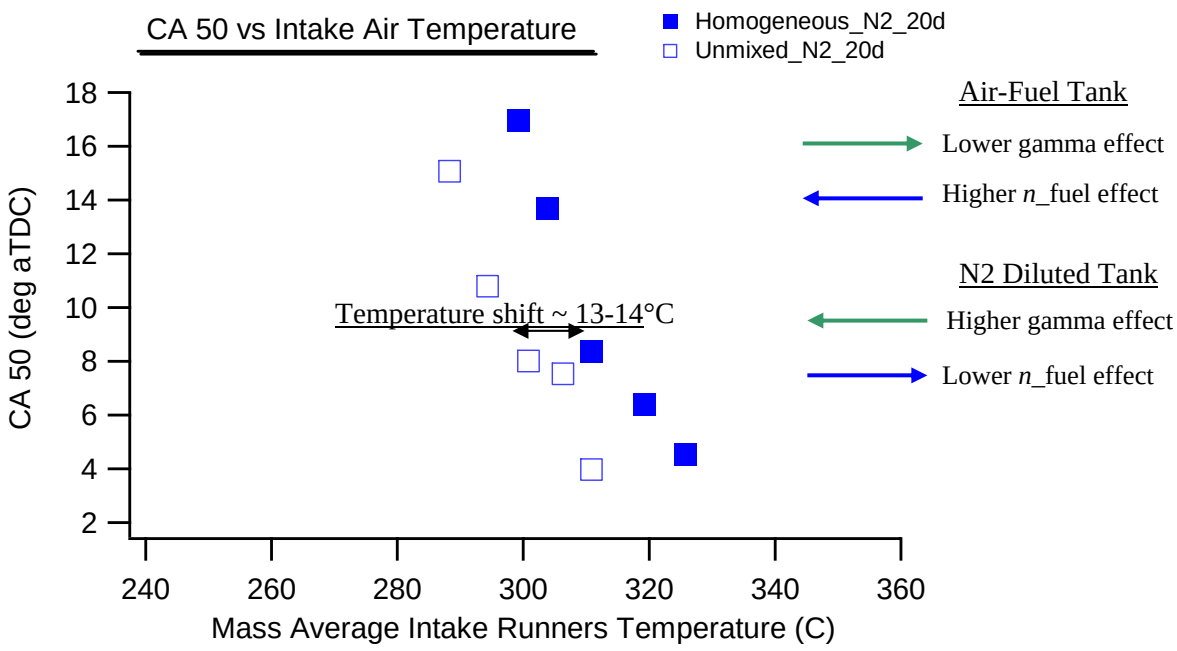

Figure 5-34 CA50 versus Mass Average Intake Charge Temperature

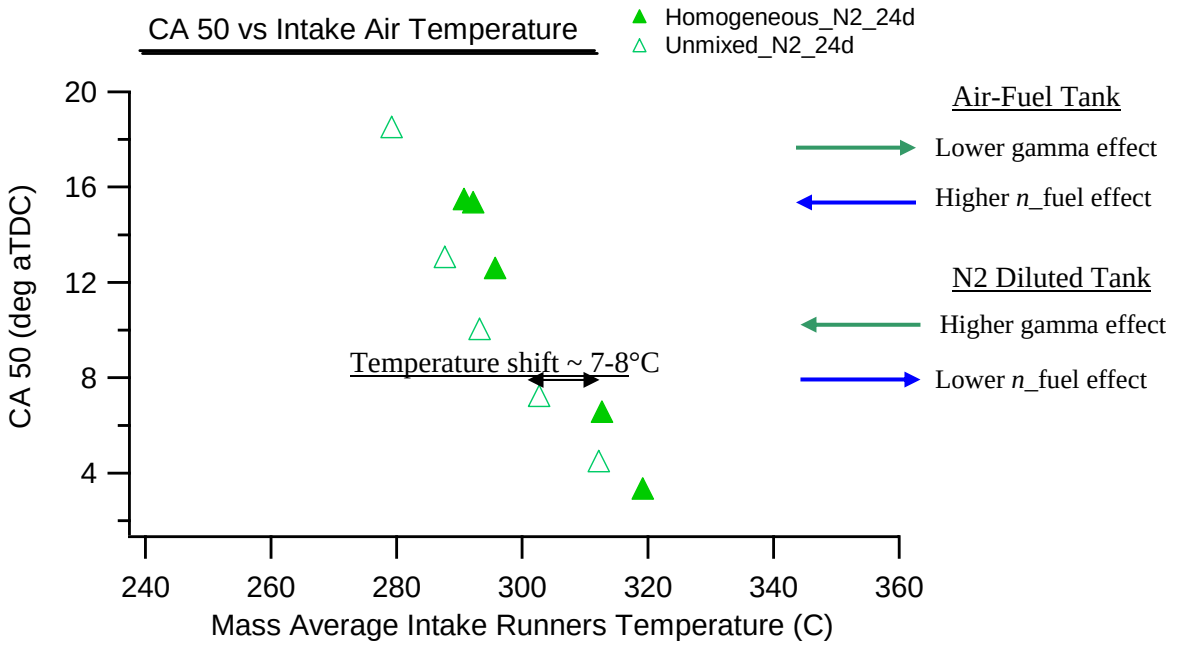

Figure 5-35 CA50 versus Mass Average Intake Charge Temperature

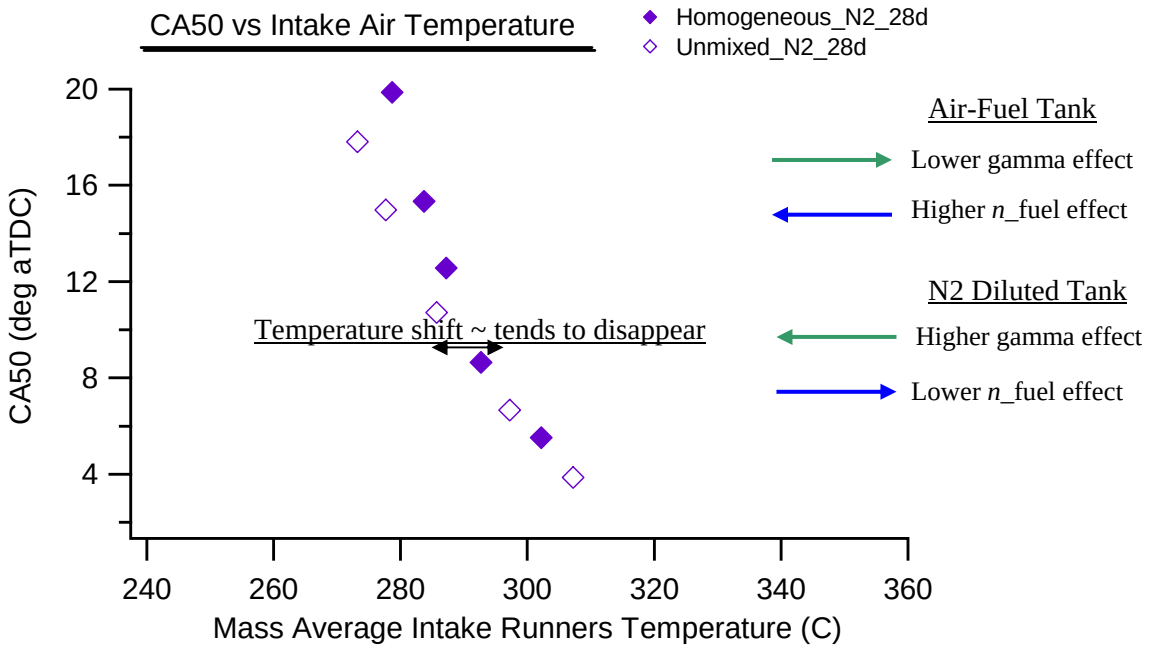

Figure 5-36 CA50 versus Mass Average Intake Charge Temperature

It is evident that the N2 gas diluent stratification effects resulted with a less pronounced shift on the operating temperature window than the EGR diluent stratification. In other words, a smaller ignition timing change was imposed by the N2 gas diluent stratification effect. The homogeneous air, fuel and N2 gas diluent mixtures did have a constant air-fuel ratio and gamma throughout the spatial fuel distribution. There was not an air-fuel ratio effect here as it was seen for the EGR diluent stratification cases, in which combustion phasing was very sensitive to changes in the air-fuel ratio.

N2 diluent Stratification Effects

Unmixed N2 Diluent Case	**Specific Heat Ratio**				**Trapped AF**				**Isentropic Temp. (rc = 7)**			
Delivered AF	**20:1**	**24:1**	**28:1**	**38:1**	**20:1**	**24:1**	**28:1**	**38:1**	**20:1**	**24:1**	**28:1**	**38:1**
AIR+FUEL (homog. mixture)	1.314	1.320	1.332		20	24	28		1055	1068	1078	
AIR+FUEL+N2 (diluted tank)	1.355	1.347	1.341		20	24	28		1144	1126	1114	

Table 5-16 Mixture Gamma, Trapped A/F and T_isentropic (C) Calculations

Nevertheless, the stratified charges with N2 did present unmixedness in the specific heat ratios. These differences in γ were larger for lower air-fuel ratio, N2 dilution cases. Similarly, as was discussed for the EGR diluent stratification cases, which contained two strong and competing stratification effects, fuel number density and air-fuel ratio; the N2 gas diluent stratification cases contain effects of unmixedness in γ and fuel number density, but not air-fuel ratio. The non diluted tank with a homogeneous air-fuel mixture had higher fuel number density with and a lower γ while the N2 gas diluted tank had a lower fuel number density and higher γ. The γ differences for the N2 diluted surge tank, approximated 3% for the air-fuel ratio of 20:1 case, this could potentially result in differences in isentropic compression temperature of 90°C, which would make the combustion phasing strongly sensitive to the differences in the mixtures γ. See Figures 5-34 through 5-36 for references.

Chapter 6 – Summary of Conclusions and Recommendations

6.1 – Summary of Conclusions

As Chapter 5 presented the different results and discussions drawn by the analysis of each of the experimental cases run, it would be very valuable to present a compact summary of results for each of the different set of experiments. Therefore, Table 6-1 was arranged to show details for each of the intake charge and diluent type strategies that were used to perform this research work and try to aid the understanding of how sensitive combustion performance, emission performance and combustion phasing variables were to charge stratification effects.

The individual effects that were identified to act in an interconnected manner to determined air, fuel and diluent mixture auto-ignition timings were: air-fuel ratio effects, spatial distributions of non-uniform specific heat ratios, spatial distributions of non-uniform fuel number densities and thermal differences throughout the mixtures. All of these listed effects can contribute to changes on the combustion phasing, hence defining different intake charge temperatures at fixed combustion phasings. Therefore, and as it was shown throughout the presentation of experimental results, these effects can be found in particular experimental cases as single effects, or dual effects combined with a second effect or multiple effects. Each of the experimental cases and the most relevant investigated intake charge effects are shown in the following experiment effects and degree of effects sensitivity table.

Row Reference	Experimental Cases	A/F_delieverd, Mixture and Diluent Type	Intake Charge Stratification Individual Effects: A/F_trapped	Gamma	DT or Isent. Comp. Temp.[°C]	N_fuel [mg/charge]	N_diluent [vol_%]	Temp. Window Shift [°C]	Temp. Window Width [°C]
	Single Effect Cases								
R-1	*Homogeneous N2_baseline*	20:1_Air_Fuel_N2	20:1	1.333	1096	10mg/cycle	45%	0	22°C
R-2	Homogeneous N2	24:1_Air_Fuel_N2	24:1	1.333	1096	10mg/cycle	35%	9-10	23°C
R-3		28:1_Air_Fuel_N2	28:1	1.333	1095	10mg/cycle	25%	18-19	24°C
R-4		38:1_Air_Fuel	38:1	1.332	1094	10mg/cycle	0%	46-48	25°C
R-5	*Homogeneous EGR_baseline*	20:1_Air_Fuel_EGR	24:1	1.316	1059	10mg/cycle	40%	0	20°C
R-6	Homogeneous N2	24:1_Air_Fuel_N2	24:1	1.333	1096	10mg/cycle	35%	24-25	24°C
R-7	Homogeneous EGR_with	20:1_Air_Fuel_EGR	24:1	1.316	30 (delta	10mg/cycle	40%	4-5	20°C
R-8	Temperature Stratification				temperature)				
	Dual Effect Cases								
R-9	*Homogeneous EGR_baseline*	20:1_Air_Fuel_EGR	24:1	1.316	1059	10mg/cycle	40%	0	20°C
R-10	Homogeneous N2	20:1_Air_Fuel_N2	20:1	1.333	1096	10mg/cycle	45%	19-20	22°C
	Multiple Effect Cases								
R-11	*Homogeneous N2_baseline*	20:1_Air_Fuel_N2	20:1	1.333	1096	10mg/cycle	45%	0	22°C
R-12	Stratified N2 [Air-Fuel tank	20:1_Air_Fuel	20:1	1.314	1055	9.1mg/cycle	0%	13-14	23°C
R-13	mixture vs Diluted Tank mixture]	20:1_Air_Fuel_N2	20:1	1.355	1144	0.9mg/cycle	90%		
R-14	*Homogeneous N2_baseline*	24:1_Air_Fuel_N2	24:1	1.333	1096	10mg/cycle	35%	0	23°C
R-15	Stratified N2 [Air-Fuel tank	24:1_Air_Fuel	24:1	1.32	1068	7.7mg/cycle	0%	7-8	26°C
R-16	mixture vs Diluted Tank mixture]	24:1_Air_Fuel_N2	24:1	1.347	1126	2.3mg/cycle	70%		
R-17	*Homogeneous N2_baseline*	28:1_Air_Fuel_N2	28:1	1.333	1095	10mg/cycle	25%	0	24°C
R-18	Stratified N2 [Air-Fuel tank	28:1_Air_Fuel	28:1	1.332	1078	6.7mg/cycle	0%	3-4	28°C
R-19	mixture vs Diluted Tank mixture]	28:1_Air_Fuel_N2	28:1	1.341	1114	3.3mg/cycle	50%		
R-20	*Homogeneous EGR_baseline*	20:1_Air_Fuel_EGR	24:1	1.316	1059	10mg/cycle	40%	0	20°C
R-21	Stratified EGR [Air-Fuel tank	20:1_Air_Fuel	20:1	1.314	1055	8.3mg/cycle	0%	33-34	29°C
R-22	mixture vs Diluted Tank mixture]	20:1_Air_Fuel_EGR	71:1	1.318	1064	1.7mg/cycle	80%		
		Column Reference	C-1	C-2	C-3	C-4	C-5	C-6	C-7

Table References:

-Cells highlighted in **red** indicate that the combustion auto-ignition was considerably sensitive to the particular effect.

-Cells highlighted in **orange** indicate that the combustion auto-ignition was less sensitive to the particular effect.

-Cells highlighted in **yellow** indicate that the combustion auto-ignition was not that sensitive to the particular effect.

Table 6-1 Experiment stratification charge effects and degree of effects sensitivity

It will be mentioned later the main details and conclusions throughout each of the experimental cases. Explanations will be presented by starting off with single charge effect cases, continuing through dual effect cases and finally presenting the diluent stratification cases which were established to hold multiple charge stratification effects.

The first set of experiments corresponding to the experimental matrix details listed in Table 5-6 dealt with the effect of air-fuel ratio on combustion phasing. As it was pointed out on Table 6-1, the effect of increasing the air-fuel ratio of the homogeneous air, fuel and N2 gas diluent mixtures was the single distinctive effect between each of these experimental cases. The last column in Table 6-1 showed the magnitude of the operating window shift for these cases (all negative temperature shifts), achieving a maximum downward temperature shift of approximately 47°C between cases with a less lean air-fuel ratio of 20:1 and the leanest air-fuel ratio case of 38:1. The conclusions drawn out of these experiments were that air-fuel ratio does affect the start of ignition or combustion phasing, and once ignition is triggered the process continues without showing any other combustion or emission performance changes. Combustion phasing sensitivity to air-fuel ratio changes was very high, hence causing very noticeable shifts on the operating temperature window.

The second set of experiment detailed in Table 6-1 which corresponds to the thermal charge stratification effects will be described as follows. Experiment running conditions for this set of experiments can be found in Table 5-2. A temperature operating window shift of approximately 4-5°C was observed between the homogeneous temperature and composition data set and the temperature stratification data set. This temperature shift caused by an imposed intake charge temperature difference of 30°C

resulted to be quite mild, while compared against the temperature shift achieved by imposing EGR diluent charge stratification. Nevertheless, it is important to keep in mind that maximum intake charge streams temperature difference was limited by hardware restrictions and the very high intake charge temperature required to achieving HCCI combustion. Therefore, it can be concluded that non-uniform spatial distribution of charge thermal gradients does affect combustion phasing, thus reducing the required intake charge temperature for a fixed ignition timing.

The third set of experiments corresponding to the experimental matrix details listed in Table 5-9 dealt with the single effect of specific heat ratio on combustion phasing. As it was pointed out on Table 6-1, the effect of the mixtures specific heat ratios was quite different depending on the value of γ for each case. Both mixtures were homogeneous mixtures of air, fuel and diluent and held an equal trapped air-fuel ratio of 24:1. The EGR diluted case with a lower γ (1.316) than the N2 gas diluted case (1.333) ended up resulting with an isentropic gas temperature 40°C lower than the γ converted isentropic compression temperature for the N2 gas diluent case. Therefore, it can be concluded that the specific heat ratio of the mixture affects the ignition timing through the change of isentropic compression temperature. It is also shown that the sensitivity to changes γ is very important; temperature shifts of up to 25°C were observed by just imposing a 40°C difference in the γ isentropic compression temperature. Mixtures with higher γ started ignition at lower intake temperatures for a fixed combustion temperature, and vice versa for cases with lower γ.

Continuing now through the set of experiments within the dual charge stratification effects category, it can be said that as the delivered air-fuel ratio of the air,

fuel and diluents (N2 gas diluent and EGR diluent cases) is matched, the effect of less lean air-fuel ratio mixture for the N2 gas diluent case affects the combustion phasing to counteract the effect exerted by the mixture's lower γ. Therefore, the required intake charge temperatures tend to experience a narrower temperature shift for these cases. With EGR as diluent the mixture trapped air-fuel ratio increases which decreases the required intake charge temperature for a fixed combustion phasing; although γ decreases which converts to a lower isentropic compression temperature requiring a higher intake charge temperature for a fixed combustion phasing. Regardless of the increase of the amount of N2 gas diluent and/or the decrease on air-fuel ratio, the isentropic compression temperature has been maintained constant. Experiment running conditions for these cases were shown in Table 5-10.

Following cases within the multiple charge stratification effects category will be presented.

The first set of experiment dealt with N2 gas diluent stratification cases. Experiment running conditions for these cases can be found in Table 5-15. These N2 gas diluent experiments were performed at three different charge air-fuel ratios of 20:1, 24:1 and 28:1 with amounts of N2 gas diluent equal to 45%, 35% and 25% of the total charge volume respectively. The stratified charge delivered from the no diluted intake surge tank is conformed by a homogeneous mixture of air and fuel at the delivered air-fuel ratio. Meanwhile, the second stratified charge delivered from the second and N2 gas diluted EGR tank was mainly N2 gas, although decreasing amounts of diluent were applied as the delivered air-fuel ratios increased. The main effects through out the stratified charges were determined by differences on the specific heat ratios and non-uniform spatial

distributions of fuel. These differences in γ between the stratified charges were larger for lower air-fuel ratio N2 gas diluent cases. Similarly as it was mentioned for the EGR diluent stratification cases which held two strong and competing stratification effects, fuel number density and air-fuel ratio; the N2 gas diluent stratification cases presented no air-fuel ratio effects, but as mentioned earlier γ and fuel number density effects. The no N2 gas diluted tank with a homogeneous air-fuel mixture had higher fuel number density with a lower γ, instead the N2 gas diluted tank had a lower fuel number density and higher γ. The γ differences of up to more than 3% for the N2 gas diluent case with a air-fuel ratio of 20:1 were converted into a difference in isentropic compression temperature of 90°C, making the combustion phasing to be strongly sensitive to the differences in mixtures γ.

The second set of experiments which introduces multiple charge stratificstion effects by the delivery of two stratified intake charges; one charge stream which contains just air and fuel at the delivered air-fuel ratio and a second charge stream which contains mainly EGR diluent with a remainder of fuel and air. The effects imposed by differences in the spatial distribution of fuel, leaner air-fuel ratio zones and different γ zones seems to define non-uniform charge characteristic zones in the chamber with combined and interconnected effects that may advance the combustion phasing due to large energy release events (i.e. higher fuel number density zones, leaner air-fuel ratios and larger mixture γ) or retard the combustion phasing due to a lower γ effects or leaner air-fuel ratio effects or larger non-uniform spatial distribution of EGR diluent.

For this EGR diluent stratified case, the effect of air-fuel ratio is very considerable. Although, it’s important to mention that both stratified charge regions do

present competing effects on the combustion phasing. For instance, regions with large amounts of EGR have leaner air-fuel ratios and less fuel spatially distributed through the oxygen molecules, and vice versa for the no EGR diluent air and fuel mixture. γ effects were considered to be mild; isentropic compression temperature calculations from mixtures γ showed small differences as the EGR diluted charge stream and air-fuel charge stream specific heat ratios are very much equal.

The following arrangement of detailed list of conclusions presents a compact layout of the conclusions extracted out of this HCCI research work. Numerical and quantitative details can be found in Table 6-1.

1- Combustion phasing is sensitive to thermal and diluent stratification effects.

2- Combustion event was a unique function of Combustion Phasing CA50.

3- With thermal charge stratification, combustion advances at a fixed mass average intake temperature.

4- With diluent stratification, combined effects take place to modify ignition timing.

4a- Stratified charge effects such as A/F, Non-uniform Spatial Distribution of Mixture Gamma, Fuel and Diluent are all interconnected.

4a(i)- Higher gamma, hence higher mixture compression temperatures advances the overall combustion timing, thus requiring a lower intake temperature.

4a(ii)- Leaner A/F advances the overall combustion timing, thus requiring a lower intake temperature.

4aa(i)- Lower intake temperature decreases the temperature of the burning charge.

4b- EGR diluted zones hold much leaner A/F, slightly higher gamma and lower fuel number density than non diluted air-fuel zones.

4b(i)- Competing effects like leaner A/F and lower fuel number density counteract each other to mitigate the offset on the effect on combustion timing.

4b(ii)- As combustion is advanced by the effect of EGR stratification, 33-34°C lower intake temperatures than the homogeneous EGR case were needed to maintain combustion metrics within the desired ranges. This is believed to be caused when the high non-uniform O2 number density effect is imposed by EGR stratification.

4b(iii)- A widening of ~10°C on the operating temperature window was observed for the EGR stratification case compared against the homogeneous EGR case. This is believed to be caused by a small increase on the CA90-10 angle related qualitatively to lower non-uniform gamma distributions imposed by EGR stratification.

4c- N2 diluted zones have considerably higher gamma and lower fuel number density (less decrease on mixture gamma) than non diluted air-fuel zones (lower mixture gamma due to fuel presence).

4c(i)- Competing effects like higher spatial distribution of gamma and lower fuel number density counteract each other to mitigate the offset on the effect on combustion.

4c(ii)- Less pronounced temperature window shifts within the N2 gas diluent stratification cases were observed as fuel number density and gamma effects started to disappear as mixture air-fuel ratio increased (Engine IMAP ~1bar is held constant).

A small decrease on EINO and Combustion Efficiency, and small increase on EIHC and EICO were observed for cases with lower intake charge temperatures.

4a(iii)- Higher fuel number density zones advance the combustion timing, thus requiring a lower intake temperature.

6.2 – Summary of Recommendations

As it was previously explained throughout the experimental setup sections, the engine intake port and intake manifold setup used to deliver into the combustion chamber fully stratified intake charges seemed to perform fairly well, nevertheless as flow field data of the combustion chamber mixture acquired on the GM optical engine shows, there is a considerable and very effective mixing occurring through the last stages of the engine's compression stroke. These data was acquired by Randy Herold on the GM Optically Accessible Gasoline HCCI engine while performing investigations on the in-cylinder mixture charge bulk unmixedness by applying Planar Laser Induced Fluorescence techniques. The results showed that effective intake charge stratification is achieved at earlier stages of the intake stroke, nonetheless the flow field evolution as the intake and compression strokes progress is quite considerable resulting in a uniform unmixed charge. Figure 6-1 below shows the evolution of the flow field as the charge induction and compression strokes are being completed. Darker regions in each of the single images can be taken as reference for tracking the mixing of EGR diluted charge stream with the brighter image regions which corresponded to air-fuel non diluent stream.

Image Location	Mean	Image Location	Mean
330 bTDC		180 bTDC	
315 bTDC		135 bTDC	
270 bTDC		90 bTDC	
225 bTDC		45 bTDC	
180 bTDC		30 bTDC	

Figure 6-1 In-cylinder Flow Field Evolution

Therefore, one of the recommendations that may help resolved with better accuracy the effects of intake charge stratification on combustion and emission performance would be to use an approach in the metal engine that could promote the unmixedness of the charges through the induction and compression engine strokes. It would be also valuable to evaluate different techniques that impose effects on the inducted intake charge, which promote less mixing in the chamber. Mixing index parameters calculated from flow field data acquired in the optical engine could then be compared against the different approaches, hence to establish different engine intake port and charge delivery strategies that would provide different levels of achievable charge unmixedness at the start of combustion.

Secondly, it is believed that the strong sensitivity of combustion phasing to the EGR diluent charge stratification effects could be probably investigated further by leveraging on the triggering of the ignition timing by imposing thermal gradients throughout the EGR diluted and/or air-fuel non diluent charge streams. It has been found that slight changes on the CA90-10 combustion duration angles were present while imposing EGR diluent stratification effects throughout combustion, emissions and combustion phasing variables at a fixed CA50 combustion phasing.

The experimental results presented in Table 6-1 define an arrangement of data that establishes which of the intake charge effects took place within an experiment, and the HCCI operating temperature window changes that are observed as these effects take place to vary the start of ignition. Nevertheless, there are single effect experiments; it is not that straight forward to compare single effect cases against dual or multiple effect cases to asses more accurately the temperature shifts found. Therefore, it would extremely useful to have a sort of parameter that quantifies the non-uniform spatial fuel distribution for the diluent stratified cases. This extra parameter would allow to asses with more detail the magnitude of each of the stratified charge competing effects and the resultant intake charge temperature tendencies. For instance, a study on the changes in operating temperature window width and shift (Parameter 1) could be characterized by changes on single charge effect (Parameter 2) to then compare these relative changes against the different experimental cases.

BIBLIOGRAPHY

1. United States Environmental Protection Agency, “Global Warming – Climate”, http://yosemite.epa.gov/oar/globalwarming.nsf/content/climate.html, 2000.

2. Sher, E., Handbook of Air Pollutions from Internal Combustion Engines – “Pollution Formation and Control”, 1st edition, Academic Press, Chestnut Hilll, MA, 1998.

3. Ellinger, R., Meitz,K., Prenninger,P., Salchenegger,S., Brandstaetter, W., “Comparison of CO_2 Emission Levels for Internal Combustion Engine and Fuel Cell Automotive Propulsion Systems”, SAE Paper 2001-01-3751, 2001.

4. Weiss, M., “Comparative Assessment of Fuel Cell Cars, Report MIT LFEE”, 2003-001 RP, Laboratory for Energy and the Environment, MIT, http://lfee.mit.edu/publications/, 2003.

5. Stanglmaier, R. and Roberts, C., “Homogeneous Charge Compression Ignition (HCCI): Benefits, Compromises, and Future Engine Applications”, SAE Paper 1999-01-3682, 1999.

6. Koopmans, L., Wallesten, J., Ogink, R., Denbratt, I., “Location of the First Auto-Ignition Sites for Two HCCI Systems in a Direct Injection Engine”, SAE Paper 2004-01 - 0564, 2004.

7. Koopmans, L. and Denbratt, I., “Cycle to Cycle Variations: Their Influence on Cycle Resolved Gas Temperature and Unburned Hydrocarbons from a Camless Gasoline Compression Ignition Engine”, SAE Paper 2002-01-0110, 2002.

8. Najt, P.M., “Compression Ignition Homogeneous Charge Combustion”, M.S. Thesis, Mechanical Engineering Department, University of Wisconsin - Madison, 1981.

9. Iverson, R.J., “The Effects of Intake Charge Preheating and Charge Stratification on HCCI Combustion”, M.S. Thesis, Mechanical Engineering Department, University of Wisconsin – Madison, 2004.

10. Milovanovic, N. and Chen, R., "A Review of Experimental and Simulation Studies on Controlled Auto-Ignition Combustion", SAE Paper 2001-01-1890, 2001.

11. Reuss, D., Eng, J, Najt, P. Personal Communication. GM Research Labs.

12. Kakuho, A., Nagamine, M., Amenomori, Y., Urushihara, T., Itoh, T., “In-Cylinder Temperature Distribution Measurements and Its Application to HCCI Combustion”, SAE Paper 2006-01-1202, 2006.

13. Sjoberg, M., Dec, J.E., Cernansky, N.P., “Potential of Thermal Stratification and Combustion Retard for Reducing Pressure-Rise Rates in HCCI Engines, Based on Multi-Zone Modeling and Experiments”, SAE Paper 2005-01-0113, 2005.

14. Tominaga, R., Morimoto, S., Kawabata, Y., Matsuo, S., Amano, T., “Effects of Heterogeneous EGR on the Natural Gas Fueled HCCI Engine Using Using Experiments, CFD and Detailed Kinetics”, SAE Paper 2004-01-0945, 2004.

15. Aroonsrisopon, T., Werner, P., Waldman, J.O., Sohm, V., Foster, D.E., Morikawa, T., and Iida, M., "Expanding the HCCI Operation with the Charge Stratification", SAE Paper 2004-01-1756, 2004.

16. Amano, T., Morimoto, S., Kawabata, Y., “Modeling of the Effect of Air/Fuel Ratio and Temperature Distribution on HCCI Engines”, SAE Paper 2001-01-1024, 2001.

17. Noda, T. and Foster, D., “A Numerical Study to Control Combustion Duration of Hydrogen-Fueled HCCI by Using Multi-zone Chemical Kinetics Simulation”, SAE Paper 2001-01-0250, 2001.

18. Richter, M., Engstrom, J., Franke, A., Alden, M., Hultqvist A., and Johansson, B., "The Influence of Charge Inhomogeneity on the HCCI Combustion Process", SAE Paper 2000-01-2868, 2000.

19. Dec, J.E., Hwang, W., Sjoeberg, M., “An Investigation of Thermal Stratification in HCCI Engines Using Chemiluminescence Imaging”, SAE Paper 2006-01-1518, 2006.

20. Grenda, J.M., “Numerical Modeling of Charge Stratification for the Combustion Control of HCCI Engines”, SAE Paper 2005-01-3722, 2005.

21. Babajimopoulos, A., Lavoie, G.A., Assanis, D.N., “Modeling HCCI combustion with high levels of residual gas fraction ~A comparison of two VVA strategies”, SAE Paper 2003-01-3220, 2003.

22. Flowers, D.L., Aceves, S.M., Babajimopoulos, A., “Effect of Charge Non-Uniformity on Heat Release and Emissions in PCCI Engine Combustion”, SAE Paper 2006-01-1363, 2006.

23. Hiraya, K., Hasegawa, K., Urushihara, T., Liyama, A., Itoh, T., “A Study on Gasoline Fueled Compression Ignition Engine ~ A Trial of Operation Region Expansion ~”, SAE Paper 2002-01-0416, 2002.

24. Christensen, M., Hultqvist, A., Johansson, B., “Demonstrating the Multi Fuel Capability of a Homogeneous Charge Compression Ignition Engine with Variable Compression Ratio”, SAE Paper 1999-01-3679, 1999.

25. Cairns, A., Blaxill, H., “The Effects of Combined Internal and External Exhaust Gas Recirculation on Gasoline Controlled Auto-Ignition”, SAE Paper 2005-01-0133, 2005.

26. Kumano, K., and Iida, N., “Analysis of the Effect of Charge Inhomogeneity on HCCI Combustion by Chemiluminescence Measurement”, SAE Paper 2004-01-1902.

27. Aceves, S., Martinez-Frias, J., Flowers, D., Smith, J. R., Dibble, R.W., Wright, J.F., Hessel, R.P., “A Decoupled Model of Detailed Fluid Mechanics Followed by Detailed Chemical Kinetics for Prediction of Iso-Octane HCCI Combustion”, SAE Paper 2001-01-3612, 2001.

28. Dec, J., “A Computational Study of the Effects of Low Fuel Loading and EGR on Heat Release Rates and Combustion Limits in HCCI Engines”, SAE Paper 2002-01-1309, 2002.

29. Christensen, M., and Johansson, B., “Influence of Mixture Quality on Homogeneous Charge Compression Ignition”, SAE Paper 982454, 1998.

30. Koopmans, L., Stroemberg, E., Denbratt, I., “The Influence of PRF and Commercial Fuels with High Octane Number on the Auto-ignition Timing of an Engine Operated in HCCI Combustion Mode with Negative Valve Overlap”, SAE Paper 2004-01-1967, 2004

31. Reuss, D. L., Sick, V., “Inhomogeneities in HCCI Combustion: An Imaging Study”, SAE Paper 2005-01-2122, 2005.

32. Aleiferis, P.G., Charalambides, A.G., Hardalupas, Y., Taylor, A.M., Urata, Y., “Modelling and Experiments of HCCI Engine Combustion with Charge Stratification and Internal EGR”, SAE Paper 2005-01-3725, 2005.

33. Sjoeberg, M., Dec., J.E., Babajimopoulos, A., Assanis, D.N., “Comparing Enhanced Natural Thermal Stratification Against Retarded Combustion Phasing for Smoothing of HCCI Heat-Release Rates”, SAE Paper 2004-01-2994, 2004.

34. Lancaster, D.R., Krieger,R.B., and Lienesch, J.H., "Measurement and Analysis of Engine Pressure Data", SAE Paper 750026, 1975.

35. Eng, J.A., "Characterization of Pressure Waves in HCCI Combustion", SAE Paper 2002-01-2859, 2002.

36. Davis, R.S. and Patterson, G.J., “Cylinder Pressure Data Quality Checks and Procedures to Maximize Data Accuracy”, SAE Paper 2006-01-1346, 2006.

37. Glassman, I., Combustion, 3rd Edition, Academic Press, Orlando, CA, 1996.

38. Heywood, J.B., Internal Combustion Engine Fundamentals, McGraw-Hill, Inc., New York, NY, ISBN 0-07-028637-X, 1988.

Appendix A –Computer Codes

A.1 Engine Intake Charge Mixture Specific Heat Ratio and A/Fs Calculations

Note: n_N2 parameter EES code calculations is shown in Appendix B.4.

```
n_fuel=1;                                   m_fuel=n_fuel*molarmass(C8H18)
m_air/m_fuel=AF;                            m_air=n_air*molarmass(Air)
T=500 "degrees C"

cp_air=cp(air,T=T);                         gamma_air=cp_air/(cp_air-R#)
cp_fuel=cp(C8H18,T=T);                      gamma_fuel=cp_fuel/(cp_fuel-R#)
cp_airfuel=(n_air*cp_air+n_fuel*cp_fuel)/(n_air+n_fuel);
gamma_airfuel=cp_airfuel/(cp_airfuel-R#)

{x_co2=1;                                   x_o2=1;;
x_H20=1;                                    name$='dd'}
xco2=x_co2/100;
xo2=x_o2/100;
xH2O=x_H2O/100
x_co=0;
x_HC=0;
x_NO=0;
x_H2=0;
x_n2ex=1- xco2 -xo2 -xH2O

n_total=n_EGR+n_fuel+n_air+n_N2*n_air/4.76
PercentEGR/100=n_EGR/n_total
PercentN2/100=n_N2*n_air/4.76/n_total

cp_EGR=xco2*cp(CO2,T=T)+xO2*cp(O2,T=T)+xH2O*cp(H2O,T=T)+x_n2ex*cp(N2,T=T);
gamma_EGR=cp_EGR/(cp_EGR-R#)

cp_mix=(n_air*cp_air+n_fuel*cp_fuel+n_EGR*cp_EGR+n_N2*n_air/4.76*cp(N2,T=T))/n_total
gamma_mix=cp_mix/(cp_mix-R#)

cp_dilutedtank=(percentEGR*cp_EGR+percentN2*cp(N2,T=T)+(50-percentEGR-
percentN2)*cp_airfuel)/0.5/100
gamma_dilutedtank=cp_dilutedtank/(cp_dilutedtank-R#)

AF_st=12.5*4.76*molarmass(Air)/molarmass(C8H18)
AF_mix=(0.21*n_air+n_EGR*xo2)*molarmass(O2) / (n_fuel*molarmass(C8H18)) /
(12.5*molarmass(O2)/molarmass(C8H18)) *AF_st
AF_dilutedtank=(0.21*(50-percentEGR-percentN2)/100*n_air+n_EGR*xo2)*molarmass(O2) /
(n_fuel*(50-percentEGR-percentN2)/100*molarmass(C8H18)) /
(12.5*molarmass(O2)/molarmass(C8H18)) *AF_st

T_IVC=273+300;                              rc=7
T_mix=T_IVC*rc^(gamma_mix-1);
T_airfuel=T_IVC*rc^(gamma_airfuel-1);
T_dilutedtank=T_IVC*rc^(gamma_dilutedtank-1);
```

-Case Results:

	Input Parameters				
	Mol number		*Mol fraction*		
Case Name	n_total	n_N2	x_CO2	x_H2O	x_O2
Homogeneous_EGR_20	137.7	0	10.43	11.79	5.83
Unmixed_EGR_20	137.7	0	10.46	11.83	5.699
Tstrat_Homogeneous_EGR_20	137.7	0	10.29	11.64	6.036
Homogeneous_N2_20	145.8	3.981	5.45	6.18	3.44
Homogeneous_N2_24	147.3	2.598	5.42	6.15	5.75
Homogeneous_N2_28	148.1	1.581	5.15	5.85	8.09
Homogeneous_N2_38	150.9	0	5.18	5.88	13.18
Unmixed_N2_20	145.8	3.981	5.39	6.11	3.35
Unmixed_N2_24	147.3	2.598	5.43	6.16	5.75
Unmixed_N2_28	148.1	1.581	5.26	5.97	8.05

	Calculated Parameters						
	Specif Heat Ratios				*Isentropic Compression Temperature [C]*		
Case Name_Diluet_A/Fdelivered	Air-Fuel	HomogeneousMixture	DilutedMixture	EGR	T_isent_airfuel	Thomog.mixture	Tdil.mixture
Homogeneous_EGR_20	1.314	1.3158	1.318	1.319	1055	1059	1064
Unmixed_EGR_20	1.314	1.3158	1.318	1.319	1055	1059	1064
Tstrat_Homogeneous_EGR_20	1.314	1.316	1.318	1.319	1055	1060	1065
Homogeneous_N2_20	1.314	1.3332	1.355	1.337	1055	1096	1144
Homogeneous_N2_24	1.32	1.3331	1.347	1.337	1068	1096	1126
Homogeneous_N2_28	1.325	1.3328	1.341	1.337	1078	1095	1114
Homogeneous_N2_38	1.332	1.3324	1.332	1.336	1094	1094	1094
Unmixed_N2_20	1.314	1.3332	1.355	1.338	1055	1096	1144
Unmixed_N2_24	1.32	1.3331	1.347	1.337	1068	1096	1126
Unmixed_N2_28	1.325	1.3328	1.341	1.337	1078	1095	1114

	Calculated Parameters		*Input Parameters*		
	Air-Fuel Ratio			*Diluent Percent*	
Case Name	A/F_amixture	A/F_dil.mixture	A/F_delivere	N2_vol%	EGR_vol%
Homogeneous_EGR_20	24.06	70.87	2.00E+01	4.86E-12	42
Unmixed_EGR_20	23.97	69.72	20	0	42
Tstrat_Homogeneous_EGR_20	24.21	72.67	20	0	42
Homogeneous_N2_20	19.99	19.99	20	45.23	0
Homogeneous_N2_24	23.99	23.99	24	35.07	0
Homogeneous_N2_28	27.99	27.99	28	24.77	0
Homogeneous_N2_38	37.98	37.98	3.80E+01	4.44E-11	0
Unmixed_N2_20	19.99	19.99	20	45.23	0
Unmixed_N2_24	23.99	23.99	24	35.07	0
Unmixed_N2_28	27.99	27.99	28	24.76	0

A.2 EES Heat Release Code

```
{!SINGLE ZONE HEAT RELEASE CALCULATOR}
{Developed by: J.B. Ghandhi
Modifications:
  V9 (25 October 2004, R.E. Herold):  Modified calculation of trapped mass by making EGR an input and using Yun and Mirsky model to estimate internal residuals
  V10 (4 May 2006, R.E. Herold):  Modified solution routine.
  The program now integrates the First Law balance and solves for the HT term directly without iterative minimization.  The differential first law is then used to solve for the rate terms.
Output of integral table to file was also added.}

{Notes:
1) Pressure is kPa
2) Volume in m^3
3) TDC compression is 0 degrees
}

"!FUNCTIONS, SUBPROGRAMS, & PROCEDURES"
"Function to evaluate the specific heat ratio"
FUNCTION Gamma (T)
Gamma=1.392-7.5e-5*T
END

SUBPROGRAM SolveHT(Q : HT)
    $COMMON LUT$, press$, R, mass_trapped, theta_start, theta_end, T_wall, speed, D, V_p, C2, V_disp, V_IVC, P_IVC, T_IVC, n_comp
    p=interpolate(LUT$,press$,'theta',theta=theta)
    dp=DIFFERENTIATE(LUT$,press$,'theta',theta=theta)
    T=p*V/R/(mass_trapped)
    V=interpolate(LUT$,'volume','theta',theta=theta)
    dV=DIFFERENTIATE(LUT$,'volume','theta',theta=theta)
    gam=Gamma (T)
    Indicated + HeatTransfer = Q
    Indicated = INTEGRAL(V/(gam-1)*dp+gam*p*dV/(gam-1),theta,theta_start,theta_end)
    HeatTransfer_integral = INTEGRAL(h*Area*(T-T_wall)*speed,theta,theta_start,theta_end)
    h=0.131*(D^0.2)*((p/101.3)^0.8)/(T^0.53)*(W^0.8)
    W=2.28*(V_p+C2*0.0136*(V_disp/V_IVC)*((p/P_IVC)-(V_IVC/V)^n_comp)*T_IVC)
    Area=2*(pi*D^2/4)+pi*D*(V/(pi*D^2/4))
"Disk-shaped chamber surface area"
    HeatTransfer = HeatTransfer_integral*HT
END

SUBPROGRAM SolveRateEqns(Q, HT:Q_ht)
    $COMMON LUT$, press$, R, mass_trapped, theta_start, theta_end, theta_step, T_wall, speed, D, V_p, C2, V_disp, V_IVC, P_IVC, T_IVC, n_comp
    p=interpolate(LUT$,press$,'theta',theta=theta)
    dp=DIFFERENTIATE(LUT$,press$,'theta',theta=theta)
    T=p*V/R/(mass_trapped)
    V=interpolate(LUT$,'volume','theta',theta=theta)
    dV=DIFFERENTIATE(LUT$,'volume','theta',theta=theta)
    gam=Gamma (T)
    h=0.131*(D^0.2)*((p/101.3)^0.8)/(T^0.53)*(W^0.8)
    W=2.28*(V_p+C2*0.0136*(V_disp/V_IVC)*((p/P_IVC)-(V_IVC/V)^n_comp)*T_IVC)
    Area=2*(pi*D^2/4)+pi*D*(V/(pi*D^2/4))
```

```
"Disk-shaped chamber surface area"
    V/(gam-1)*dp+gam*p*dV/(gam-1)+dQ_ht=dQ_hr
    dQ_ht=HT*h*Area*(T-T_wall)*speed
    Q_tot=integral(dQ_hr,theta, theta_start,theta_end,theta_step)
    cum_hr=Q_tot/Q
    Q_ht=integral(dQ_ht,theta,theta_start,theta_end)
END

{Procedure to determine the 10, 50 and 90 % burn times}
Procedure Crank (theta_start,theta_end,theta:CA_10,CA_50,CA_90, CA_5)
CA_10=-99; CA_50=-99; CA_90=-99; CA_5=-99
if (theta<theta_end) then  goto 10; {Get out because integration is not done}
i:=theta_start;
V1=0.1; V5=0.5; V9=0.9; V05=0.05
repeat
    i:=i+.5
    z1=IntegralValue(i,cum_hr)
    z2=IntegralValue(i-0.5,cum_hr)
    if ((z1  > V05-0.001) and (z2<V05+0.001)) then CA_5=i
    if ((z1 > V1-0.001) and (z2<V1+0.001)) then CA_10=i
    if ((z1 > V5-0.001) and (z2<V5+0.001)) then CA_50=i
    if ((z1 > V9-0.001) and (z2<V9+0.001)) then CA_90=i
Until (i>=theta_end)
10:
End

{!Added by Bob Iverson June 12, 2004}
Procedure TDC(Theta, Theta_end, CA_5: T_TDC, P_TDC, T_CA5)
{!Pick out the temperature and pressure @ TDC}
T_TDC = 20; P_TDC = 101; T_CA5 = 20
{!Initialization of the TDC Temperature and Pressure Variables}
if (Theta < Theta_end) then goto 20;
{!Get out because integration is not done}
    if (theta >= Theta_end) then
    T_TDC = IntegralValue(0, T)
    P_TDC = IntegralValue(0, P)
    T_CA5 = IntegralValue(CA_5, T)
endif
20:
End

{Values input in diagram window}
{    C2 = 0                                  "Expansion velocity flag (0 = ignore, 1 =
consider)"
    ca = 0.5                                "Crankangle per data point - i.e. encoder
resolution"
    press$='pressure'                       "Use 'pressure' for supplied raw pressure,
'fpressure' for supplied filtered pressure"
    theta_start = -45                       "Angle for start of integration"
    theta_end = 45                          "Angle for end of integration"
    IVC = -125                              "Crank angle of intake valve closing"
    EVO = 131                               "Crank angle of exhaust valve opening"
    EVC = 375                               "Crank agle of exhaust valve closing"
    LHV = 43030 [kJ/kg]                     "Lower heating value of the fuel"
    D = 0.086                               "Bore"
    stroke = 0.086                          "Stroke"
```

```
    T_wall = 400                                    "Wall temperature for heat transfer
calculations"
    q$=''
     r$=''
    s$=''
}

$IFNOT PARAMETRICTABLE
    LUT$ = 'run_1'
    eta_c = 0.9514
    mass_air = 0.0001502 [kg]
    mass_fuel = 0.000005  [kg]
    RPM = 1000 [rev/min]
{   T_exhaust = 542.5 [K]
    T_intake = 633 [K]}
    EGR = 50.6 [%]
    Out$ = 'output.txt'
$ENDIF

"Specify and calculate trivial values"
theta_step=0.25                                     "Integration step size"
NumPts = 361                                        "Number of points in output array"
V_disp=lookup(LUT$,1,'volume')-lookup(LUT$,180/ca,'volume')
"Displacement Volume"
Q=mass_fuel*LHV*eta_c                               "Total energy release from fuel"
Ru=8.314[kJ/kmol·K]                                 "Universal Gas constant"
R=Ru/molarmass(air)  "kJ/kg-K"                      "Gas constant for Air"
speed=time*convert(sec/rev,sec/degree)              "Engine speed in seconds/degree"
strokeperrev = 2*stroke/revunits                    "Number of strokes per revolution"
revunits = 1 [rev]                                  "For units purposes"
V_p=(strokeperrev)/time                             "Mean piston speed"
time=1/(RPM*convert(rev/min, rev/sec))              "Engine speed in time/revolution"

"Lookup important volumes and pressures"
V_IVC=interpolate(LUT$,'volume','theta',theta=IVC);
P_IVC=interpolate(LUT$,press$,'theta',theta=IVC)
V_EVO=interpolate(LUT$,'volume','theta',theta=EVO);
P_EVO=interpolate(LUT$,press$,'theta',theta=EVO)
V_EVC=interpolate(LUT$,'volume','theta',theta=EVC);
P_EVC=interpolate(LUT$,press$,'theta',theta=EVC)

"Determine the compression polytropic coefficient"
P1=interpolate(LUT$,press$,'theta',theta=IVC+5);
V1=interpolate(LUT$,'volume','theta',theta=IVC+5)
P2=interpolate(LUT$,press$,'theta',theta=-30);
V2=interpolate(LUT$,'volume','theta',theta=-30)
n_comp=abs(log10(P2/P1)/log10(V2/V1))

"Used measured EGR and Yun&Mirski correlation to calculate residuals"
"Added to V9"
y_res_int=(V_EVC/V_EVO)*(P_EVC/P_EVO)^(1/n_comp)
"Yun & Mirsky correlation"
mass_trapped = (mass_air+mass_fuel)*(1+(EGR*convert(%, ))/(1-(EGR*convert(%, ))))/(1-
y_res_int)                                          "Total trapped mass based on measured
external EGR"
mass_res_int = y_res_int*mass_trapped
```

```
"Calculated mass of internal residual"
mass_res_ext = mass_trapped - mass_res_int - (mass_air+mass_fuel)
"Calculated mass of external residual"
mass_res = mass_res_int + mass_res_ext
"Calculated mass of total residual"
y_res = mass_res/mass_trapped
"Calculated total residual mass fraction"

"Temperature at IVC"
T_IVC=P_IVC*V_IVC/R/(mass_trapped)

"Solve integrated first law for HT term"
CALL SolveHT(Q : HT)

"Solve instantaneous first law for crank-angle dependent terms"
p=interpolate(LUT$,press$,'theta',theta=theta)
dp=DIFFERENTIATE(LUT$,press$,'theta',theta=theta)
T=p*V/R/(mass_trapped)
V=interpolate(LUT$,'volume','theta',theta=theta)
dV=DIFFERENTIATE(LUT$,'volume','theta',theta=theta)
gam=Gamma (T)
h=0.131*(D^0.2)*((p/101.3)^0.8)/(T^0.53)*(W^0.8)
W=2.28*(V_p+C2*0.0136*(V_disp/V_IVC)*((p/P_IVC)-(V_IVC/V)^n_comp)*T_IVC)
Area=2*(pi*D^2/4)+pi*D*(V/(pi*D^2/4))
"Disk-shaped chamber surface area"
V/(gam-1)*dp+gam*p*dV/(gam-1)+dQ_ht=dQ_hr
dQ_ht=HT*h*Area*(T-T_wall)*speed
Q_tot=integral(dQ_hr,theta, theta_start,theta_end,theta_step)
cum_hr=Q_tot/Q
Q_ht=integral(dQ_ht,theta,theta_start,theta_end,theta_step)
$integraltable theta:0.25, dQ_hr,dQ_ht,cum_hr, T, p


"Extract phasing, temperature, and pressure terms"
call Crank (theta_start,theta_end,theta:CA_10,CA_50,CA_90, CA_5)
call TDC(Theta, Theta_end, CA_5: T_TDC, P_TDC, T_CA5) "!Added by Bob Iverson June 12,
2004"

"Output integral table to file"
{$SaveTable 'Integral' Out$}
```

A.3 EES N2 Diluent Moles Calculations

-Acquired engine exhaust species concentrations:

GM/ERC Collaborative Research Laboratory HCCI Project 28-Jul-06						
		Homogeous_Air AF=38:1	**Homogeneous_Air-N2 AF=28:1**	**Homogeneous_Air-N2 AF=24:1**	**Homogeneous_Air-N2 AF=20:1**	**Homogenous_Air-AirGR AF=20:1**
Run Number Engine Run Time		1 Metal 7/28/2006 20:37	2 Metal 7/28/2006 20:48	3 Metal 7/28/2006 20:55	4 Metal 00:32.0	5 Metal 05:08.0
Raw Emissions:						
CO2	vol %	0.07	0.05	0.05	0.05	0.07
CO	vol %	0	0	0	0	0.01
EGR-CO2	vol %	0.04	0.03	0.03	0.02	0.04
O2	vol %	20.74	15.77	13.59	11.44	20.49
Calculated O2	vol %	21.46	21.18	21.34	21.92	21.14
HC	ppm	26	16	15	15	15
NO	ppm	4.4	3.3	2.9	3.1	3
H2O	vol %	0.08	0.06	0.06	0.06	0.08
Calculated H2	vol %	0.0009	0.0013	0.0013	0.0013	0.0016

-EES code for n_N2 caculcations:

"Motoring Engine Tests - N2 gas diluent exhaust concentration (n_N2) calculations"

"Code input: x_O2"
"Code output result: n_N2"

"Reactant - Product Species equation"

"(O2 + 3.76*N2) + n_N2*N2 => O2 + N2*(n+3.76)"

x_o2 = 1 / ((1+3.76)+n_N2)

"Case#1: A/F=28:1 _ N2 diluent"
"x_O2 = 0.1577" "(from vol_% emissions bench output)"

"Case#1: A/F=24:1 _ N2 diluent"
"x_O2 = 0.1359" "(from vol_% emissions bench output)"

"Case#1: A/F=20:1 _ N2 diluent"
"x_O2 = 0.1144" "(from vol_% emissions bench output)"

-EES code n_N2 results:

Case name	n_N2	x_O2
Homogeneous_N2_28d	1.581	0.1577
Homogeneous_N2_24d	2.598	0.1359
Homogeneous_N2_20d	3.981	0.1144

Appendix B – Experimental Cases Data Summary and Heat Release Results

The following set of data results correspond to data cases that were used through out this thesis to aid the understanding of the HCCI combustion analysis performed. Data will be organized by cases specifying intake charge handling strategy, mixture delivered air-fuel ratio and diluent used.

- EES Heat Release Code Input and Calculated Parameters:

		Input Parameters						
		Etta_comb	Mass_air	Mass_fuel	Engine Speed	T_exhaust	T_intake_avg	EGR_vol%
Experimental Case	Run#		[kg/cycle]	[kg/cycle]	[RPM]	[K]	[K]	
Homogeneous_Air	1	0.9629	0.000374	0.00001	1000	603.5	571.7	0
A/F_d = 38:1	2	0.9557	0.000374	0.00001	1000	606.4	563.7	0
	3	0.9399	0.000374	0.00001	1000	613.4	545.2	0
	4	0.9126	0.000374	0.00001	1000	619	535.2	0
	5	0.8162	0.000374	0.00001	1000	606.8	527.7	0
Homogeneous_N2	6	0.9451	0.000374	0.000021	1000	604.2	587.7	0
A/F_d = 28:1	7	0.944	0.000374	0.00002	1000	609.5	578.2	0
	8	0.9231	0.000374	0.000008	1000	620	572.7	0
	9	0.8957	0.000374	0.000008	1000	609.7	569.2	0
	10	0.6269	0.000374	0.000008	1000	576.5	564.2	0
Homogeneous_N2	11	0.9473	0.000374	0.000008	1000	619.9	598.2	0
A/F_d = 24:1	12	0.9596	0.000374	0.000008	1000	619.4	604.7	0
	13	0.9296	0.000374	0.000008	1000	631.3	581.2	0
	14	0.9043	0.000374	0.000008	1000	632.3	577.7	0
	15	0.8979	0.000374	0.000008	1000	631.2	576.2	0
Homogeneous_N2	16	0.9486	0.000374	0.000007	1000	623	604.7	0
A/F_d = 20:1	17	0.9541	0.000374	0.000007	1000	623.1	611.2	0
	18	0.9434	0.000374	0.000007	1000	629.5	596.2	0
	19	0.9158	0.000374	0.000007	1000	633	589.2	0
	20	0.869	0.000374	0.000007	1000	609.2	584.7	0
Unmixed_N2	21	0.9442	0.000374	0.000007	1000	617.8	591.7	0
A/F_d = 20:1	22	0.9546	0.000374	0.000007	1000	617.6	596.2	0
	23	0.9428	0.000374	0.000007	1000	621	586.2	0
	24	0.9317	0.000374	0.000008	1000	609.9	579.7	0
	25	0.9317	0.000374	0.000008	1000	609.9	573.7	0
Unmixed_N2	26	0.955	0.000374	0.000009	1000	608.6	592.7	0
A/F_d = 28:1	27	0.9477	0.000374	0.000009	1000	614	582.7	0
	28	0.9317	0.000374	0.000009	1000	606.6	571.2	0
	29	0.8965	0.000374	0.000008	1000	610.5	563.2	0
	30	0.8261	0.000374	0.000008	1000	545.6	558.7	0
Unmixed_N2	31	0.9542	0.000374	0.000008	1000	611.8	597.7	0
A/F_d = 24:1	32	0.9451	0.000374	0.000008	1000	614.8	588.2	0
	33	0.9316	0.000374	0.000008	1000	613.3	578.7	0
	34	0.9136	0.000374	0.000008	1000	615.6	573.2	0
	35	0.7676	0.000374	0.000008	1000	565.9	564.7	0
Homogeneous_EGR	36	96.11	0.0001988	0.000008	1000	639.5	607.7	43.7
A/F_d = 20:1	37	96.48	0.0002000	0.000008	1000	644.3	612.6	43.3
	38	96.7	0.0002000	0.000008	1000	646.8	615.2	43.1
	39	95.62	0.0002000	0.000008	1000	634.8	603.0	44.0
	40	95.37	0.0001989	0.000008	1000	632.7	600.9	44.2
	41	94.77	0.0002011	0.000008	1000	628.7	596.8	44.5
	42	94.07	0.0002011	0.000008	1000	625.1	593.1	44.7
Homogeneous_EGR	43	96.83	0.0001988	0.00001	1000	610.3	589.9	45.0
Temp. Stratification	44	97.211	0.0001989	0.00001	1000	635	597.4	44.4
A/F_d = 20:1	45	97.408	0.0002001	0.00001	1000	640.3	603.9	43.9
	46	94.92	0.0001996	0.000007	1000	599.1	565.1	46.8
	47	93.961	0.0001996	0.000008	1000	594	558	47.3
	48	96.06	0.0001989	0.000008	1000	607	577	45.9
	49	96.55	0.0002003	0.00001	1000	615	584	45.4
Unmixed_EGR	50	96.394	0.0002001	0.00001	1000	636.8	605	72.4
A/F_d = 20:1	51	96.888	0.0002001	0.000008	1000	647.0	615.36	71.1
	52	96.7	0.0002000	0.000008	1000	641.9	610.22	71.7
	53	96	0.0002000	0.000008	1000	632.7	600.85	72.9
	54	95.574	0.0002000	0.000008	1000	628.4	596.49	73.4
	55	94.814	0.0001989	0.000007	1000	622.2	590.17	74.2
	56	94.181	0.0001989	0.000008	1000	618.3	586.13	74.6

		Calculated Parameters				
Experimental Case	Run#	CA 10 [dATDC]	CA 50 [dATDC]	CA 90 [dATDC]	Q_ht [kJ]	Q_tot [kJ]
Homogeneous_Air A/F_d = 38:1	1	-0.5	2	4	0.07479	0.4093
	2	2	5	7.5	0.05903	0.403
	3	6.5	10.5	14.5	0.05055	0.4025
	4	9	15	23	0.0464	0.3902
	5	10	19	32.5	0.05394	0.3469
Homogeneous_N2 A/F_d = 28:1	6	-7	6.5	29.5	0.5073	0.8483
	7	-7	9.5	28	0.4684	0.8187
	8	8	12	15.5	1.00E-06	0.351
	9	10	15	20	0.000001	0.3417
	10	13	21	32.5	0.000001	0.2236
Homogeneous_N2 A/F_d = 24:1	11	3.5	6	8	1.00E-06	0.3531
	12	1	3	4.5	1.00E-06	0.3483
	13	8	12	15.5	1.00E-06	0.3598
	14	9.5	14.5	19.5	1.00E-06	0.35
	15	10	15	20	1.00E-06	0.3512
Homogeneous_N2 A/F_d = 20:1	16	3.5	5.5	7.5	1.00E-06	0.3549
	17	2	4	5.5	1.00E-06	0.3519
	18	5	7.5	9.5	1.00E-06	0.3583
	19	8.5	12.5	15.5	1.00E-06	0.3565
	20	10.5	16	20.5	1.00E-06	0.3365
Unmixed_N2 A/F_d = 20:1	21	4	6.5	8.5	1.00E-06	0.3521
	22	1.5	3.5	5	1.00E-06	0.3454
	23	4.5	7.5	9	1.00E-06	0.3515
	24	6.5	10.5	13.5	0.000001	0.3524
	25	9	14.5	20.5	1.00E-06	0.3406
Unmixed_N2 A/F_d = 28:1	26	1.5	3.5	5.5	0.02673	0.3681
	27	3.5	6.5	9	0.01439	0.3639
	28	6.5	10.5	14.5	0.0002081	0.3533
	29	9.5	14.5	19.5	1.00E-06	0.3436
	30	11	17.5	25.5	1.00E-06	0.3083
Unmixed_N2 A/F_d = 24:1	31	2	4	6	1.00E-06	0.3439
	32	4	7	9	1.00E-06	0.3491
	33	6	9.5	12.5	1.00E-06	0.3502
	34	8	12.5	16.5	1.00E-06	0.3469
	35	11.5	18.5	27.5	1.00E-06	0.2826
Homogeneous_EGR A/F_d = 20:1	36	2.72	6	9.17	0.10310	0.4330
	37	0.95	4.67	6.75	0.09727	0.4280
	38	0.03	3.78	6.25	0.09415	0.4253
	39	4.29	7.95	12.33	0.10880	0.4379
	40	5.02	8.95	13.83	0.11128	0.4400
	41	6	10.9	17.58	0.11620	0.4442
	42	7.31	13.4	22	0.12056	0.4480
Homogeneous_EGR Temp. Stratification A/F_d = 20:1	43	0.27	3.12	6.9	0.12439	0.4513
	44	-2.22	1.5	4	0.09727	0.4280
	45	-3.71	0	2.5	0.09415	0.4253
	46	5.18	10.45	21.42	0.10880	0.4379
	47	7.39	14.3	28.25	0.11128	0.4400
	48	2.72	6.3	11.67	0.11620	0.4442
	49	1.12	4.1	9	0.12056	0.4480
Unmixed_EGR A/F_d = 20:1	50	2	5.25	7.92	0.10636	0.4358
	51	-0.39	3.24	4.96	0.09398	0.4252
	52	1	3.78	5.78	0.10012	0.4305
	53	3.41	6.4	10.26	0.11131	0.4401
	54	4.42	8.38	13.39	0.11652	0.4445
	55	6.13	11.42	18.63	0.12407	0.4510
	56	7.53	14.46	22.82	0.12889	0.4551

		Calculated Parameters					
Experimental Case	Run#	y_residuals	y_res_interna	HT	T @ CA 5 [K]	CA 5 [dATDC]	T @ IVC [K]
Homogeneous_Air	1	0.07447	0.07447	4.102	1006	-1.5	492.3
A/F_d = 38:1	2	0.07316	0.07316	3.389	998.4	0.5	492
	3	0.07164	0.07164	3.207	987.7	4	492.5
	4	0.07089	0.07089	3.277	974.3	5.5	492.4
	5	0.0722	0.0722	4.374	960	4	491.3
Homogeneous_N2	6	0.07344	0.07344	29.96	858	-19	481.7
A/F_d = 28:1	7	0.0724	0.0724	28.91	859.2	-19	482.8
	8	0.07177	0.07177	6.421E-05	1043	7	497.7
	9	0.07138	0.07138	6.888E-05	1028	8.5	497.5
	10	0.07808	0.07808	8.648E-05	987.6	11	493.4
Homogeneous_N2	11	0.07269	0.07269	5.852E-05	1043	3	498.4
A/F_d = 24:1	12	0.07326	0.07326	5.505E-05	1054	0.5	498.6
	13	0.07088	0.07088	6.545E-05	1018	7	498.6
	14	0.07047	0.07047	0.0000698	1015	8.5	499
	15	0.07056	0.07056	6.906E-05	1021	8.5	498.4
Homogeneous_N2	16	0.0726	0.0726	5.762E-05	1041	2.5	500
A/F_d = 20:1	17	0.07298	0.07298	0.0000559	1039	1	499.7
	18	0.07206	0.07206	6.009E-05	1032	4	500.1
	19	0.07098	0.07098	6.609E-05	1024	7	500.1
	20	0.0707	0.0707	7.294E-05	1005	8.5	499.5
Unmixed_N2	21	0.07257	0.07257	5.907E-05	1038	3	500.3
A/F_d = 20:1	22	0.07344	0.07344	0.0000557	1044	0.5	499.8
	23	0.07244	0.07244	5.962E-05	1038	3.5	499.6
	24	0.07198	0.07198	6.315E-05	1030	5.5	498.7
	25	0.07144	0.07144	6.868E-05	1028	7.5	497.9
Unmixed_N2	26	0.07344	0.07344	1.496	1035	0.5	493.7
A/F_d = 28:1	27	0.07251	0.07251	0.8419	1045	3	494
	28	0.0716	0.0716	0.01284	1045	5.5	494.3
	29	0.07092	0.07092	6.793E-05	1030	8	495.7
	30	0.07197	0.07197	0.0000752	1016	9.5	494.7
Unmixed_N2	31	0.0729	0.0729	5.728E-05	1029	1	496
A/F_d = 24:1	32	0.0725	0.0725	5.895E-05	1035	3	495.6
	33	0.07216	0.07216	6.068E-05	1054	5	495.8
	34	0.0715	0.0715	6.467E-05	1039	6.5	495.6
	35	0.07371	0.07371	7.801E-05	1012	9.5	493.8
Homogeneous_EGR	36	0.47390	0.06807	5.907	1032	3.0	481.1
A/F_d = 20:1	37	0.47095	0.06868	5.580	1042	2.3	489.5
	38	0.46937	0.06900	5.406	1047	1.8	493.9
	39	0.47678	0.06748	6.227	1022	4.1	473.0
	40	0.47804	0.06723	6.365	1018	4.6	469.5
	41	0.48053	0.06672	6.641	1010	5.6	462.4
	42	0.48273	0.06626	6.885	1002	6.9	456.2
Homogeneous_EGR	43	0.48467	0.06587	7.100	996	1.5	450.7
Temp. Stratification	44	0.48014	0.06680	6.598	1011	0.6	489.5
A/F_d = 20:1	45	0.47621	0.06760	6.163	1024	-0.2	493.9
	46	0.49966	0.06280	8.759	946	5.4	473.0
	47	0.50395	0.06192	9.234	931	7.4	469.5
	48	0.49247	0.06427	7.963	970	3.2	462.4
	49	0.48824	0.06514	7.494	984	2.0	456.2
Unmixed_EGR	50	0.71218	0.01927	6.090	1026	2.6	476.5
A/F_d = 20:1	51	0.70185	0.02139	5.396	1047	1.6	494.2
	52	0.70697	0.02034	5.740	1037	1.8	485.4
	53	0.71631	0.01842	6.367	1018	3.2	469.4
	54	0.72066	0.01753	6.659	1009	4.3	462.0
	55	0.72696	0.01624	7.082	996	5.9	451.2
	56	0.73099	0.01542	7.352	988	7.5	444.3

- Data Summary Acquired and Calculated Parameters:

Experimental Case	RN#	Eng Spd [RPM]	SprkTimng [dBTDC]	CombEff [%]	ThermEff [%]	VolEff [%]	EGR [%]	OrAIRfl [mg/sec]
Homogeneous_Air	1	1000.02	1111.1	96.288	38.813	57.437	0.24	3025.721
A/F_d = 38:1	2	1000.02	1111.1	95.567	39.734	57.421	0.214	3027.817
	3	1000.02	1111.1	93.991	39.3	57.431	0.067	3027.952
	4	1000.02	1111.1	91.262	36.872	57.389	0.06	3026.948
	5	1000.02	1111.1	81.625	31.029	57.371	0.013	3028.201
Homogeneous_N2	6	1000.02	1111.1	94.513	18.681	106.768	-0.133	5516.771
A/F_d = 28:1	7	1000.02	1111.1	94.396	19.464	103.234	-0.266	5515.512
	8	1000.02	1111.1	92.314	45.278	43.214	-0.295	2258.574
	9	1000.03	1111.1	89.573	42.927	43.207	-0.286	2258.519
	10	1000.03	1111.1	62.695	28.543	43.181	-0.491	2258.828
Homogeneous_N2	11	1000.02	1111.1	94.728	50.228	36.699	-0.206	1900.23
A/F_d = 24:1	12	1000.03	1111.1	95.96	50.059	36.715	-0.222	1899.997
	13	1000.03	1111.1	92.963	48.943	36.736	-0.248	1900.601
	14	1000.03	1111.1	90.435	46.678	36.728	-0.274	1900.318
	15	1000.03	1111.1	89.786	47.004	36.719	-0.297	1900.38
Homogeneous_N2	16	1000.03	1111.1	94.863	56.091	30.93	-0.333	1586.033
A/F_d = 20:1	17	1000.03	1111.1	95.414	55.865	30.932	-0.301	1586.041
	18	1000.02	1111.1	94.337	55.738	30.953	-0.332	1586.956
	19	1000.03	1111.1	91.576	53.623	30.927	-0.373	1585.893
	20	1000.02	1111.1	86.904	49.872	30.509	-0.385	1586.569
Unmixed_N2	21	1000.03	1111.1	94.42	55.833	30.971	0.252	1586.457
A/F_d = 20:1	22	1000.02	1111.1	95.457	55.855	30.923	0.341	1586.234
	23	1000.02	1111.1	94.283	55.846	30.98	0.363	1586.404
	24	1000.03	1111.1	93.167	49.198	34.625	0.335	1586.531
	25	1000.02	1111.1	93.167	45.73	34.626	0.335	1586.531
Unmixed_N2	26	1000.02	1111.1	95.503	45.935	43.296	0.403	2261.921
A/F_d = 28:1	27	1000.03	1111.1	94.772	46.14	43.294	0.413	2261.956
	28	1000.03	1111.1	93.168	42.417	46.854	0.511	2263.226
	29	1000.03	1111.1	89.646	42.97	43.314	0.518	2263.588
	30	1000.02	1111.1	82.614	40.688	40.49	0.572	2139.596
Unmixed_N2	31	1000.02	1111.1	95.422	49.905	36.66	0.561	1903.23
A/F_d = 24:1	32	1000.03	1111.1	94.508	50.535	36.673	0.513	1903.902
	33	1000.02	1111.1	93.16	50.566	36.67	0.488	1903.617
	34	1000.03	1111.1	91.355	48.99	36.666	0.607	1903.549
	35	1000.02	1111.1	76.761	38.332	36.864	0.619	1903.476
Homogeneous_EGR	36	1000.02	1111.1	96.11	36.81117385	30.31798892	40.704	1568.503
A/F_d = 20:1	37	1000.02	1111.1	96.48	36.95288787	30.43470577	40.476	1568.155
	38	1000.03	1111.1	96.7	37.03715026	30.50410497	40.212	1571.991
	39	1000.03	1111.1	95.62	36.62349853	30.16341797	40.763	1571.229
	40	1000.02	1111.1	95.37	36.52774581	30.08455523	40.919	1571.563
	41	1000.03	1111.1	94.77	36.29793929	29.89528468	41.236	1571.61
	42	1000.02	1111.1	94.07	36.02983169	29.67446903	41.341	1570.501
Homogeneous_EGR	43	1000.02	1111.1	96.342	40.051	30.922	44.339	1566.674
Temp. Stratification	44	1000.02	1111.1	96.888	40.182	30.72	44.414	1567.884
A/F_d = 20:1	45	1000.03	1111.1	96.7	39.916	30.805	43.941	1571.991
	46	1000.03	1111.1	96	40.084	30.804	46.766	1571.616
	47	1000.02	1111.1	95.574	39.624	30.79	47.283	1571.563
	48	1000.03	1111.1	94.814	34.003	33.449	45.899	1572.438
	49	1000.03	1111.1	94.66	34.918	33.973	45.743	1570.528
Unmixed_EGR	50	1000.03	1111.1	96.83	37.08694167	30.54511359	72.371	1574.427
A/F_d = 20:1	51	1000.02	1111.1	97.211	37.23286881	30.6653004	71.126	1573.831
	52	1000.02	1111.1	97.408	37.30832194	30.72744423	71.744	1573.552
	53	1000.03	1111.1	94.92	36.35539092	29.94260232	72.869	1573.124
	54	1000.02	1111.1	93.961	35.98808351	29.64008487	73.393	1571.835
	55	1000.03	1111.1	96.06	36.7920233	30.30221638	74.152	1575.283
	56	1000.02	1111.1	96.55	36.97969863	30.45678733	74.637	1574.457

Experimental Case	RN#	PremInj AirFl [mg/sec]	StratAIRfl [mg/sec]	TotAIRfl [mg/sec]	PreMixFUELfl [mg/sec]	StratInjFUELfl [mg/sec]	TotFUELfl [mg/sec]	Strat [%]
Homogeneous_Air	1	91.257	0	3116.978	82.429	0	72.17	0
A/F_d = 38:1	2	88.291	0	3116.108	81.893	0	75.763	0
	3	88.72	0	3116.672	81.647	0	75.333	0
	4	87.417	0	3114.365	81.301	0	82.2	0
	5	85.183	0	3113.384	80.009	0	175.677	0
Homogeneous_N2	6	277.286	0	5794.057	173.847	0	77.877	0
A/F_d = 28:1	7	86.754	0	5602.266	167.876	0	77.666	0
	8	86.566	0	2345.14	69.708	0	78.18	0
	9	86.234	0	2344.753	69.63	0	73.095	0
	10	84.554	0	2343.382	67.038	0	231.395	0
Homogeneous_N2	11	91.36	0	1991.59	66.077	0	122.984	0
A/F_d = 24:1	12	92.474	0	1992.472	66.472	0	109.33	0
	13	92.977	0	1993.578	65.881	0	98.467	0
	14	92.84	0	1993.158	65.4	0	94.28	0
	15	92.274	0	1992.654	65.131	0	230.176	0
Homogeneous_N2	16	92.503	0	1678.536	59.629	0	325.144	0
A/F_d = 20:1	17	92.589	0	1678.63	59.851	0	93.976	0
	18	92.777	0	1679.733	59.666	0	93.074	0
	19	92.486	0	1678.379	58.999	0	86.231	0
	20	69.08	0	1655.649	58.024	0	129.134	0
Unmixed_N2	21	94.274	0	1680.732	58.94	0	86.169	0
A/F_d = 20:1	22	91.909	0	1678.142	58.882	0	87.944	0
	23	94.789	0	1681.193	58.643	0	87.575	0
	24	292.526	0	1879.057	65.352	0	84.316	0
	25	292.526	0	1879.057	65.352	0	84.316	0
Unmixed_N2	26	87.651	0	2349.573	70.995	0	83.297	0
A/F_d = 28:1	27	87.514	0	2349.47	71.324	0	88.224	0
	28	279.446	0	2542.671	76.239	0	84.284	0
	29	87	0	2350.588	70.313	0	85.628	0
	30	57.68	0	2197.276	65.231	0	91.135	0
Unmixed_N2	31	86.229	0	1989.459	65.561	0	86.859	0
A/F_d = 24:1	32	86.269	0	1990.17	64.846	0	84.725	0
	33	86.383	0	1990	63.906	0	84.8	0
	34	86.263	0	1989.812	63.559	0	86.149	0
	35	97.029	0	2000.505	63.51	0	93.934	0
Homogeneous_EGR	36	99.554	0	1668.057	83.968	0	83.489	0
A/F_d = 20:1	37	99.143	0	1667.298	84.088	0	85.42	0
	38	99.743	0	1671.734	84.06	0	86.448	0
	39	99.337	0	1670.567	83.976	0	86.726	0
	40	99.36	0	1670.923	84.031	0	85.352	0
	41	273.12	0	1843.648	84.566	0	84.456	0
	42	274.288	0	1843.652	85.104	0	83.142	0
Homogeneous_EGR	43	99.775	0	1757.003	83.999	0	85.558	0
Temp. Stratification	44	99.211	0	1667.096	83.543	0	85.476	0
A/F_d = 20:1	45	99.743	0	1671.734	84.06	0	86.448	0
	46	100.04	0	1672.656	83.971	0	86.593	0
	47	99.36	0	1770.923	84.031	0	85.352	0
	48	270.32	0	1854.012	91.727	0	80.509	0
	49	273.12	0	1843.648	92.564	0	80.402	0
Unmixed_EGR	50	91.771	0	1666.199	83.252	0	84.828	0
A/F_d = 20:1	51	95.303	0	1669.134	83.718	0	87.618	0
	52	95.246	0	1668.797	83.678	0	85.152	0
	53	95.143	0	1668.267	83.805	0	86.627	0
	54	93.771	0	1665.607	83.131	0	83.03	0
	55	93.497	0	1668.78	83.523	0	85.711	0
	56	93.617	0	1668.074	83.45	0	87.537	0

Experimental Case	RN#	PreAIRfl [mg/cycle]	StratAIRfl [mg/cycle]	TotAIRfl [mg/cycle]	PreMixAIRfl [mg/cycle]	TotFUELfl [mg/cycle]	CalcAIRflCyc [mg/Cycle]	CalcFUELflCyc [mg/cycle]
Homogeneous_Air	1	10.951	0	374.03	9.891	8.66	Inf	9.891
A/F_d = 38:1	2	10.595	0	373.925	9.827	9.091	Inf	9.827
	3	10.646	0	373.993	9.797	9.04	Inf	9.797
	4	10.49	0	373.716	9.756	9.864	Inf	9.756
	5	10.222	0	373.599	9.601	21.081	Inf	9.601
Homogeneous_N2	6	33.274	0	695.273	20.861	9.345	Inf	20.861
A/F_d = 28:1	7	10.41	0	672.258	20.145	9.32	Inf	20.145
	8	10.388	0	281.411	8.365	9.381	Inf	8.365
	9	10.348	0	281.362	8.355	8.771	Inf	8.355
	10	10.146	0	281.197	8.044	27.767	Inf	8.044
Homogeneous_N2	11	10.963	0	238.986	7.929	14.758	Inf	7.929
A/F_d = 24:1	12	11.097	0	239.089	7.976	13.119	Inf	7.976
	13	11.157	0	239.222	7.905	11.816	Inf	7.905
	14	11.14	0	239.172	7.848	11.313	Inf	7.848
	15	11.073	0	239.111	7.815	27.62	Inf	7.815
Homogeneous_N2	16	11.1	0	201.418	7.155	39.016	Inf	7.155
A/F_d = 20:1	17	11.11	0	201.43	7.182	11.277	Inf	7.182
	18	11.133	0	201.564	7.16	11.169	Inf	7.16
	19	11.098	0	201.399	7.08	10.347	Inf	7.08
	20	8.289	0	198.674	6.963	15.496	Inf	6.963
Unmixed_N2	21	11.313	0	201.682	7.073	10.34	Inf	7.073
A/F_d = 20:1	22	11.029	0	201.373	7.066	10.553	Inf	7.066
	23	11.374	0	201.739	7.037	10.509	Inf	7.037
	24	35.102	0	225.48	7.842	10.118	Inf	7.842
	25	35.102	0	225.482	7.842	10.118	Inf	7.842
Unmixed_N2	26	10.518	0	281.943	8.519	9.995	Inf	8.519
A/F_d = 28:1	27	10.501	0	281.928	8.559	10.587	Inf	8.559
	28	33.533	0	305.111	9.148	10.114	Inf	9.148
	29	10.44	0	282.062	8.437	10.275	Inf	8.437
	30	6.921	0	263.668	7.828	10.936	Inf	7.828
Unmixed_N2	31	10.347	0	238.73	7.867	10.423	Inf	7.867
A/F_d = 24:1	32	10.352	0	238.813	7.781	10.167	Inf	7.781
	33	10.366	0	238.795	7.669	10.176	Inf	7.669
	34	10.351	0	238.77	7.627	10.338	Inf	7.627
	35	11.643	0	240.056	7.621	11.272	Inf	7.621
Homogeneous_EGR	36	11.946	0	200.161	10.076	10.018	Inf	10.076
A/F_d = 20:1	37	11.897	0	200.072	10.09	10.25	Inf	10.09
	38	11.969	0	200.602	10.087	10.373	Inf	10.087
	39	11.92	0	200.462	10.077	10.407	Inf	10.077
	40	11.923	0	200.507	10.084	10.242	Inf	10.084
	41	11.867	0	200.623	10.129	10.121	Inf	10.103
	42	11.922	0	200.144	10.094	10.411	Inf	10.065
Homogeneous_EGR	43	11.9192	0	200.032	10.12	10.254	Inf	10.01
Temp. Stratification	44	11.913207	0	200.12	10.071	10.334	Inf	10.08
A/F_d = 20:1	45	11.917666	0	200.611	10.087	10.373	Inf	10.087
	46	11.918472	0	200.5	10.076	10.391	Inf	10.076
	47	11.914988	0	200.123	10.064	10.242	Inf	10.084
	48	11.90438	0	221.01	11.007	9.699	Inf	11.127
	49	11.890483	0	219.02	11.002	9.732	Inf	11.005
Unmixed_EGR	50	11.012	0	199.938	9.99	10.179	Inf	9.99
A/F_d = 20:1	51	11.436	0	200.292	10.046	10.514	Inf	10.046
	52	11.429	0	200.252	10.041	10.218	Inf	10.041
	53	11.417	0	200.188	10.056	10.395	Inf	10.056
	54	11.252	0	199.869	9.975	9.963	Inf	9.975
	55	11.219	0	200.25	10.023	10.285	Inf	10.023
	56	11.234	0	200.165	10.014	10.504	Inf	10.014

Experimental Case	RN#	StratInjPlenPress [kPa]	StratInjPlenTemp [C]	CalcAIRfl [mg/Cycle]	CalcFUELfl [mg/Cycle]	IntkMAP [kPa]	ExhstMAP [kPa]	AEAP [kPa]
Homogeneous_Air	1	1111.1	2222.2	327.478	9.891	33.54	26.69	111.66
A/F_d = 38:1	2	1111.1	2222.2	345.936	9.827	33.49	26.61	111.6
	3	1111.1	2222.2	345.071	9.797	33.22	26.4	110.38
	4	1111.1	2222.2	377.848	9.756	31.7	24.85	108.97
	5	1111.1	2222.2	820.318	9.601	33.41	26.6	108.66
Homogeneous_N2	6	1111.1	2222.2	311.457	20.861	34.27	27.41	109.62
A/F_d = 28:1	7	1111.1	2222.2	311.013	20.145	34.46	27.57	109.13
	8	1111.1	2222.2	315.614	8.365	32.7	25.74	107.09
	9	1111.1	2222.2	295.364	8.355	34.88	27.91	106.07
	10	1111.1	2222.2	970.608	8.044	33.54	26.59	105.88
Homogeneous_N2	11	1111.1	2222.2	444.807	7.929	34.88	27.91	111.2
A/F_d = 24:1	12	1111.1	2222.2	393.242	7.976	34.87	27.87	111.7
	13	1111.1	2222.2	357.549	7.905	34.87	27.89	109.41
	14	1111.1	2222.2	344.789	7.848	34.9	27.9	107.57
	15	1111.1	2222.2	845.029	7.815	35.19	27.9	106.66
Homogeneous_N2	16	1111.1	2222.2	1098.284	7.155	35.36	27.99	110.49
A/F_d = 20:1	17	1111.1	2222.2	316.28	7.182	35.35	27.93	110.96
	18	1111.1	2222.2	314.426	7.16	35.29	27.88	110.63
	19	1111.1	2222.2	294.358	7.08	35.19	27.88	107.35
	20	1111.1	2222.2	442.156	6.963	35.08	27.88	106.54
Unmixed_N2	21	1111.1	2222.2	294.855	7.073	35.45	27.94	109.66
A/F_d = 20:1	22	1111.1	2222.2	300.762	7.066	35.3	27.95	110.83
	23	1111.1	2222.2	301.271	7.037	35.7	27.97	109.64
	24	1111.1	2222.2	290.912	7.842	35.71	27.99	108.92
	25	1111.1	2222.2	290.915	7.842	35.74	28	105.83
Unmixed_N2	26	1111.1	2222.2	330.799	8.519	35.22	28.19	111.36
A/F_d = 28:1	27	1111.1	2222.2	348.732	8.559	35.04	27.94	111.18
	28	1111.1	2222.2	337.31	9.148	35.26	28.01	108.08
	29	1111.1	2222.2	343.5	8.437	35.29	28.01	106.66
	30	1111.1	2222.2	368.373	7.828	35.29	27.97	105.88
Unmixed_N2	31	1111.1	2222.2	316.282	7.867	35.29	27.96	112.53
A/F_d = 24:1	32	1111.1	2222.2	312.021	7.781	35.31	28	110.56
	33	1111.1	2222.2	316.869	7.669	35.4	28.03	107.64
	34	1111.1	2222.2	323.633	7.627	34.39	26.86	106.54
	35	1111.1	2222.2	355.052	7.621	34.24	26.66	104.93
Homogeneous_EGR	36	1111.1	2222.2	199.02	10.076	31.49	29.65	105.46
A/F_d = 20:1	37	1111.1	2222.2	203.241	10.09	31.55	29.62	106.16
	38	1111.1	2222.2	206.302	10.087	31.52	29.64	106.18
	39	1111.1	2222.2	207.028	10.077	31.52	29.6	105.96
	40	1111.1	2222.2	203.658	10.084	31.54	29.65	105.85
	41	1111.1	2222.2	203.667	10.05	31.61	29.63	105.25
	42	1111.1	2222.2	206.011	10.064	31.43	29.6	105.43
Homogeneous_EGR	43	1111.1	2222.2	203.1	10.01	31.554	29.630	105.932
Temp. Stratification	44	1111.1	2222.2	203.497	10.08	31.542	29.624	105.801
A/F_d = 20:1	45	1111.1	2222.2	206.302	10.087	31.551	29.629	105.898
	46	1111.1	2222.2	206.856	10.076	31.553	29.629	105.916
	47	1111.1	2222.2	203.658	10.084	31.546	29.626	105.840
	48	1111.1	2222.2	192.081	11.127	31.526	29.615	105.607
	49	1111.1	2222.2	195.081	11.005	31.499	29.601	105.302
Unmixed_EGR	50	1111.1	2222.2	203.724	9.99	34.46	29.74	105.97
A/F_d = 20:1	51	1111.1	2222.2	209.622	10.046	31.81	29.65	109.92
	52	1111.1	2222.2	203.778	10.041	31.76	29.65	110.38
	53	1111.1	2222.2	206.929	10.056	31.7	29.71	105.99
	54	1111.1	2222.2	199.627	9.975	31.75	29.65	104.38
	55	1111.1	2222.2	205.497	10.023	31.87	29.64	107.64
	56	1111.1	2222.2	209.969	10.014	31.84	29.67	108.86

Experimental Case	RN#	OrUpstmPress [kPa]	OrUpstmTemp [C]	ntkAIRTem [C]	ColntTemp [C]	OilTemp [C]	ExhstPrt_Temp [C]	ISFC [g/kW-hr]
Homogeneous_Air	1	284.714	24.689	286.3	214.077	88.557	330.309	176.732
A/F_d = 38:1	2	284.794	24.579	278.3	189.526	87.051	333.263	182.252
	3	284.76	24.531	259.8	216.68	91.106	340.26	183.893
	4	284.637	24.495	249.8	254.1	87.306	345.817	214.766
	5	284.751	24.499	242.3	190.003	88.297	333.671	550.591
Homogeneous_N2	6	504.871	24.701	302.3	232.377	87.186	331.003	189.209
A/F_d = 28:1	7	504.723	24.679	292.8	270.334	86.254	336.386	187.658
	8	504.783	24.665	287.3	184.766	87.543	346.86	196.385
	9	504.763	24.661	283.8	183.983	141.306	336.546	193.956
	10	504.84	24.665	278.8	205.28	82.786	303.34	947.377
Homogeneous_N2	11	424.763	24.61	312.8	193.8	88.317	346.76	291.453
A/F_d = 24:1	12	424.697	24.6	319.3	306.534	84.74	346.26	258.461
	13	424.823	24.594	295.8	212.64	89.497	358.177	240.512
	14	424.774	24.604	292.3	201.554	86.517	359.106	243.659
	15	424.777	24.597	290.8	181.289	86.58	358.083	595.381
Homogeneous_N2	16	354.689	24.615	319.3	257.22	113.123	349.84	766.901
A/F_d = 20:1	17	354.646	24.577	325.8	212.331	84.123	349.917	221.45
	18	354.831	24.562	310.8	226.831	86.549	356.337	220.432
	19	354.597	24.564	303.8	230.397	89.277	359.823	215.847
	20	354.754	24.569	299.3	187.343	86.6	336.046	352.826
Unmixed_N2	21	354.731	24.571	306.3	192.717	141.191	344.617	206.618
A/F_d = 20:1	22	354.691	24.579	310.8	250.746	84.503	344.403	210.632
	23	354.711	24.564	300.8	186.36	84.626	347.826	210.983
	24	354.726	24.553	294.3	212.469	85.469	336.797	207.048
	25	354.726	24.553	288.3	212.469	85.469	336.797	223.854
Unmixed_N2	26	504.426	24.015	307.3	238.017	84.7	335.463	201.065
A/F_d = 28:1	27	504.246	23.904	297.3	186.034	87.094	340.849	211.075
	28	504.366	23.809	285.8	225.58	85.071	333.463	206.621
	29	504.46	23.817	277.8	228.911	87.271	337.363	224.888
	30	476.863	23.805	273.3	192.691	84.577	272.48	271.789
Unmixed_N2	31	424.211	23.756	312.3	233.4	124.517	338.617	208.383
A/F_d = 24:1	32	424.349	23.747	302.8	199.686	117.803	341.611	203.984
	33	424.323	23.773	293.3	202.103	89.257	340.151	208.552
	34	424.323	23.784	287.8	234.269	84.529	342.469	220.067
	35	424.331	23.801	279.3	212.789	87.223	292.774	305.923
Homogeneous_EGR	36	348.04	22.29	334.73	230.449	88.211	301.249	195.734
A/F_d = 20:1	37	348.037	22.353	339.61	217.131	88.877	300.357	201.098
	38	349.003	22.452	342.22	267.52	88.977	299.44	203.895
	39	348.96	22.558	329.95	215.694	89.4	306.197	205.123
	40	349.029	22.554	327.88	285.863	89.454	306.36	203.031
	41	348.926	22.661	323.76	210.26	89.431	302.957	196.967
	42	348.563	22.652	320.11	211.23	89.464	303.122	197.132
Homogeneous_EGR	43	348.966	22.33	332	262.306	88.009	302.319	201.747
Temp. Stratification	44	347.966	22.343	342.36	260.301	88.669	302.673	200.801
A/F_d = 20:1	45	349.003	22.452	337.22	267.52	88.977	302.409	201.505
	46	348.989	22.51	327.85	257.334	89.097	302.362	201.632
	47	349.029	22.554	323.49	285.863	89.454	302.568	201.082
	48	348.643	22.661	317.17	210.31	89.431	303.194	199.408
	49	348.926	22.668	313.13	210.26	89.731	304.015	197.214
Unmixed_EGR	50	353.286	25.617	316.9	236.091	89.146	284.914	211.977
A/F_d = 20:1	51	351.589	24.295	324.4	197.174	88.957	282.631	224.868
	52	351.631	24.383	330.9	239.843	86.497	284.871	220.499
	53	351.574	24.416	292.1	250.557	86.657	288.851	219.655
	54	350.774	23.981	285	284.754	87.1	280.474	237.335
	55	351.711	24.125	304	258.08	87.511	282.583	230.007
	56	351.64	24.22	311	211.923	85.369	282.951	238.327

Experimental Case	RN#	NSFC [g/kW-hr]	ISAC [g/kW-hr]	NSAC [g/kW-hr]	IndicatdTorq [N-m]	NetTorq [N-m]	PumpngTorq [N-m]	IndicatdPwr [kW]
Homogeneous_Air	1	183.316	7632.96	7917.326	14.038	13.534	-0.504	1.47
A/F_d = 38:1	2	189.212	7495.979	7782.233	14.291	13.765	-0.526	1.497
	3	190.789	7608.016	7893.32	14.083	13.574	-0.509	1.475
	4	222.831	8136.994	8442.546	13.157	12.681	-0.476	1.378
	5	575.051	9757.682	10191.176	10.969	10.502	-0.467	1.149
Homogeneous_N2	6	194.87	14077.201	14498.319	14.149	13.738	-0.411	1.482
A/F_d = 28:1	7	193.154	13536.276	13932.738	14.228	13.823	-0.404	1.49
	8	201.29	5890.892	6038.039	13.685	13.352	-0.333	1.433
	9	198.73	6221.762	6374.889	12.955	12.644	-0.311	1.357
	10	982.723	9594.27	9952.227	8.396	8.094	-0.302	0.879
Homogeneous_N2	11	301.13	4719.766	4876.464	14.506	14.04	-0.467	1.519
A/F_d = 24:1	12	267.004	4710.297	4865.984	14.541	14.076	-0.465	1.523
	13	248.168	4869.442	5024.445	14.074	13.64	-0.434	1.474
	14	250.976	5151.157	5305.84	13.301	12.914	-0.388	1.393
	15	610.995	5154.264	5289.439	13.29	12.95	-0.34	1.392
Homogeneous_N2	16	789.984	3959.082	4078.245	14.575	14.149	-0.426	1.526
A/F_d = 20:1	17	228.406	3955.621	4079.861	14.588	14.144	-0.444	1.528
	18	227.433	3978.192	4104.556	14.515	14.068	-0.447	1.52
	19	221.494	4201.195	4311.109	13.733	13.383	-0.35	1.438
	20	362.64	4523.641	4649.473	12.582	12.241	-0.341	1.318
Unmixed_N2	21	212.789	4030.098	4150.472	14.337	13.921	-0.415	1.501
A/F_d = 20:1	22	217.298	4019.265	4146.464	14.353	13.913	-0.44	1.503
	23	217.309	4050.286	4171.719	14.269	13.854	-0.415	1.494
	24	213.112	4614.255	4749.379	13.999	13.601	-0.398	1.466
	25	229.271	4988.792	5109.518	12.948	12.642	-0.306	1.356
Unmixed_N2	26	207.566	5671.489	5854.841	14.242	13.796	-0.446	1.491
A/F_d = 28:1	27	217.857	5621.087	5801.699	14.368	13.921	-0.447	1.505
	28	211.804	6233.317	6389.674	14.023	13.68	-0.344	1.468
	29	230.309	6173.426	6322.254	13.089	12.781	-0.308	1.371
	30	279.035	6552.857	6727.579	11.527	11.228	-0.299	1.207
Unmixed_N2	31	215.737	4772.896	4941.335	14.329	13.841	-0.488	1.501
A/F_d = 24:1	32	210.102	4791.531	4935.248	14.278	13.863	-0.416	1.495
	33	213.253	4894.083	5004.397	13.978	13.67	-0.308	1.464
	34	224.835	5082.967	5193.089	13.457	13.172	-0.285	1.409
	35	313.555	6515.215	6677.749	10.555	10.299	-0.256	1.105
Homogeneous_EGR	36	200.713	3910.643	4010.112	14.663	14.299	-0.364	1.536
A/F_d = 20:1	37	206.26	3925.188	4025.949	14.602	14.237	-0.365	1.529
	38	209.371	3942.92	4048.818	14.575	14.194	-0.381	1.526
	39	210.531	3951.202	4055.37	14.534		-0.373	1.522
	40	208.311	3974.705	4078.08	14.452	14.085	-0.366	1.513
	41	202.065	4510.523	4627.271	14.051	13.697	-0.355	1.471
	42	202.23	4510.688	4627.436	14.216	13.862	-0.19	1.636
Homogeneous_EGR	43	207.015	3899.088	4001.220	14.587	14.222	-0.394	1.519
Temp. Stratification	44	206.038	4045.999	4151.829	14.480	14.120	-0.359	1.535
A/F_d = 20:1	45	206.765	3936.692	4039.771	14.560	14.196	-0.385	1.523
	46	206.896	3916.934	4019.515	14.574	14.210	-0.390	1.521
	47	206.328	4002.340	4107.071	14.512	14.150	-0.370	1.530
	48	204.599	4262.383	4373.658	14.323	13.968	-0.308	1.560
	49	202.334	4603.052	4722.900	14.075	13.730	-0.226	1.598
Unmixed_EGR	50	216.208	4163.674	4246.769	13.757	13.487	-0.269	1.441
A/F_d = 20:1	51	232.479	4283.762	4428.764	13.395	12.956	-0.439	1.403
	52	228.218	4321.304	4472.593	13.276	12.827	-0.449	1.39
	53	225.15	4230.119	4335.942	13.557	13.227	-0.331	1.42
	54	244.407	4761.018	4902.869	12.026	11.679	-0.348	1.259
	55	237.925	4478.201	4632.354	12.81	12.384	-0.426	1.342
	56	247.373	4541.475	4713.859	12.627	12.165	-0.461	1.322

Experimental Case	RN#	NetPwr [kW]	PumpngPwr [kW]	IndicatdWrk [J]	NetWrk [J]	PumpngWrk [J]	IMEP [kPa]	NMEP [kPa]
Homogeneous_Air	1	1.417	-0.053	176.407	170.071	-6.331	320.74	309.22
A/F_d = 38:1	2	1.441	-0.055	179.581	172.975	-6.606	326.51	314.5
	3	1.421	-0.053	176.968	170.572	-6.397	321.76	310.13
	4	1.328	-0.05	165.341	159.357	-5.984	300.62	289.74
	5	1.1	-0.049	137.836	131.972	-5.863	250.61	239.95
Homogeneous_N2	6	1.439	-0.043	177.804	172.639	-5.17	323.28	313.89
A/F_d = 28:1	7	1.448	-0.042	178.788	173.701	-5.082	325.07	315.82
	8	1.398	-0.035	171.974	167.783	-4.186	312.68	305.06
	9	1.324	-0.033	162.8	158.889	-3.911	296	288.89
	10	0.848	-0.032	105.512	101.717	-3.795	191.84	184.94
Homogeneous_N2	11	1.47	-0.049	182.287	176.429	-5.863	331.43	320.78
A/F_d = 24:1	12	1.474	-0.049	182.732	176.886	-5.841	332.24	321.61
	13	1.428	-0.045	176.858	171.402	-5.451	321.56	311.64
	14	1.352	-0.041	167.151	162.278	-4.878	303.91	295.05
	15	1.356	-0.036	167.007	162.739	-4.268	303.65	295.89
Homogeneous_N2	16	1.482	-0.045	183.15	177.799	-5.352	333	323.27
A/F_d = 20:1	17	1.481	-0.047	183.321	177.738	-5.583	333.31	323.16
	18	1.473	-0.047	182.402	176.787	-5.616	331.64	321.43
	19	1.402	-0.037	172.579	168.179	-4.4	313.78	305.78
	20	1.282	-0.036	158.109	153.83	-4.279	287.47	279.69
Unmixed_N2	21	1.458	-0.043	180.158	174.933	-5.22	327.56	318.06
A/F_d = 20:1	22	1.457	-0.046	180.367	174.834	-5.533	327.94	317.88
	23	1.451	-0.043	179.311	174.091	-5.214	326.02	316.53
	24	1.424	-0.042	175.918	170.913	-5.005	319.85	310.75
	25	1.324	-0.032	162.712	158.868	-3.845	295.84	288.85
Unmixed_N2	26	1.445	-0.047	178.965	173.36	-5.61	325.39	315.2
A/F_d = 28:1	27	1.458	-0.047	180.56	174.939	-5.621	328.29	318.07
	28	1.433	-0.036	176.215	171.903	-4.317	320.39	312.55
	29	1.338	-0.032	164.483	160.611	-3.872	299.06	292.02
	30	1.176	-0.031	144.854	141.091	-3.762	263.37	256.53
Unmixed_N2	31	1.449	-0.051	180.065	173.927	-6.138	327.39	316.23
A/F_d = 24:1	32	1.452	-0.044	179.427	174.202	-5.225	326.23	316.73
	33	1.432	-0.032	175.654	171.781	-3.867	319.37	312.33
	34	1.379	-0.03	169.109	165.523	-3.586	307.47	300.95
	35	1.078	-0.027	132.644	129.415	-3.223	241.17	235.3
Homogeneous_EGR	36	1.497	-0.038	184.261	179.691	-4.576	334	326.71
A/F_d = 20:1	37	1.491	-0.038	183.497	178.904	-4.593	333.25	325.28
	38	1.486	-0.04	183.156	178.365	-4.791	332.08	324.3
	39	1.483	-0.039	182.644	177.953	-4.692	331.1	323.55
	40	1.475	-0.038	181.605	177.001	-4.604	328.56	321.82
	41	1.434	-0.037	176.572	172.117	-4.455	322.3	323.35
	42	1.599	0.128	176.737	172.282	-4.29	311.84	323.92
Homogeneous_EGR	43	1.481	-0.065	183.579	178.936	-4.697	334	324.59
Temp. Stratification	44	1.498	-0.033	181.872	177.278	-4.617	329.39	324.26
A/F_d = 20:1	45	1.485	-0.057	183.142	178.512	-4.677	332.82	324.50
	46	1.483	-0.061	183.371	178.735	-4.688	333.44	324.55
	47	1.493	-0.043	182.379	177.770	-4.641	330.76	324.36
	48	1.523	0.013	179.359	174.834	-4.499	322.6	323.78
	49	1.563	0.087	175.401	170.988	-4.313	311.91	323.03
Unmixed_EGR	50	1.412	-0.028	172.871	169.488	-3.383	329.41	308.16
A/F_d = 20:1	51	1.357	-0.046	168.322	162.811	-5.511	324.51	296.02
	52	1.343	-0.047	166.826	161.183	-5.643	320.34	293.06
	53	1.385	-0.035	170.368	166.21	-4.158	324.91	302.2
	54	1.223	-0.036	151.129	146.757	-4.373	310.34	266.83
	55	1.297	-0.045	160.98	155.623	-5.357	335.19	282.95
	56	1.274	-0.048	158.67	152.867	-5.797	332.3	277.94

Experimental Case	RN#	PMEP [kPa]	LNVofIMEP	COVofIMEP [%]	PeakPress [kPa]	LocatPkPress [dATDC]	PressIVO [kPa]	PressIVC [kPa]
Homogeneous_Air	1	-11.51	94.969	1.68	3938.17	5.13	105.11	115.01
A/F_d = 38:1	2	-12.01	95.964	1.329	3708.38	7.86	106.4	114.92
	3	-11.63	95.723	1.381	3101.99	13.54	107.15	115.02
	4	-10.88	51.262	5.966	2492.87	16.97	106.92	115.23
	5	-10.66	21.367	17.824	2110.99	7.2	106.21	115.34
Homogeneous_N2	6	-9.4	-36.348	11.029	3636.49	8.6	105.81	115.83
A/F_d = 28:1	7	-9.24	95.977	1.378	3322.77	11.81	106.59	115.87
	8	-7.61	91.646	2.055	2832.62	15.73	105.75	116.17
	9	-7.11	78.33	4.471	2453.64	17.07	105.31	116.15
	10	-6.9	4.421	36.771	2104.09	1.6	103.32	116.34
Homogeneous_N2	11	-10.66	96.323	1.218	3550.61	9.69	107.75	115.4
A/F_d = 24:1	12	-10.62	94.265	1.36	3872.09	6.41	108.13	115.53
	13	-9.91	89.819	1.969	2835.72	15.85	108.39	115.65
	14	-8.87	24.816	7.028	2475.69	16.3	107.29	115.76
	15	-7.76	71.324	4.715	2456.05	17.25	106.82	116.02
Homogeneous_N2	16	-9.73	96.164	1.245	3573.69	9.57	106.73	115.61
A/F_d = 20:1	17	-10.15	95.297	1.328	3756.33	7.66	107.86	115.48
	18	-10.21	96.036	1.127	3348.82	11.6	108.89	115.52
	19	-8	88.991	2.88	2678.56	16.86	107.09	115.99
	20	-7.78	62.016	7.719	2256.31	13.88	107.01	115.93
Unmixed_N2	21	-9.49	95.864	1.378	3420.79	10.73	105.65	115.66
A/F_d = 20:1	22	-10.06	95.133	1.315	3771.41	7.19	107.65	115.59
	23	-9.48	95.994	1.259	3362.19	11.24	107.59	115.73
	24	-9.1	93.853	1.452	3025.46	14.06	107.85	115.71
	25	-6.99	70.851	6.007	2477.09	15.98	105.66	116.17
Unmixed_N2	26	-10.2	94.62	1.256	3783.65	6.96	100.57	114.99
A/F_d = 28:1	27	-10.22	96.213	1.173	3533.45	9.75	101.65	115.01
	28	-7.85	92.155	1.809	3075.37	13.9	100.6	115.49
	29	-7.04	71.744	5.506	2510.77	16.63	100.59	115.55
	30	-6.84	22.282	15.216	2209.36	9.59	101.16	115.52
Unmixed_N2	31	-11.16	95.314	1.279	3702.25	7.6	104.44	114.7
A/F_d = 24:1	32	-9.5	95.915	1.224	3455.85	10.4	104.34	114.94
	33	-7.03	95.838	1.423	3145.99	13.21	102.32	115.51
	34	-6.52	84.951	2.951	2748.69	16.12	102.2	115.5
	35	-5.86	26.342	20.527	2162.48	5.81	101.86	115.78
Homogeneous_EGR	36	-8.32	97.798	0.68	3500.11	9.3	105.42	113.15
A/F_d = 20:1	37	-8.35	97.121	0.9	3627.84	7.28	107.55	113.6
	38	-8.71	96.716	1.03	3709.58	6.5	107.86	113.53
	39	-8.53	96.924	0.82	3200	11.53	108.08	113.56
	40	-8.37	94.55	1.07	3080	12.48	107.94	113.78
	41	-8.1	96.72	2.03	2833	14.54	107.73	113.61
	42	-8.02	96.643	6.49	2517	16.16	110.075	115.955
Homogeneous_EGR	43	-8.50	96.794	0.82	3570	8.51	107.20	113.27
Temp. Stratification	44	-8.39	96.686	0.82	3826	6	106.69	112.86
A/F_d = 20:1	45	-8.47	96.766	1.03	3742	7	106.86	112.99
	46	-8.49	96.781	0.76	3403	10.2	107.53	113.54
	47	-8.43	96.718	1.07	3199	11.97	107.94	113.86
	48	-8.24	96.526	3.13	2861	15.15	108.62	114.40
	49	-8.00	96.275	7.07	2472	16.76	109.40	115.02
Unmixed_EGR	50	-6.15	95.762	1.194	3672.45	6.18	105.93	115.31
A/F_d = 20:1	51	-10.02	93.137	1.968	3817	4.26	107.96	113.19
	52	-10.26	91.42	2.189	3889	3.05	108.69	113.19
	53	-7.56	90.153	2.57	2717	14.8	106.44	113.74
	54	-7.95	79.254	6.43	2222	18.8	103.28	112.17
	55	-9.74	97.34	1.052	3317	9.81	107.57	112.05
	56	-10.54	90.929	1.09	3560	7.97	108.3	111.51

Experimental Case	RN#	PressEVO [kPa]	PressEVC [kPa]	MPRR [kPa/Deg]	MPRRLocat [dATDC]	BurnDur10-90 [Deg]	CA10 [dATDC]	CA50 [dATDC]	CA90 [dATDC]
Homogeneous_Air	1	197	99.87	617.23	1.55	5.33	-0.07	2	5.26
A/F_d = 38:1	2	199.6	99.18	467.96	4.34	6.2	2.24	4.8	8.44
	3	201.93	97.97	225.84	9.61	8.99	6.32	10.36	15.31
	4	202.34	96.87	94.17	7.56	12.83	8.93	14.94	21.76
	5	195.61	95.9	52.28	-14.35	17.38	9.81	18.55	27.18
Homogeneous_N2	6	199.4	99.35	397.78	4.84	6.97	2.61	5.48	9.58
A/F_d = 28:1	7	201.95	98.9	274.9	7.92	8.34	5.04	8.62	13.38
	8	202.37	97.82	140.03	11.2	11.2	7.53	12.53	18.73
	9	202.24	97.11	77.78	6.2	13.46	9.12	15.31	22.57
	10	179.11	96.44	49.76	-19.89	21.86	8.22	19.83	30.08
Homogeneous_N2	11	202.49	100.07	363.03	5.95	7.28	3.43	6.54	10.71
A/F_d = 24:1	12	201.79	100.59	526.81	2.87	6.15	0.9	3.33	7.05
	13	205.22	98.36	150.57	11.36	10.96	7.6	12.58	18.56
	14	204.69	97.21	89.25	5.85	13.34	9.1	15.33	22.44
	15	204.96	97.19	81.64	5.44	13.52	9.17	15.47	22.7
Homogeneous_N2	16	203.08	100.02	359.74	5.85	7.6	3.22	6.41	10.82
A/F_d = 20:1	17	202.38	100.26	442.47	4.01	6.88	1.74	4.52	8.62
	18	203.8	99.64	281.26	7.68	8.41	4.7	8.38	13.11
	19	204.64	97.85	113.08	11.03	12.44	7.99	13.69	20.43
	20	203.58	97	59.62	-6.22	15.31	9.56	16.98	24.87
Unmixed_N2	21	201.87	99.39	296.52	6.92	8.3	3.92	7.54	12.23
A/F_d = 20:1	22	200.67	100.19	447.33	3.47	6.89	1.19	3.98	8.08
	23	201.98	99.23	279.83	7.32	8.52	4.29	8.01	12.82
	24	202.36	98.63	184.11	9.84	10.32	6.14	10.8	16.46
	25	201.75	97.02	80.24	3.09	14.13	8.37	15.07	22.5
Unmixed_N2	26	200.15	99.7	468.32	3.35	6.5	1.29	3.84	7.79
A/F_d = 28:1	27	202.17	99.16	352.91	6.05	7.63	3.52	6.63	11.14
	28	202.73	97.4	193.35	9.71	10.09	6.34	10.69	16.42
	29	202.89	96.36	85.11	6.94	13.3	8.85	14.95	22.15
	30	197.96	95.89	55.37	-12.6	16.51	9.81	17.78	26.32
Unmixed_N2	31	201.05	99.67	433.85	3.98	6.9	1.69	4.48	8.59
A/F_d = 24:1	32	201.66	98.81	314.02	6.56	8.22	3.82	7.21	12.03
	33	201.6	97.65	204.77	9.06	10	5.73	10.01	15.73
	34	201.78	96.65	117.65	10.71	12.22	7.57	13.04	19.79
	35	192.2	95.91	51.33	-17.27	18.46	9.16	18.49	27.62
Homogeneous_EGR	36	204.98	95.89	330.78	5.63	6.45	2.72	6	9.17
A/F_d = 20:1	37	203.33	96.8	381.12	4.35	5.8	0.95	4.67	6.75
	38	202.86	96.71	414.7	3.53	6.22	0.03	3.78	6.25
	39	208.8	96.34	218.36	8.6	8.04	4.29	7.95	12.33
	40	209.6	96.33	191.33	9.37	8.81	5.02	8.95	13.83
	41	211.87	95.87	120.66	10.24	11.58	6	10.9	17.58
	42	214.215	98.215	123.005	12.585	14.69	7.31	13.4	22
Homogeneous_EGR	43	204.43	96.18	349.96	5.18	5.92	2	5.25	7.92
Temp. Stratification	44	201.89	95.98	418.03	3.26	5.35	-0.39	3.24	4.96
A/F_d = 20:1	45	202.72	96.04	395.70	3.89	4.78	1	3.78	5.78
	46	206.08	96.31	305.56	6.43	6.85	3.41	6.4	10.26
	47	208.10	96.48	251.31	7.96	8.97	4.42	8.38	13.39
	48	211.45	96.75	161.44	10.50	12.5	6.13	11.42	18.63
	49	215.30	97.06	58.00	13.42	15.29	7.53	14.46	22.82
Unmixed_EGR	50	190.43	97.33	414.09	2.72	6.63	0.27	3.12	6.9
A/F_d = 20:1	51	190.42	99.68	509.53	0.25	6.22	-2.22	1.5	4
	52	189.87	99.97	562.7	-1.06	6.21	-3.71	0	2.5
	53	198.03	97.08	161.98	9.28	16.24	5.18	10.45	21.42
	54	188.81	95.22	90.43	5.39	20.86	7.39	14.3	28.25
	55	185.16	97.4	322.02	4.71	8.95	2.72	6.3	11.67
	56	182.31	97.98	490.27	0.57	7.88	1.12	4.1	9

Experimental Case	RN#	PolyCoefComp	PolyCoefExp	Temp-IVC [C]	Delivered AF	EmisBasAFCO2	EmisBasAFO2	EmisBasAFave
Homogeneous_Air	1	1.29	1.34	219.300	43.189	37.992	37.636	37.814
A/F_d = 38:1	2	1.29	1.33	219.000	41.13	38.227	37.875	38.051
	3	1.29	1.33	219.500	41.372	38.362	37.983	38.172
	4	1.28	1.27	219.400	37.888	38.506	38.107	38.306
	5	1.28	1.17	218.300	17.722	39.134	38.692	38.913
Homogeneous_N2	6	1.29	1.34	208.700	74.4	38.036	28.621	33.328
A/F_d = 28:1	7	1.29	1.34	209.800	72.133	38.093	28.65	33.371
	8	1.29	1.32	224.700	29.997	38.656	28.629	33.642
	9	1.29	1.27	224.500	32.078	38.68	28.669	33.675
	10	1.29	1.17	220.400	10.127	40.223	29.689	34.956
Homogeneous_N2	11	1.29	1.33	225.400	16.194	36.279	24.002	30.141
A/F_d = 24:1	12	1.29	1.33	225.600	18.224	36.086	23.863	29.974
	13	1.28	1.31	225.600	20.246	36.394	24.127	30.261
	14	1.28	1.26	226.000	21.141	36.823	24.13	30.477
	15	1.29	1.26	225.400	8.657	37.231	23.958	30.595
Homogeneous_N2	16	1.29	1.33	227.000	5.162	36.165	20.134	28.149
A/F_d = 20:1	17	1.29	1.33	226.700	17.862	35.953	20.141	28.047
	18	1.29	1.33	227.100	18.047	36.013	20.292	28.152
	19	1.29	1.3	227.100	19.464	36.717	20.178	28.447
	20	1.29	1.22	226.500	12.821	36.758	20.31	28.534
Unmixed_N2	21	1.29	1.34	227.300	19.505	36.9	20.132	28.516
A/F_d = 20:1	22	1.29	1.33	226.800	19.082	36.815	20.185	28.5
	23	1.29	1.34	226.600	19.197	37.11	20.227	28.669
	24	1.29	1.33	225.700	22.286	37.175	20.331	28.753
	25	1.29	1.27	224.900	22.286	37.175	20.331	28.753
Unmixed_N2	26	1.29	1.33	220.700	28.207	37.655	28.535	33.095
A/F_d = 28:1	27	1.29	1.33	221.000	26.631	37.47	28.412	32.941
	28	1.3	1.33	221.300	30.168	38.432	28.271	33.352
	29	1.3	1.28	222.700	27.451	38.553	28.308	33.43
	30	1.29	1.2	221.700	24.11	38.874	28.495	33.684
Unmixed_N2	31	1.29	1.33	223.000	22.904	36.503	24.187	30.345
A/F_d = 24:1	32	1.29	1.34	222.600	23.49	37.364	24.017	30.691
	33	1.3	1.34	222.800	23.467	38.417	23.862	31.139
	34	1.3	1.31	222.600	23.097	38.651	23.962	31.306
	35	1.29	1.19	220.800	21.297	38.93	24.068	31.499
Homogeneous_EGR	36	1.3	1.33	208.149	19.979	19.924	19.807	19.865
A/F_d = 20:1	37	1.29	1.33	216.475	19.519	19.888	19.768	19.828
	38	1.29	1.33	220.928	19.338	19.946	19.829	19.888
	39	1.29	1.31	199.993	19.263	19.928	19.859	19.894
	40	1.29	1.31	196.461	19.577	19.915	19.854	19.884
	41	1.29	1.31	189.432	19.366	19.918	19.847	19.883
	42	1.29	1.32	183.204	19.273	20.093	20.022	20.058
Homogeneous_EGR	43	1.262	1.326	177.727	19.395	19.997	19.738	19.957
Temp. Stratification	44	1.262	1.335	216.475	19.525	19.909	19.838	19.863
A/F_d = 20:1	45	1.262	1.331	220.928	19.506	19.922	19.824	19.877
	46	1.262	1.322	199.993	19.487	19.934	19.810	19.890
	47	1.262	1.318	196.461	19.506	19.922	19.824	19.877
	48	1.262	1.313	189.432	19.534	19.903	19.846	19.856
	49	1.262	1.309	183.204	19.386	20.003	19.731	19.964
Unmixed_EGR	50	1.27	1.35	203.491	19.642	20.03	19.998	20.014
A/F_d = 20:1	51	1.27	1.33	221.167	19.05	19.963	19.912	19.937
	52	1.27	1.33	212.397	19.598	19.969	19.917	19.943
	53	1.27	1.32	196.410	19.258	19.937	19.876	19.907
	54	1.27	1.28	188.971	20.06	20.08	19.992	20.036
	55	1.27	1.34	178.188	19.47	20.004	19.956	19.98
	56	1.27	1.34	171.295	19.056	20.002	19.976	19.989

Experimental Case	RN#	EmisBasDeltAF	FuelHCratio	StoichAF	PHI Ave	LAMBDA Ave	CO2 [vol %]	CO [vol %]
Homogeneous_Air	1	0.356	2.25	15.084	0.399	2.507	5.263	0.055
A/F_d = 38:1	2	0.352	2.25	15.084	0.396	2.523	5.183	0.065
	3	0.379	2.25	15.084	0.395	2.531	5.064	0.084
	4	0.399	2.25	15.084	0.394	2.54	4.871	0.121
	5	0.442	2.25	15.084	0.388	2.58	4.213	0.21
Homogeneous_N2	6	9.415	2.25	15.084	0.453	2.21	5.151	0.063
A/F_d = 28:1	7	9.443	2.25	15.084	0.452	2.212	5.132	0.071
	8	10.027	2.25	15.084	0.448	2.23	4.926	0.092
	9	10.011	2.25	15.084	0.448	2.232	4.755	0.119
	10	10.534	2.25	15.084	0.432	2.317	3.073	0.258
Homogeneous_N2	11	12.277	2.25	15.084	0.5	1.998	5.421	0.064
A/F_d = 24:1	12	12.223	2.25	15.084	0.503	1.987	5.532	0.054
	13	12.267	2.25	15.084	0.498	2.006	5.288	0.082
	14	12.693	2.25	15.084	0.495	2.02	5.063	0.105
	15	13.273	2.25	15.084	0.493	2.028	4.964	0.111
Homogeneous_N2	16	16.031	2.25	15.084	0.536	1.866	5.449	0.061
A/F_d = 20:1	17	15.812	2.25	15.084	0.538	1.859	5.518	0.057
	18	15.721	2.25	15.084	0.536	1.866	5.438	0.066
	19	16.539	2.25	15.084	0.53	1.886	5.153	0.091
	20	16.448	2.25	15.084	0.529	1.892	4.85	0.13
Unmixed_N2	21	16.768	2.25	15.084	0.529	1.891	5.308	0.065
A/F_d = 20:1	22	16.63	2.25	15.084	0.529	1.889	5.387	0.057
	23	16.883	2.25	15.084	0.526	1.901	5.268	0.067
	24	16.844	2.25	15.084	0.525	1.906	5.187	0.078
	25	16.844	2.25	15.084	0.525	1.906	5.187	0.078
Unmixed_N2	26	9.12	2.25	15.084	0.456	2.194	5.264	0.059
A/F_d = 28:1	27	9.058	2.25	15.084	0.458	2.184	5.244	0.067
	28	10.161	2.25	15.084	0.452	2.211	5.009	0.084
	29	10.245	2.25	15.084	0.451	2.216	4.775	0.121
	30	10.379	2.25	15.084	0.448	2.233	4.314	0.178
Unmixed_N2	31	12.316	2.25	15.084	0.497	2.012	5.431	0.059
A/F_d = 24:1	32	13.347	2.25	15.084	0.491	2.035	5.244	0.067
	33	14.555	2.25	15.084	0.484	2.064	5.012	0.08
	34	14.689	2.25	15.084	0.482	2.076	4.868	0.101
	35	14.862	2.25	15.084	0.479	2.088	3.968	0.211
Homogeneous_EGR	36	0.117	2.25	15.084	0.759	1.317	10.328	0.093
A/F_d = 20:1	37	0.12	2.25	15.084	0.761	1.315	10.376	0.091
	38	0.117	2.25	15.084	0.758	1.318	10.361	0.09
	39	0.069	2.25	15.084	0.758	1.319	10.217	0.107
	40	0.061	2.25	15.084	0.759	1.318	10.183	0.112
	41	0.071	2.25	15.084	0.759	1.318	10.034	0.132
	42	0.074	2.425	15.259	0.743	1.493	10.012	0.141
Homogeneous_EGR	43	0.083	2.25	15.084	0.752	1.33	10.366	0.067
Temp. Stratification	44	0.094	2.25	15.084	0.760	1.316	10.366	0.059
A/F_d = 20:1	45	0.093	2.25	15.084	0.759	1.318	10.410	0.062
	46	0.091	2.25	15.084	0.758	1.32	10.303	0.072
	47	0.093	2.25	15.084	0.759	1.318	10.200	0.079
	48	0.095	2.25	15.084	0.760	1.315	10.040	0.105
	49	0.082	2.25	15.084	0.751	1.331	10.040	0.126
Unmixed_EGR	50	0.032	2.25	15.084	0.754	1.327	10.486	0.066
A/F_d = 20:1	51	0.051	2.25	15.084	0.757	1.322	10.577	0.059
	52	0.052	2.25	15.084	0.756	1.322	10.6	0.054
	53	0.061	2.25	15.084	0.758	1.32	10.325	0.108
	54	0.088	2.25	15.084	0.753	1.328	10.1	0.118
	55	0.048	2.25	15.084	0.755	1.325	10.459	0.071
	56	0.026	2.25	15.084	0.755	1.325	10.552	0.056

Experimental Case	RN#	EGR-CO2 [vol %]	EGR-O2 [vol%]	CalcO2 [vol%]	HC [ppm]	NO [ppm]	CalcH2O [vol%]	CalcH2 [vol%]
Homogeneous_Air	1	0.063	13.075	13.348	587.431	10.312	5.966	0.016
A/F_d = 38:1	2	0.061	13.182	13.452	697.225	5.426	5.885	0.019
	3	0.053	13.314	13.597	946.726	3.579	5.766	0.025
	4	0.053	13.537	13.83	1370.053	3.675	5.58	0.036
	5	0.051	14.35	14.664	2884.327	4.617	4.911	0.064
Homogeneous_N2	6	0.043	8.094	13.497	897.08	9.818	5.847	0.019
A/F_d = 28:1	7	0.036	8.107	13.516	903.297	5.713	5.832	0.021
	8	0.036	8.137	13.784	1225.026	4.181	5.618	0.028
	9	0.037	8.369	13.995	1667.665	4.109	5.447	0.036
	10	0.036	10.586	16.229	5908.26	5.797	3.666	0.081
Homogeneous_N2	11	0.039	5.735	13.103	904.084	10.865	6.152	0.019
A/F_d = 24:1	12	0.038	5.576	12.959	689.353	34.96	6.268	0.016
	13	0.037	5.941	13.272	1206.741	4.629	6.017	0.025
	14	0.036	6.083	13.568	1626.781	3.845	5.782	0.032
	15	0.035	5.969	13.701	1716.346	3.465	5.676	0.033
Homogeneous_N2	16	0.032	3.436	13.068	886.504	17.207	6.181	0.018
A/F_d = 20:1	17	0.034	3.412	12.974	792.921	28.143	6.255	0.017
	18	0.032	3.591	13.076	983.808	11.249	6.172	0.02
	19	0.031	3.69	13.455	1440.92	4.703	5.872	0.027
	20	0.032	4.161	13.835	2249.76	4.305	5.563	0.039
Unmixed_N2	21	0.063	3.402	13.265	942.767	13.39	6.025	0.019
A/F_d = 20:1	22	0.068	3.352	13.164	763.238	27.207	6.107	0.017
	23	0.069	3.449	13.322	959	10.668	5.982	0.02
	24	0.067	3.597	13.423	1146.44	6.063	5.9	0.023
	25	0.067	3.597	13.423	1146.44	6.063	5.9	0.023
Unmixed_N2	26	0.071	8.049	13.34	731.651	14.622	5.971	0.018
A/F_d = 28:1	27	0.071	8.079	13.358	857.86	6.881	5.955	0.02
	28	0.075	7.918	13.678	1093.3	4.226	5.704	0.025
	29	0.074	8.19	13.967	1657.69	4.064	5.472	0.036
	30	0.074	8.771	14.553	2787.475	5.151	4.999	0.054
Unmixed_N2	31	0.08	5.749	13.096	774.048	22.632	6.159	0.018
A/F_d = 24:1	32	0.077	5.591	13.357	909.621	9.029	5.955	0.02
	33	0.074	5.454	13.675	1101.864	5.414	5.705	0.024
	34	0.079	5.62	13.855	1381.315	4.574	5.56	0.03
c	35	0.074	6.788	15.001	3752.629	5.902	4.636	0.065
Homogeneous_EGR	36	4.234	5.779	5.983	1127.602	17.31	11.696	0.028
A/F_d = 20:1	37	4.23	5.709	5.917	1051.539	22.455	11.748	0.027
	38	4.196	5.736	5.941	999.644	27.139	11.731	0.027
	39	4.194	5.974	6.125	1413.241	9.949	11.583	0.032
	40	4.196	6.025	6.166	1520.688	8.848	11.548	0.033
	41	4.167	6.201	6.353	1901.736	7.057	11.397	0.039
	42	4.023	6.376	6.433	2001.335	7.232	11.572	0.037
Homogeneous_EGR	43	4.085	6.398	6.475	604.116	25.588	11.855	0.022
Temp. Stratification	44	4.133	6.173	6.295	491.860	42.185	11.904	0.020
A/F_d = 20:1	45	4.175	5.979	6.138	551.904	32.780	11.878	0.021
	46	3.925	7.141	7.073	677.213	22.181	11.823	0.023
	47	3.879	7.354	7.244	831.238	20.900	11.757	0.026
	48	4.002	6.785	6.786	1115.793	19.852	11.633	0.032
	49	4.047	6.575	6.618	1324.641	18.949	11.543	0.036
Unmixed_EGR	50	7.578	5.682	5.792	552.849	30.637	11.851	0.02
A/F_d = 20:1	51	7.373	5.539	5.67	417.301	64.828	11.948	0.018
	52	7.323	5.51	5.642	355.025	97.212	11.97	0.016
	53	7.446	5.833	5.975	1064.983	7.521	11.705	0.032
	54	4.063	6.11	6.28	1467.56	5.398	11.46	0.035
	55	4.072	5.699	5.826	667.291	26.167	11.825	0.021
	56	4.004	5.605	5.707	434.811	73.637	11.917	0.017

Experimental Case	RN#	EICO2 [g/kg]	EICO [g/kg]	EINO [g/kg]	EIHC [g/kg]	Knck/RngIndAve [V]	Knck/RngIndStdDev [V]
Homogeneous_Air	1	2958	19.68	0.3952	10.69	5.29	0.071
A/F_d = 38:1	2	2933	23.41	0.2094	12.78	4.32	0.694
	3	2879	30.4	0.1387	17.43	1.71	0.167
	4	2784	44.02	0.1432	25.36	0.1	0.022
	5	2460	78.06	0.1838	54.54	0.09	0.166
Homogeneous_N2	6	2901	22.58	0.377	16.36	4.05	1.144
A/F_d = 28:1	7	2895	25.49	0.2198	16.5	2.47	0.927
	8	2825	33.58	0.1635	22.75	0.9	0.711
	9	2733	43.52	0.161	31.03	0.12	0.604
	10	1860	99.37	0.2392	115.8	0.81	0.699
Homogeneous_N2	11	2909	21.85	0.3975	15.71	3.59	1.080
A/F_d = 24:1	12	2949	18.32	1.271	11.9	4.95	1.267
	13	2849	28.12	0.17	21.05	0.4	0.643
	14	2765	36.49	0.1431	28.76	0.3	0.629
	15	2743	39.03	0.1305	30.7	0.24	0.621
Homogeneous_N2	16	2914	20.76	0.6273	15.35	3.4	1.054
A/F_d = 20:1	17	2932	19.27	1.019	13.64	4.52	1.208
	18	2896	22.37	0.4085	16.96	2.54	0.936
	19	2804	31.51	0.1745	25.38	0.4	0.643
	20	2649	45.19	0.1603	39.78	0.23	0.619
Unmixed_N2	21	2898	22.59	0.4985	16.67	3.2	1.027
A/F_d = 20:1	22	2933	19.75	1.01	13.45	4.54	1.211
	23	2894	23.42	0.3995	17.06	2.75	0.965
	24	2856	27.33	0.2276	20.44	1.8	0.835
	25	2856	27.33	0.2276	20.44	0.31	0.630
Unmixed_N2	26	2933	20.92	0.5555	13.2	4.55	1.212
A/F_d = 28:1	27	2909	23.65	0.2602	15.41	3.62	1.085
	28	2854	30.46	0.1642	20.17	1.6	0.807
	29	2734	44.1	0.1587	30.74	0.12	0.604
	30	2501	65.67	0.2036	52.32	0.21	0.617
Unmixed_N2	31	2931	20.27	0.8328	13.53	4.5	1.205
A/F_d = 24:1	32	2900	23.59	0.3405	16.29	3.22	1.030
	33	2855	29	0.2102	20.32	1.9	0.849
	34	2793	36.88	0.1789	25.66	0.68	0.681
c	35	2310	78.18	0.2343	70.74	0.15	0.608
Homogeneous_EGR	36	2958.607	16.952	0.518	31.9	3.51	1.871
A/F_d = 20:1	37	2966.041	16.505	0.671	29.2	4.28	2.316
	38	2970.448	16.371	0.813	27.9	4.95	2.868
	39	2929.986	19.16	0.298	37	2.77	1.159
	40	2919.167	20.17	0.265	40	2.36	0.996
	41	2880.334	21.77	0.212	46.1	1.6	0.729
	42	2879.313	25.2	0.18	54.2	0.65	0.684
Homogeneous_EGR	43	2959.774	16.716	0.44	29.3	3.68	1.883
Temp. Stratification	44	2959.774	14.89	1.01	25	5.62	1.883
A/F_d = 20:1	45	2970.448	15.7	0.687	27.3	4.65	2.868
	46	2944.343	17.78	0.323	32.1	2.75	1.673
	47	2919.167	19.48	0.279	38	1.97	0.996
	48	2880.334	25.19	0.243	48.9	1.04	0.729
	49	2880.334	29.81	0.212	56.9	0.57	0.729
Unmixed_EGR	50	3015.499	15.96	0.965	24	5.01	1.725
A/F_d = 20:1	51	3029.311	15.1	1.941	21.4	5.96806	0.631
	52	3036.28	14.276	2.974	20.4	7.22194	0.754
	53	2959.738	23.28	0.195	45.5	2.24	0.188
	54	2920.73	29.74	0.163	62.8	1.47	0.176
	55	3004.349	17.416	0.448	32.2	3.66928	0.449
	56	3028.643	16.21	0.731	26.8	4.82	0.617

Appendix C – Metal Engine Blow-by Measurement

Engine blow-by measurements must be performed every 100 engine ruuning hours and also when new piston rings are installed. Blow-by measurements are performed by measuring the volumetric flow of engine combustion chamber charge that escapes through the piston rings to the engine crankcase compartment. Engine is run in spark-ignited firing mode. The following table presents details on engine running conditions and engine intake charge conditions for each of the engine firing mode stages required to fully break-in the piston rings.

Test#	EngineSpeed [RPMs]	IMAP [kPa]	Orif.#	PressureOrif. [kPa]	Fueling Rate [mg / cycle]	KRIndex [V]	TestTime [mins.]	A/F	SparkTiming BTDC [degs.]	Blow-by [L / min] 1st 11hrs. Tests	Blow-by [L / min] 2nd 11hrs. Tests
Blow-by	1300	50	2	225	13.2	0.6	20	17:01	20		
0	2200	50	2	420	Motoring	--	30	--	--		
1	2200	45	2	380	14.7	4.6	30	15 -16 : 1	21		
2	2200	60	2	500	18.75	4.65	30	15 -16 : 1	13.2		
3	1300	50	2	210	14	4.6	30	15 -16 : 1	43		
Blow-by	1300	50	2	225	13.2	0.6	10	17:01	20		
4	1500	50	2	270	15.5	4.7	60	15 -16 : 1	35		
5	1700	60	2	390	19.5	4.6	60	15 -16 : 1	20		
6	1900	60	2	440	18.5	4.5	60	15 -16 : 1	18		
7	1300	50	2	210	14	4.6	30	15 -16 : 1	43		
Blow-by	1300	50	2	225	13.2	0.6	10	17:01	20		
8	2200	60	2	500	18.75	4.6	60	15 -16 : 1	15.5		
9	2300	60	2	525	18.7	4.6	60	15 -16 : 1	14		
10	2500	60	2	585	18.8	4.6	60	15 -16 : 1	15		
11	1300	50	2	210	14	4.6	30	15 -16 : 1	43		
Blow-by	1300	50	2	225	13.2	0.55	10	17:01	20		
12	2000	45	2	330	14.5	4.7	30	15 -16 : 1	31		
13	2200	60	2	500	18.75	4.6	30	15 -16 : 1	14		
14	2200	50	2	420	Motoring	--	30	--	--		
15	2000	45	2	330	14.5	4.7	30	15 -16 : 1	31		
16	2200	60	2	500	18.75	4.6	30	15 -16 : 1	13.2		
17	1300	50	2	210	14	4.6	30	15 -16 : 1	43		
Blow-by	1300	50	2	225	13.2	0.6	10	17:01	20		

Note: Test# ~ Blow-by: Indicates to take reading of the engine blow-by